The *Toxoplasma* effector GRA28 promotes parasite dissemination by inducing dendritic cell-like migratory properties in infected macrophages

Arne L. ten Hoeve, Laurence Braun, Matias E Rodriguez, Gabriela C Olivera, Alexandre Bougdour, Lucid Belmudes, Yohann Couté, Jeroen P. J. Saeij, Mohamed-Ali Hakimi, Antonio Barragan

Article

Cell Host & Microbe

The *Toxoplasma* effector GRA28 promotes parasite dissemination by inducing dendritic cell-like migratory properties in infected macrophages

Graphical abstract

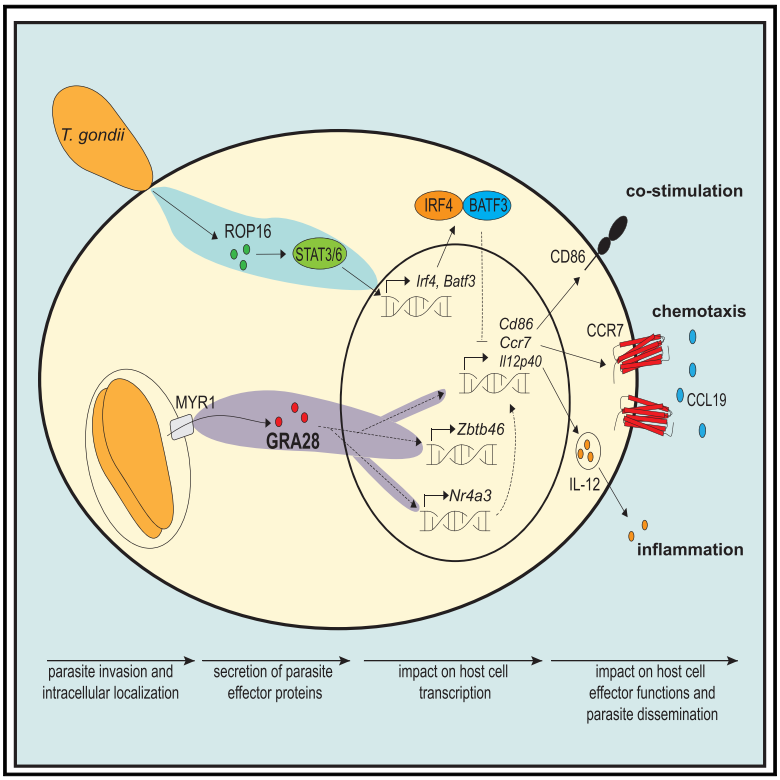

Highlights

- *Toxoplasma* effector protein GRA28 drives a pro-migratory transcriptional remodeling
- In parasitized macrophages, GRA28 cooperates with host chromatin modifiers
- Parasitized macrophages upregulate CCR7 GRA28-dependently and chemotax
- GRA28 facilitates systemic migration of adoptively transferred macrophages in mice

Authors

Arne L. ten Hoeve, Laurence Braun, Matias E. Rodriguez, ..., Jeroen P.J. Saeij, Mohamed-Ali Hakimi, Antonio Barragan

Correspondence

mohamed-ali.hakimi@univ-grenoble-alpes.fr (M.-A.H.), antonio.barragan@su.se (A.B.)

In brief

Toxoplasma gondii exploits the trafficking of phagocytes for dissemination. Ten Hoeve et al. show that parasitized macrophages acquire dendritic cell-like CCR7-dependent migratory properties via parasite effector GRA28-mediated transcriptional remodeling of the host cell, which facilitates *T. gondii* dissemination. This work highlights a remarkable migratory plasticity in differentiated mononuclear phagocytes.

ten Hoeve et al., 2022, Cell Host & Microbe *30*, 1570–1588
November 9, 2022
https://doi.org/10.1016/j.chom.2022.10.001

CellPress

CellPress
OPEN ACCESS

Cell Host & Microbe

Article

The *Toxoplasma* effector GRA28 promotes parasite dissemination by inducing dendritic cell-like migratory properties in infected macrophages

Arne L. ten Hoeve,[1,5] Laurence Braun,[2,5] Matias E. Rodriguez,[1] Gabriela C. Olivera,[1] Alexandre Bougdour,[2] Lucid Belmudes,[3] Yohann Couté,[3] Jeroen P.J. Saeij,[4] Mohamed-Ali Hakimi,[2,*] and Antonio Barragan[1,6,*]

[1]Department of Molecular Biosciences, The Wenner-Gren Institute, Stockholm University, 106 91 Stockholm, Sweden
[2]Institute for Advanced Biosciences, INSERM U1209, CNRS UMR5309, Université Grenoble Alpes, Grenoble, France
[3]Univ. Grenoble Alpes, INSERM, CEA, UMR BioSanté U1292, CNRS, CEA, FR2048, 38000 Grenoble, France
[4]Department of Pathology, Microbiology, and Immunology, University of California Davis, Davis, CA 95616, USA
[5]These authors contributed equally
[6]Lead contact
*Correspondence: mohamed-ali.hakimi@univ-grenoble-alpes.fr (M.-A.H.), antonio.barragan@su.se (A.B.)
https://doi.org/10.1016/j.chom.2022.10.001

SUMMARY

Upon pathogen detection, macrophages normally stay sessile in tissues while dendritic cells (DCs) migrate to secondary lymphoid tissues. The obligate intracellular protozoan *Toxoplasma gondii* exploits the trafficking of mononuclear phagocytes for dissemination via unclear mechanisms. We report that, upon *T. gondii* infection, macrophages initiate the expression of transcription factors normally attributed to DCs, upregulate CCR7 expression with a chemotactic response, and perform systemic migration when adoptively transferred into mice. We show that parasite effector GRA28, released by the MYR1 secretory pathway, cooperates with host chromatin remodelers in the host cell nucleus to drive the chemotactic migration of parasitized macrophages. During *in vivo* challenge studies, bone marrow-derived macrophages infected with wild-type *T. gondii* outcompeted those challenged with MYR1- or GRA28-deficient strains in migrating and reaching secondary organs. This work reveals how an intracellular parasite hijacks chemotaxis in phagocytes and highlights a remarkable migratory plasticity in differentiated cells of the mononuclear phagocyte system.

INTRODUCTION

The mononuclear phagocyte system plays pivotal roles in immune responses and comprises principally monocytes, macrophages and dendritic cells (DCs) (Guilliams et al., 2014). The identification of DC-restricted precursors indicates ontological differences between DCs and macrophages (Sathe et al., 2014). While DCs arise from bone marrow-derived common DC precursors, various tissue-resident macrophages develop from yolk-sac or erythro-myeloid progenitors during fetal development (Guilliams et al., 2014). Macrophages and monocyte-derived DCs (Mo-DCs) also differentiate from monocytic precursors (Helft et al., 2015).

Ontology and differences in tissue localization are reflected in the transcriptomes of macrophages and DCs, which can be distinguished by transcriptional signatures (Miller et al., 2012). Marked by the expression of ZBTB46 (Satpathy et al., 2012), conventional DCs (cDCs) develop *in vivo* in response to STAT3-activating growth factor FLT3L (Laouar et al., 2003) and under the control of IRF8, BATF3, or IRF4 (Amon et al., 2019). Similarly, Mo-DCs depend on IRF4 for their differentiation, while monocytes divert toward macrophages independently of IRF4 (Briseño et al., 2016). Together, STAT3, BATF3, IRF4, and IRF8 form part of the regulatory network that controls cDC development (Lin et al., 2015).

The study of host-pathogen interactions provides a powerful approach to gain insight into cellular processes in immune cells. The protozoan *Toxoplasma gondii* commonly infects humans and other warm-blooded vertebrates, for example, rodents. It is estimated that one third of the global human population encounters *T. gondii* during a life-time (Pappas et al., 2009). Following oral infection, *T. gondii* disseminates widely from the intestine to reach peripheral organs, such as the central nervous system. Although principally asymptomatic in healthy individuals, infection can cause life-threatening encephalitis in immune-compromised persons, severe neurological manifestations in the developing fetus, and recurrent ocular disease in immune-competent individuals (Montoya and Liesenfeld, 2004; Schlüter and Barragan, 2019).

The disseminating stage of *T. gondii*—the tachyzoite—is obligate intracellular. Thus, active invasion of host cells, including leukocytes, is essential for parasite survival (Dobrowolski and

CellPress
OPEN ACCESS

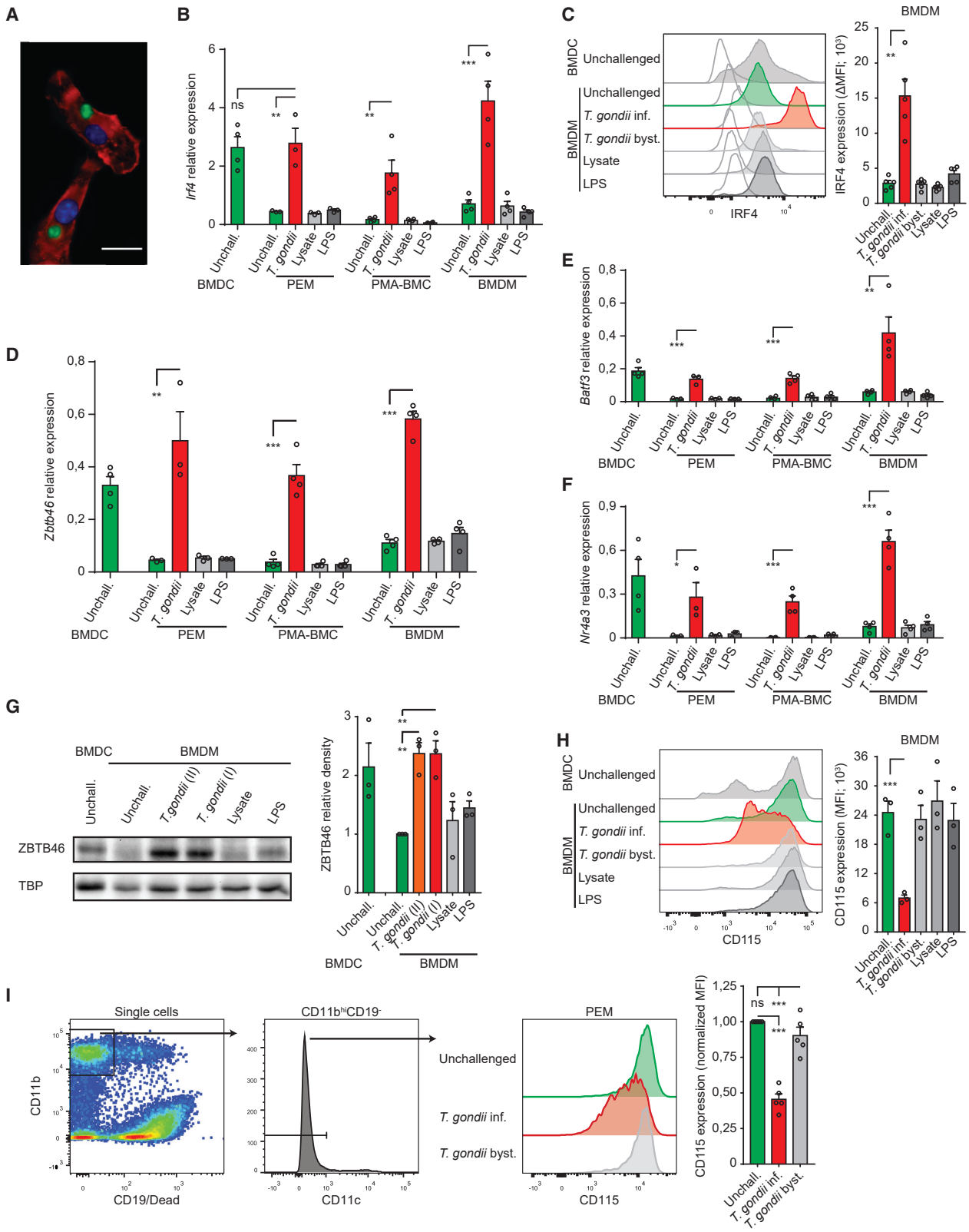

Figure 1. Expression of DC-associated transcription factors in *T. gondii*-challenged macrophages

(A) Representative micrograph shows primary bone marrow-derived macrophages (BMDMs) stained for F-actin (red) and nuclei (blue), with replicating intracellular GFP-expressing *T. gondii* tachyzoites (green) 18 h post-challenge. Scale bars, 20 μm.

(legend continued on next page)

Sibley, 1996). Invasion of host cells encompasses the discharge of secretory organelles, called rhoptries, into the cytosol and the secreted proteins (ROPs) modulate cellular responses of parasitized cells (Frickel and Hunter, 2021; Hakimi et al., 2017). The virulence-associated rhoptry kinase ROP16 activates STAT signaling in infected cells, which results in inhibition of inflammatory cytokine secretion (Butcher et al., 2011; Saeij et al., 2007). Further, a secretory machinery (MYR) ensures transport of dense granule proteins (GRAs) across the intracellular parasitophorous vacuole where the parasite resides (Franco et al., 2016).

Shortly after oral infection, *T. gondii* crosses the intestinal epithelium (Barragan and Sibley, 2003; Dubey, 1997). Systemic spread from the intestine to peripheral organs via the blood circulation is largely mediated by parasitized CD11c^{+} and CD11b^{+} leukocytes (Courret et al., 2006). DCs can act as "Trojan horses" for *T. gondii* dissemination in mice (Lambert et al., 2006) in a parasite genotype-related fashion (Lambert et al., 2009). Upon active invasion by *T. gondii*, DCs are induced to migrate via activation of non-canonical GABAergic signaling and mitogen-activated protein (MAP) kinase activation (Bhandage et al., 2020; Kanatani et al., 2017; Ólafsson et al., 2019, 2020). This migratory activation, termed hypermigratory phenotype (Weidner and Barragan, 2014), implicates secreted parasite effectors (Drewry et al., 2019; Sangaré et al., 2019; Weidner et al., 2016) and does not rely on chemotaxis (Fuks et al., 2012; Weidner et al., 2013).

Intestinal macrophages are present at higher densities along the villi and are located more closely to the epithelial cells than DCs (Schulz et al., 2009). Although macrophages and DCs share many functions, they differ in their migration under steady-state and inflammatory conditions. Upon inflammation, DCs migrate from peripheral tissues via lymphatic vessels to lymph nodes, for which the upregulation of the chemokine receptor CCR7 is indispensable (Alvarez et al., 2008; Förster et al., 1999). By and large, macrophages can be distinguished from DCs by their lack of *Ccr7* expression (Miller et al., 2012). In line with this, macrophages along the intestinal epithelium are sessile and do not normally migrate to draining lymph nodes upon Toll-like receptor (TLR) stimulation, unlike neighboring DCs (Schulz et al., 2009).

Here, we show that *T. gondii* imparts a DC-like transcriptional signature on macrophages and that parasitized macrophages upregulate CCR7 expression with the onset of chemotaxis. Our data highlight a mechanism by which *T. gondii* exploits the migratory plasticity of parasitized macrophages to potentiate its dissemination.

RESULTS

T. gondii induces expression of DC-associated transcription factors in parasitized macrophages

The transcription factor IRF4 was found to be essential for the differentiation of monocytes to DCs but not macrophages (Briseño et al., 2016; Goudot et al., 2017). Because *T. gondii* encounters mononuclear phagocytes in tissues and modulates their migratory properties (Bhandage et al., 2020), we investigated the impact of infection on transcriptional signatures that define DCs and macrophages. Interestingly, upon challenge with live *T. gondii* tachyzoites (Figure 1A), an elevated expression of *Irf4*, similar to that in bone marrow-derived DCs (BMDCs), was measured in resident peritoneal macrophages (PEMs), macrophage-like phorbol 12-myristate 13-acetate (PMA) bone marrow-derived cells (PMA-BMCs), and bone marrow-derived macrophages (BMDMs) (Figure 1B). In contrast, neither challenge with tachyzoite lysate nor LPS altered *Irf4* expression. Flow cytometry analyses confirmed markedly elevated IRF4 protein expression in *T. gondii*-infected BMDMs but not in bystander BMDMs (Figure 1C). IRF4 expression in infected BMDMs reached levels comparable with expression in BMDCs (CD11c^{+}MHCII^{hi}) (Figure S1A), and with prominent nuclear staining (Figure S1B).

Additional DC signature genes include the transcription factors *Zbtb46*, *Batf3*, *Nr4a3*, and *Runx3* (Miller et al., 2012), and ChIP data suggest that these genes are targeted by IRF4 (Figure S1C; Boulet et al., 2019). In line with this, challenge with *T. gondii* resulted in a significant increase in *Zbtb46*, *Batf3*, *Nr4a3*, and *Runx3* mRNA in macrophages, approaching or surpassing their relative expression in BMDCs (Figures 1D–1F and S1D). In contrast, expression was non-significantly altered by *T. gondii* lysate or LPS. Elevated ZBTB46 protein expression in *T. gondii*-challenged macrophages was confirmed by western blotting (Figure 1G). Notably, challenge with *T. gondii* minorly impacted expression of the pDC-associated transcription factor *Spib*, receptor *Flt3*, and Ly6C (Figures S1E–S1G), while expression of the M-CSF receptor CD115 was reduced on both BMDMs and PEMs, in the absence of a measurable bystander effect (Figures 1H, 1I, and S1H). We confirmed that *Zbtb46* and *Irf4* are induced by a variety of *T. gondii* strains (Figure S1I). Additionally, we could largely confirm the induction of *Zbtb46*, *Batf3*, *Nr4a3*, and *Irf4* by *T. gondii* in previously published transcriptomics data (Figures S2A and S2B). However, comparing

(B) qPCR analyses of *Irf4* cDNA from PEMs, PMA-BMCs, and BMDMs challenged for 18 h with *T. gondii* type I tachyzoites (RH, MOI 2), tachyzoite lysate (MOI 2 equivalent), or LPS (10 ng/mL). For reference, macrophages and BMDCs were incubated in complete medium, unchallenged (unchall.).
(C) Flow cytometric analysis of IRF4 expression by BMDCs and BMDMs challenged as in (B) with MOI 1. *T. gondii*-infected and bystander cells are distinguished by GFP$^{+/-}$. Bar graph depicts the differences between anti-IRF4 and isotype mean fluorescence intensity (MFI, mean + SE) from 5 independent experiments (n = 5).
(D–F) qPCR analyses of *Zbtb46* (D), *Batf3* (E), and *Nr4a3* (F) cDNA, respectively, in cells challenged as in (B).
(G) Western blot analysis of ZBTB46 expression in BMDCs and BMDMs challenged for 18 h with *T. gondii* type I or type II tachyzoites, tachyzoite lysate, or LPS. Bar graph depicts density (mean + SE) related to unchallenged BMDMs (=1, n = 3).
(H) Flow cytometry analysis of CD115 expression in BMDCs and BMDMs challenged as in (C). Bar graph depicts MFI (mean + SE) from 3 independent experiments.
(I) Flow cytometric analysis of CD115 expression on PEMs challenged as in (C) with *T. gondii* (MOI 0,5) or left unchallenged, gated from live peritoneal cells as indicated. Bar graph depicts MFI (mean + SE) related to unchallenged PEM (=1, n = 5).
Relative expression ($2^{-\Delta Cq}$) is displayed as mean + SE and individual measurements (n = 3–4). Statistical comparisons were made with ANOVA and Dunnett's (B and E–H) or Holm-Bonferroni (C, D, and I) post-hoc tests (*p $\leq$ 0.05, **p $\leq$ 0.01, ***p $\leq$ 0.001, ns p > 0.05).
See also Figure S1.

CellPress
OPEN ACCESS

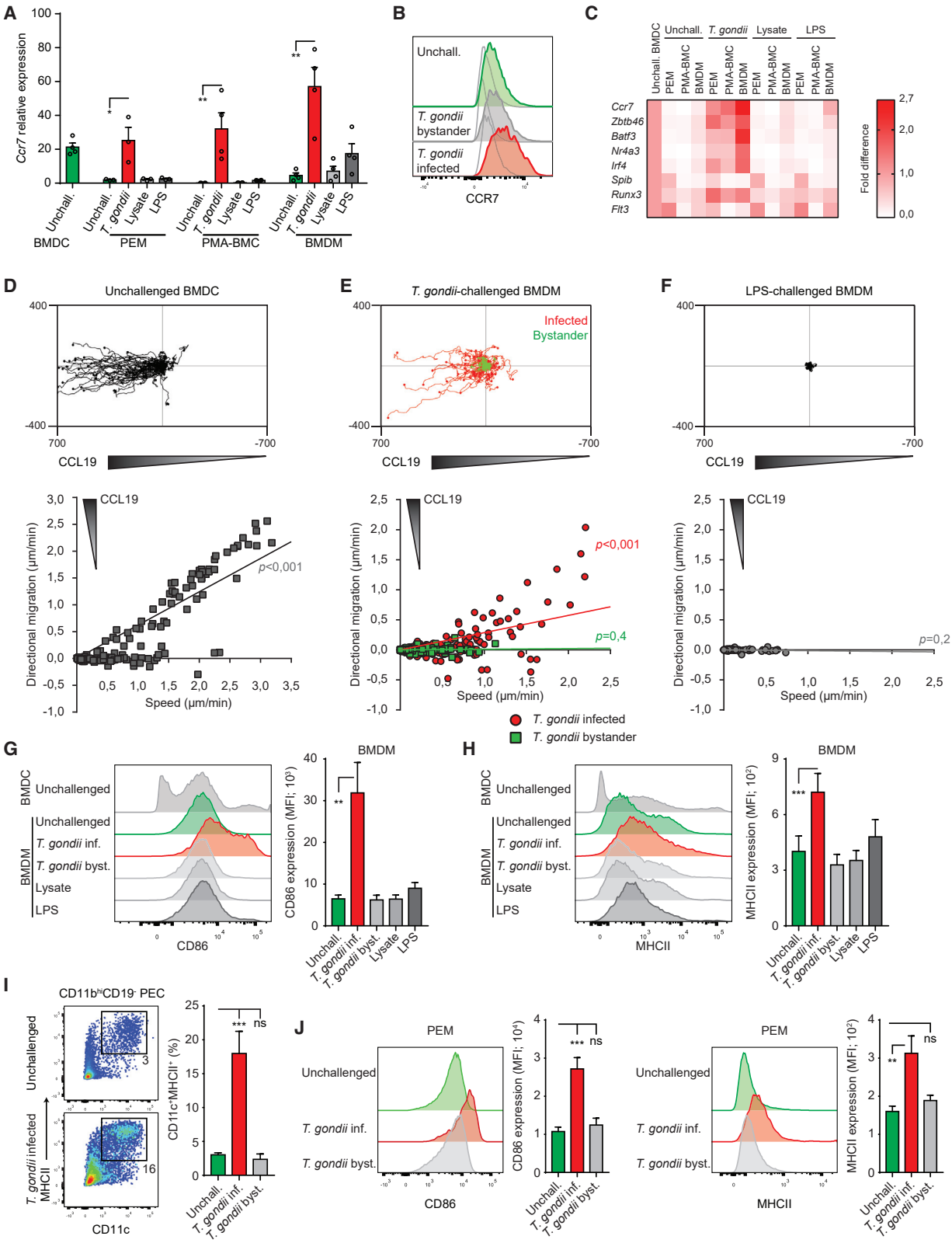

Figure 2. Expression of *Ccr7* and chemotaxis toward CCL19 by *T. gondii*-challenged macrophages

(A) qPCR analyses of *Ccr7* cDNA from BMDCs, PEMs, PMA-BMCs, and BMDMs challenged for 18 h with *T. gondii* type I tachyzoites (RH), tachyzoite lysate, LPS, or left unchallenged (unchall.). Relative expression ($2^{-\Delta Cq}$) is displayed as mean + SE and individual measurements (n = 3–4).

(legend continued on next page)

T. gondii-induced transcriptional changes with Mo-DC differentiation and gene expression differences between BMDMs and BMDCs, we found no broad similarities. We conclude that the challenge of different types of macrophages with *T. gondii* induces the expression of transcription factors associated with cDCs, but not with DC differentiation per se.

T. gondii-infected macrophages perform chemotaxis in response to CCL19

Because *Zbtb46*, *Batf3*, *Nr4a3*, and *Irf4* mediate DC development and differentiation, including associations to CCR7-mediated DC migration (Bajaña et al., 2012), we addressed whether infection impacted chemotaxis in macrophages. First, challenge with *T. gondii* tachyzoites induced a significantly superior transcriptional expression of *Ccr7*, related to LPS or MOI-equivalent doses of parasite lysate, and similar or superior to BMDCs (Figures 2A and S2C). BMDMs infected with *T. gondii* displayed elevated surface CCR7 expression over unchallenged macrophages (Figure 2B), all consistent with the relative expression profiles of DC-associated transcription factors (Figure 2C). Next, in chemotaxis assays with the CCR7-ligand chemokine CCL19, *T. gondii*-infected BMDM displayed a distinct migratory response toward the CCL19 source. Similarly, BMDCs chemotaxed (Figures 2D and 2E), as described (Helft et al., 2015), with undetectable chemotaxis by non-infected bystander BMDMs (Figure 2E) and LPS-challenged macrophages (Figure 2F). Additional control characterizations excluded chemokinetic or haptokinetic effects by CCL19 (Figures S2D and S2E). Of note, parasitized macrophages exhibited hypermotility, in line with previous results in monocytes and DCs (Bhandage et al., 2020), and this component of the migratory response was independent of CCL19 and was absent in bystander macrophages (Figures S2D and S2E). Further, we found that *T. gondii*-infected BMDMs expressed significantly higher levels of CD86 and MHCII, but not CD40 and CD80 (Figures 2G, 2H, and S2F), consistent with the impact of *T. gondii* on macrophage phenotypical maturation, cytokine responses, and proliferative responses in leukocytes (Figures S2G–S2J). While noting an increase in $CD11c^{+}MHCII^{+}$-expressing cells among resident $CD11b^{hi}CD19^{-}$ peritoneal cells (PECs) infected *in vitro* (Figure 2I), we also found increases of CD86 and MHCII on *T. gondii*-infected PEMs (Figure 2J). We conclude that challenge with *T. gondii* elevates the expression of CCR7 in parasitized macrophages with chemotactic responses to CCL19, in absence of a detectable bystander effect.

The *T. gondii* MYR1 secretory pathway and ROP16-STAT signaling differently impact chemotaxis and migration-associated transcription in infected macrophages

Because the migratory responses indicated effects related to intracellularly located parasites, we assessed two main pathways utilized by *T. gondii* to modulate host cell responses and transcriptome: rhoptry (ROP) protein-mediated activation of STAT signaling (Saeij et al., 2007) and effector protein secretion via the MYR1 pathway (Franco et al., 2016; Naor et al., 2018). Importantly, chemotaxis was abrogated in macrophages infected with MYR1-deficient parasites (TgΔ*myr1*) but maintained upon challenge with ROP16-deficient parasites (TgΔ*rop16*) (Figure 3A). Consistently, *Ccr7* expression was reduced (TgΔ*myr1*) and elevated (TgΔ*rop16*), respectively, upon challenge with the mutant parasites (Figure 3B). In line with this, contrasting effects were observed on *Zbtb46, Irf4*/IRF4, *Batf3*, and *Nr4a3* expression (Figures 3B, S3A, and S3B). Moreover, the downregulation of CD115 was abrogated and partially reduced by MYR1 and ROP16 deficiency, respectively (Figure S3C). Consistent with the downmodulation of inflammatory cytokine responses by ROP16 (Jensen et al., 2013), macrophages challenged with TgΔ*rop16* expressed higher levels of *Il12p40* and CD86, and elicited higher *Ifng* expression in mixed leukocyte reaction (MLR) (Figures 3C, 3D, and S3D). STAT inhibition confirmed the implication of STATs in the observed transcriptional changes (Figure S3E). In sharp contrast, *Il12p40* and CD86 expression was significantly reduced upon challenge with TgΔ*myr1* parasites (Figures 3C and 3D).

To confirm that the observed phenotypic effects were linked to the MYR1 secretory pathway and not MYR1 expression itself, we assessed two additional mutants (TgΔ*rop17*, TgΔ*gra45*) associated with this secretory pathway (Panas et al., 2019; Wang et al., 2020) with similar effects on *Ccr7*, *Il12p40, Zbtb46*, and *Irf4* expression (Figures 3E and S3F). In contrast, a mutant deficient in TgWIP, a rhoptry protein associated with non-chemotactic hypermotility of parasitized DCs (Sangaré et al., 2019), maintained elevated expression of *Ccr7* and chemotaxis of macrophages, similar to wild type (Figures 3E, 3F, and S3F). Jointly, these data show that the expression of DC-associated transcripts and markers in *T. gondii*-challenged macrophages depends on

(B) Flow cytometric analysis of anti-CCR7 and isotype control stainings on BMDMs challenged for 18 h with *T. gondii* type I tachyzoites or left unchallenged (unchall.). Representative of 2 independent experiments.
(C) Heatmap depicting relative mRNA expression changes of indicated genes for different types of macrophages and challenges. Color scale indicates mean fold difference in expression related to unchallenged BMDCs (=1) from 3 to 4 independent experiments.
(D–F) Motility plots depict the displacement of unchallenged BMDCs and BMDMs challenged with *T. gondii* type I (RH) or LPS for 12 h in a collagen matrix with a CCL19 gradient, as detailed in method details (scale in μm). For each condition, directional migration (μm/min) toward the CCL19 source and speed (μm/min) of individual cells are displayed in graphs, with linear regression lines. For *T. gondii*-challenged BMDMs (E), infected cells (GFP^{+}, red), and non-infected bystander cells (GFP^{-}, green) were analyzed. p values indicate the directional migration compared with hypothetical zero directionality (one-sample permutation test). Data from 2 (BMDCs) or ≥3 independent experiments.
(G and H) Flow cytometric analysis of CD86 (G) and MHCII (H) expression in BMDCs and BMDMs challenged as in (A), with *T. gondii*-infected and bystander BMDMs distinguished by $GFP^{+/-}$. Bar graph depicts the MFI (mean + SE, n = 4).
(I) Flow cytometric analysis of CD11c and MHCII expression on $CD11b^{hi}CD19^{-}$ peritoneal cells (PECs), challenged as in (C) with *T. gondii* or left unchallenged. Bar graph depicts the percentage of $CD11c^{+}MHCII^{+}$ cells (mean + SE, n = 5).
(J) Flow cytometric analysis of CD86 and MHCII on PEMs ($CD11b^{hi}CD11c^{-}CD19^{-}$), challenged as in (I). Bar graphs depict MFI (mean + SE, n = 5).
$^{*}p \leq 0.05$, $^{**}p \leq 0.01$, $^{***}p \leq 0.001$, ns $p > 0.05$ (ANOVA and Holm-Bonferroni post-hoc test, A and G–J).
See also Figure S2.

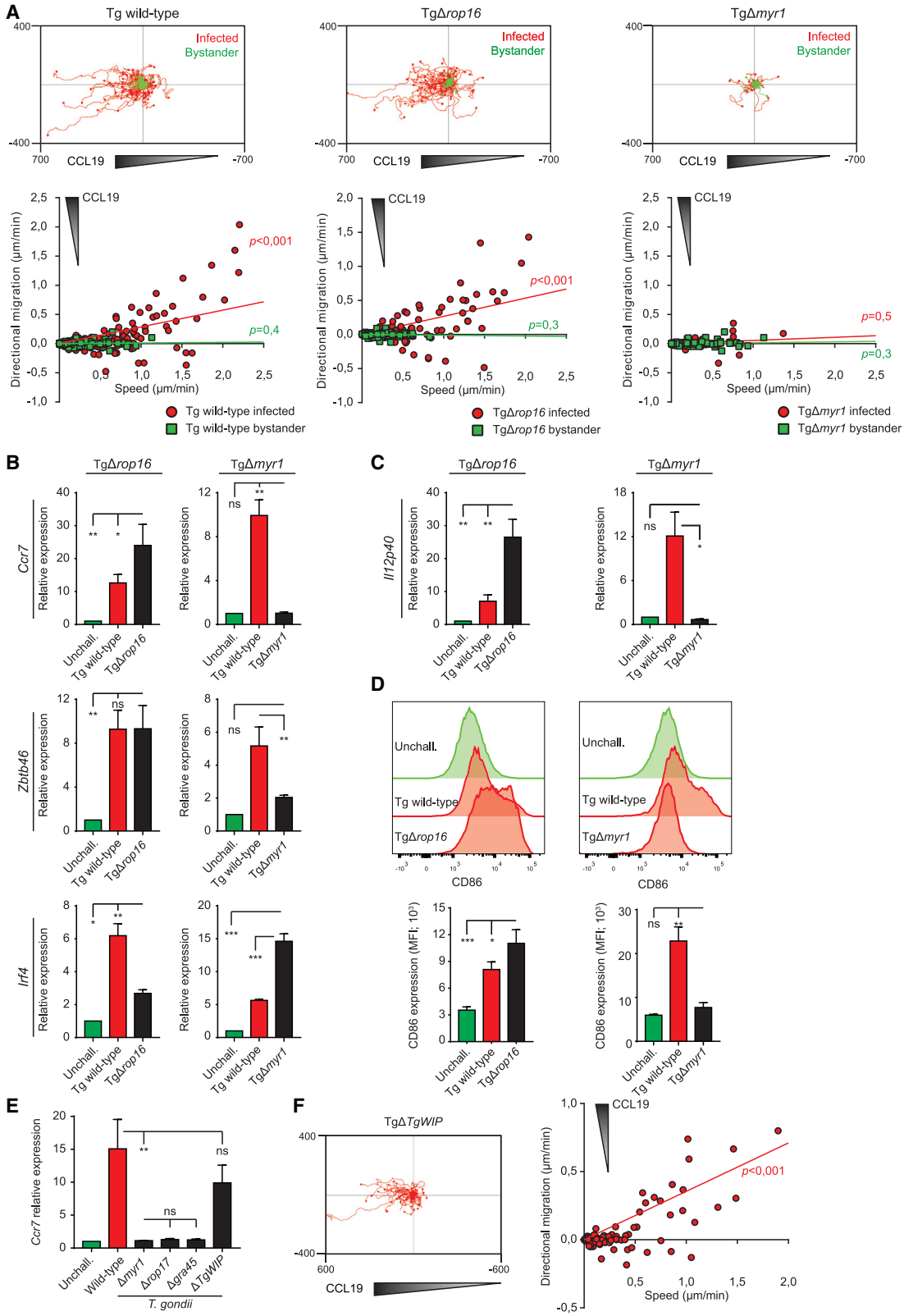

Figure 3. Impact of parasite-derived secreted effectors on macrophage chemotaxis

(A) Motility plots depict displacement of BMDMs challenged with *T. gondii* type I (RH, Tg) wild-type, MYR1-deficient (Δ*myr1*), or ROP16-deficient (Δ*rop16*) tachyzoites for 12 h in a collagen matrix with a CCL19 gradient (scale in μm). Directional migration (μm/min) toward the CCL19 source and speed (μm/min) of

(legend continued on next page)

both parasite-derived ROP16 and MYR1-mediated secretions, which partly have opposite effects. ROP16 inhibited phenotypical maturation of macrophages with the reduction of *Ccr7* expression but with maintained CCL19-dependent chemotaxis. In contrast, the MYR1 secretion system heavily impacted pro-inflammatory cytokine response, elevated *Ccr7* expression, and mediated CCL19-dependent chemotaxis.

The MYR1-associated parasite effector GRA28 mediates CCR7-dependent chemotaxis of macrophages

Given the impact of the MYR1 secretion system on chemotaxis and transcription, we hypothesized that MYR1-secreted effector molecules that target the host cell nucleus mediated the observed phenotypes in macrophages. GRA28, a 200 kDa highly disordered dense granule protein, was initially suspected because the protein is exported to the host cell nuclei in a MYR1- and ASP5-dependent manner (Figures 4A and 4B; Nadipuram et al., 2016) and, like other exported GRAs, contributes to the re-orchestration of host gene expression in macrophages but uniquely triggers CCR7 gene expression (Figures 4C–4E, S4A, and S4B). Comparing the Δ*gra28* mutant to the parental strain, we found that the expression of a relatively small number of host genes was indeed upregulated in a GRA28-dependent manner in human and murine macrophages, including CCL22 (Figures 4E, S4C, and S4D), a previously described GRA28-regulated gene (Rudzki et al., 2021). Reintroduction of one copy of the gene into *gra28*-deficient parasites was sufficient to restore the expression of these genes (Figures 4E and S4B–S4D). Although transcriptomics clearly identified GRA28 as a transcriptional activator in infected cells, it also showed that the protein triggers repression of a substantial fraction of host genes (Figures 4C and 4D). Quantitative reverse transcription PCR of mRNA from four of the repressed genes (i.e., *Cxcl3, Cxcl5, Vcam1*, and *Il1a*) documented a robust and persistent pattern of GRA28-mediated cytokine and *Vcam1* repression (Figure S4E).

Having identified GRA28 as a regulator of CCR7 expression, we investigated its role in the chemotaxis phenotype by comparing it with GRA24, another effector known to regulate the expression of chemokines and their receptors (Braun et al., 2013). Notably, while macrophages challenged with GRA24-deficient *T. gondii* (TgΔ*gra24*) maintained *Ccr7* expression and chemotaxis, challenge with GRA28-deficient tachyzoites (TgΔ*gra28*) dramatically reduced *Ccr7* expression, with abrogated chemotaxis to CCL19 (Figures 4F and 4G). Consistent with these results, ablation of GRA28, but not GRA24, abrogated the induction of *Il12p40* (Figure 4H) and the expression of CD86 (Figure 4I), compared with wild type. In contrast, a downregulation of the M-CSF receptor CD115 (Figure 1H) was maintained for both mutants (Figure S4F). Finally, we confirmed the differential effects of GRA24- and GRA28-deficiency of transcription factors. In particular, the GRA24-dependent early growth response 1 (*Egr1*) upregulation (Braun et al., 2013; ten Hoeve et al., 2019) was maintained upon GRA28-deficiency (Figure 4J). Further, *Zbtb46* expression was reduced by both GRA24- and GRA28-deficiency compared with wild-type parasites, whereas *Irf4* expression was maintained or increased (Figure 4J). Consistently, the induction of *Nr4a3* and *Runx3*, but not *Batf3*, was also partially dependent on GRA28 (Figure S4G). Taken together, these results show that GRA24 and GRA28 differently impact transcription and effector functions of macrophages and that the MYR1-mediated induction of *Ccr7* and chemotaxis in parasitized macrophages is dependent on GRA28 secretion.

GRA28 forms versatile complexes with chromatin modifiers with antagonistic activities

GRA28 is an inherently unstructured protein (Hakimi et al., 2017) and, in this respect, has no discernible protein motifs or defined domains that might indicate specific interaction partners in the host cell nucleus, where it accumulates after infection. To gain functional insight into how GRA28 regulates host gene expression, we searched for host cell partners by applying conventional and affinity chromatography to extracts from murine macrophages infected with tachyzoites expressing a HAFlag-tagged version of GRA28 (Figures 5A and 5B). Silver staining analysis of the eluate showed that GRA28 binds to multiple proteins under very stringent wash conditions (0.5 M NaCl and 0.1% NP-40), forming two distinct complexes with apparent molecular weights of approximately 2 MDa (complex 1, fractions F14–F19) and 500–600 kDa (complex 2, fractions F20–F22) once resolved in size-exclusion chromatography (Figure 5B). These partnerships were subsequently elucidated by proteomics based on mass spectrometry (Table S1), suggesting that GRA28 forms versatile complexes with (1) the multi-subunit NuRD repressor complex, which includes chromatin-remodeling ATPase (CHD4) and deacetylation enzymes (HDAC1,2) (Xue et al., 1998), and (2) the SWI/SNF (BAF) chromatin remodeler, a 2 MDa multi-subunit complex characterized by, among others, its core members SMARCB1, SMARCC1/SMARCC2, and SMARCA4 (also known as BRG1), which use energy from ATP hydrolysis to mobilize nucleosomes (Cairns et al., 1998; Kingston and Narlikar, 1999; Figure 5C). Of note, GRA28 binds to a NuRD complex distinct from that of TgIST in that it does not contain STAT1, nor the transcriptional corepressors CtBP1 and CtBP2 (Figure S5A; Gay et al., 2016).

individual cells are displayed in graphs, with linear regression lines. Infected cells (red) and non-infected bystander cells (green) were analyzed. p values indicate the directional migration compared with hypothetical zero directionality (one-sample permutation test).

(B and C) qPCR analysis of *Ccr7*, *Zbtb46* and *Irf4* (B), and *Il12p40* (C) cDNA in BMDMs challenged for 18 h with freshly egressed *T. gondii* wild-type, Δ*myr1*, or Δ*rop16* tachyzoites, or left unchallenged. Relative expression ($2^{-\Delta\Delta Cq}$) is displayed as mean + SE related to unchallenged (=1).

(D) Flow cytometric analyses of CD86 expression on BMDMs challenged as in (B). For wild-type/Δ*myr1* experiments, cells were gated for GFP^+.

(E) qPCR analysis of *Ccr7* cDNA expression in BMDMs challenged with type I (Tg) wild-type, Δ*myr1*, Δ*rop17*, Δ*gra45*, and Δ*TgWIP* tachyzoites, and displayed as in (B).

(F) Motility plot shows displacement of BMDMs challenged with Δ*TgWIP* tachyzoites in a CCL19 gradient and analysis as in (A).

All datasets are from 3 to 5 independent experiments and displayed as mean + SE. *$p \leq 0.05$, **$p \leq 0.01$, ***$p \leq 0.001$, ns $p > 0.05$ (ANOVA and Dunnett's [B–D] or Holm-Bonferroni [E] post-hoc tests).

See also Figure S3.

CellPress
OPEN ACCESS

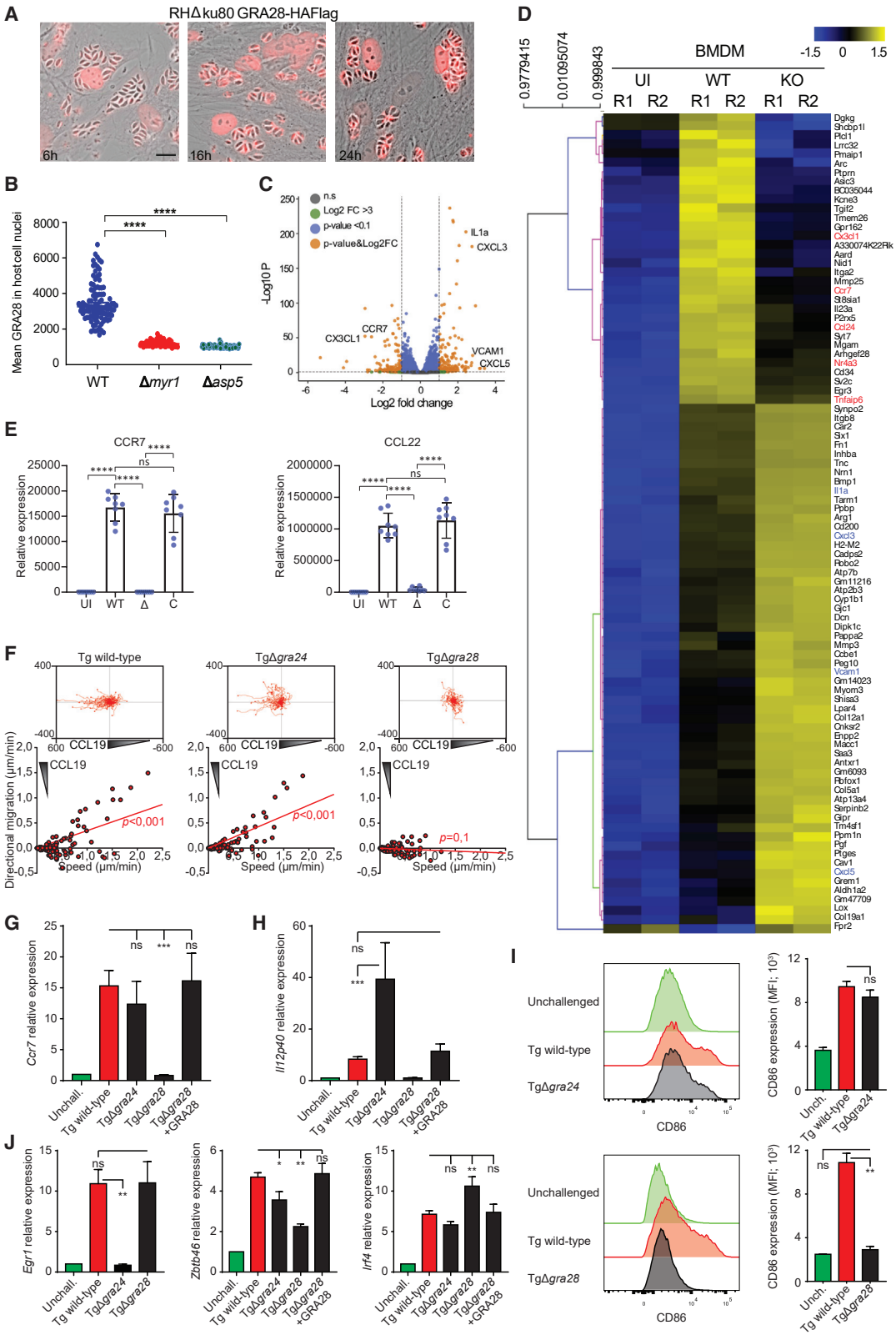

(legend on next page)

These data suggest the intriguing possibility that once GRA28 enters the host cell nucleus, it cooperates with NuRD and SWI/SNF to repress and activate host gene expression, respectively. Accordingly, GRA28 is expected to bind to chromatin. ChIP analyses on samples of human fibroblasts infected with HAFlag knockin tachyzoites showed that GRA28 was highly enriched in a specific manner near 1,976 genes (10-fold enrichment; Figure S5B; Table S2) compared with control GRAx, which also accumulated in host nuclei after infection but was rarely bound to chromatin (137 genes, 10-fold enrichment) (Figure S5B; Table S2). GRA28 is bound to upstream and intergenic regions, and at the promoter level, the protein is enriched upstream and downstream of the transcription start site (TSS) (Figures 5D, 5E, and S5C). Introns were also highly represented (33%) among GRA28-enriched regions, as reported for BRG1 in human cells (Attanasio et al., 2014). Of note, GRA28 was clearly enriched at the *CCR7* locus (Figure 5F), and its induction may be mediated by the recruitment of SWI/SNF (BAF) by GRA28, a chromatin remodeler known to activate transcription by promoting nucleosome repositioning. Chromatin occupancy of GRA28 downstream and upstream of *CCR7*, sometimes far from TSS, suggests that GRA28 cooperates with chromatin remodelers to increase DNA accessibility by creating an open chromatin conformation over long distances that favors transcription factor binding to site-specific sequences and RNA polymerase progression (Figure 5F).

Role of macrophage migratory activation on the dissemination of *T. gondii in vivo* in mice

To address the impact of *T. gondii*-induced migratory activation of BMDMs on dissemination *in vivo*, we designed separate approaches in mice. For the different conditions, equivalent numbers of pre-treated and pre-labeled cells were simultaneously adoptively transferred intraperitoneally (i.p.) to mice in competition assays. 14–18 h post-inoculation, organs were harvested and cells were characterized by flow cytometry (Figures 6A and S6A–S6D). First, unchallenged and *T. gondii*-challenged BMDMs were assessed for migration. Interestingly, challenged BMDMs ($CMTMR^+GFP^{+/-}$) migrated to the omentum, mesenteric lymph nodes (MLNs), and spleen at a higher rate than unchallenged BMDM (Deed Red^+), and this difference was further accentuated in infected ($CMTMR^+GFP^+$) cells (Figure 6B). Next, when BMDMs challenged with wild-type or MYR1-deficient (TgΔ*myr1*) *T. gondii* were allowed to compete, relatively lower numbers of Δ*myr1*-infected BMDMs were retrieved in organs (Figure 6C). Similarly, BMDMs challenged with GRA28-deficient *T. gondii* (TgΔ*gra28*) migrated at a relative lower frequency compared with BMDMs challenged with wild-type *T. gondii* (Figure 6D), with a relative re-elevation of migration in BMDMs challenged with reconstituted parasites (TgΔ*gra28* + GRA28) (Figure 6E). Jointly, this indicated an implication of MYR1-associated GRA28 secretion in the migration of parasitized BMDMs.

These results, together with a previously observed enhanced migration of parasitized BMDCs (Bhandage et al., 2020; Lambert et al., 2006), motivated a comparison of the migratory behaviors of parasitized BMDCs and parasitized BMDMs. Both cell populations exhibited a comparable high migration rate, with BMDMs relatively enriched in spleen and omentum (Figure 6G), indicative of a migration capability by parasitized BMDMs. Finally, we found that the migration frequencies of CCR7-deficient BMDMs were reduced related to wild-type BMDMs (Figure 6G), confirming a relative dependency of parasitized BMDMs on CCR7 for migration. As in *in vitro* assays (Figure 3D), wild-type infected adoptively transferred BMDMs collected from spleen expressed significantly higher levels of CD86 (Figure 6H), and chemotaxis phenotypes were confirmed *in vitro* for all conditions (Figures S6E and S6F). Altogether, the data show that *T. gondii*-infected BMDMs can traffic to secondary lymphoid organs, with an impact of the MYR1 pathway, secreted effector GRA28, and

Figure 4. GRA28 is secreted in host cell nuclei in a Myr1 and Asp5-dependent manner to activate and repress gene expression in macrophages, with an impact on *Ccr7* expression and chemotaxis

(A) Time course of GRA28 secretion and export to the host cell nucleus. HFFs were challenged with RHΔku80 GRA28-HA-FLAG tachyzoites, stained with anti-HA antibodies (red) and visualized by epifluorescence and transmitted light microscopy at indicated time points (6, 12, 24 h). Scale bars, 10 μm.

(B) RHΔ*ku80* WT, Δ*asp5* and Δ*myr1* parasites were transiently transfected with pTUB8-GRA28-HAFlag. The amount of GRA28 in the nucleus was quantified in at least 100 host cells for each parasite strain.

(C) Genome-wide expression profiling of BALB/c BMDMs left uninfected or infected with WT and Δ*gra28* type II (Pru) tachyzoites. The results of tests for differential expression between WT and Δ*gra28* tachyzoites are presented in a volcano plot that plots the statistical significance against the fold change for each gene. The orange dots indicate transcripts that were significantly upregulated and downregulated, using adjusted $p < 0.1$ (Bonferroni-corrected) and ±3-fold change as the cutoff corresponding to each comparison. x axis showing $\log_2$ fold change, y axis showing $-\log_{10}$(p value). Vertical dashed lines indicate 3-fold upregulation and downregulation.

(D) Heatmap representation of the differentially expressed mouse genes (>3-fold, RPKM > 5 in at least one sample) between parental and Δ*gra28*-infected cells. RPKM values were $\log_2$ transformed, gene/row normalized, and mean centered using MeV.

(E) RAW macrophages were infected for 24 h with WT, Δ*gra28* (Δ), or TgΔ*gra28*+GRA28 (C), the complemented line of type I (RH) tachyzoites, or left unchallenged (UI). Gene of interest (GOI) and TBP mRNA levels were determined by RT-qPCR and GOI values were normalized to TBP. $^{**}p \leq 0.01$, $^{***}p \leq 0.001$, $^{****}p \leq 0.0001$, ns $p > 0.05$ (one-way ANOVA and Tukey's multiple comparison test). Data are the mean ± SD ($n \geq 3$).

(F) Motility plots and analyses of BMDMs challenged with type I (RH) wild-type, Δ*gra24*, or Δ*gra28 T. gondii* tachyzoites (Tg) for 12h and allowed to migrate in a CCL19 gradient. p values indicate the directional migration compared with hypothetical zero directionality (one-sample permutation test).

(G and H) qPCR analysis of *Ccr7* (G) and *IL12p40* (H) cDNA expression in BMDMs challenged with type I wild-type, Δ*gra24*, Δ*gra28*, or Δ*gra28*+GRA28 tachyzoites (Tg) for 18 h (RH) or left unchallenged. Relative expression ($2^{-\Delta\Delta Cq}$) is displayed as mean + SE related to unchallenged (=1; $n \geq 4$).

(I) Flow cytometric analyses of anti-CD86 staining on BMDMs challenged as in (B).

(J) qPCR analysis of *Egr1*, *Zbtb46*, and *Irf4* in BMDMs challenged with type I wild-type (Tg), Δ*gra24* or Δ*gra28*, or Δ*gra28*+GRA28 tachyzoites, or left unchallenged as in (G). Relative expression ($2^{-\Delta\Delta Cq}$) related to unchallenged (=1; $n \geq 3$).

Datasets are from at least 3 independent experiments and displayed as mean + SE. $^{*}p \leq 0.05$, $^{**}p \leq 0.01$, $^{***}p \leq 0.001$, ns $p > 0.05$ (ANOVA and Dunnett's [G, H, J] or Holm-Bonferroni [I] post-hoc test).

See also Figure S4.

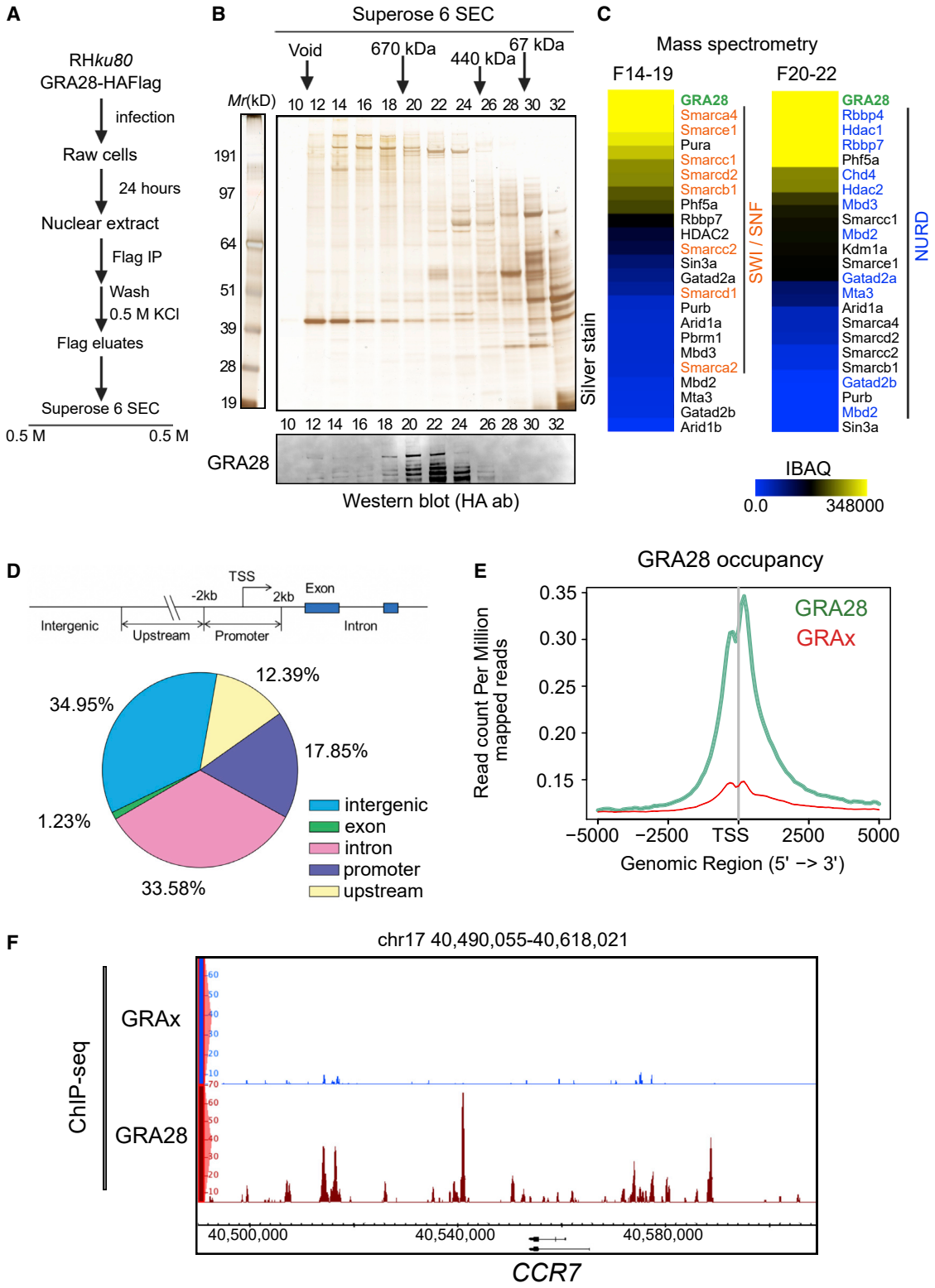

Figure 5. GRA28 binds to chromatin and partners with chromatin remodelers NuRD and SWI/SNF

(A and B) GRA28-associated proteins were purified by FLAG chromatography from protein extracts of the murine RAW macrophage line infected with RHΔ*ku80* GRA28-HA-FLAG. Fractions from size-exclusion chromatography of GRA28-containing complexes after Flag-affinity selection were analyzed on gels by silver staining and then by mass spectrometry-base proteomics to detect GRA28 and the aforementioned partners.

(C) Heatmap showing the abundance ranks of each protein in each purified fraction derived from extracted iBAQ values. The identity of the proteins is indicated.

(legend continued on next page)

homing receptor CCR7. We conclude that parasitized BMDMs exhibit enhanced systemic migration and can potentiate dissemination of intracellularly located *T. gondii*.

Impact of *T. gondii* effectors on transcriptional activation and chemotaxis of human monocytes and macrophages

Because hypermigratory responses upon *T. gondii* challenge were also observed in infected human mononuclear phagocytes (Bhandage et al., 2020), we sought to confirm our key findings in human peripheral blood monocytes and monocyte-derived macrophages. Interestingly, parasitized human macrophages chemotaxed in a CCL19 gradient, unlike bystander macrophages (Figure 7A). Extending data in murine macrophages, TgΔ*myr1* parasites, and LPS treatments failed to significantly induce chemotaxis (Figure 7A). Consistent with these findings, challenge with *T. gondii* wild-type induced *CCR7* expression in both monocytes and macrophages, in contrast with TgΔ*myr1* (Figure 7B). Despite undetectable chemotactic responses under these conditions, LPS challenge induced *CCR7* expression (Figures 7A, 7C, and 7D). As in murine macrophages, we found that *IRF4* and *BATF3* were upregulated by *T. gondii* challenge in monocytes and macrophages, but not by tachyzoite lysates or LPS (Figures S7A–S7C). Furthermore, the induction of *IRF4* expression in human monocytes and macrophages was dependent on MYR1 (Figure S7D), while the induction of *BATF3* expression in human cells was in line with findings in murine macrophages (Figure S7E), and *ZBTB46* was not significantly affected (Figure S7F). Altogether, these data corroborate and extend our findings on the MYR1-dependent induction of chemotactic migratory activation to human monocytes and macrophages.

DISCUSSION

In peripheral tissues, the encounter of *T. gondii* with mononuclear phagocytes can result in neutralization of the parasite or in infection of the host cell. Here, we addressed the impact of infection on the migratory responses of macrophages. The data demonstrate that infection with *T. gondii* allows normally sessile macrophages to acquire migratory features typically attributed to DCs. First, infection led to transcriptional signatures consistent with the acquisition of DC-like migratory properties. Second, we identified the parasite effector GRA28 as the mediator of upregulated CCR7 expression and chemotaxis in parasitized macrophages. Third, the migratory responses of macrophages impacted parasite dissemination in mice.

We report that challenge of separate types of murine and human macrophages with *T. gondii* induces the expression of transcription factors typically associated with cDCs. Importantly, *T. gondii* infection, but not challenge with parasite lysates or LPS, induced expression of IRF4, ZBTB46, *Batf3*, and *Nr4a3*. These responses coincided with CCR7-mediated chemotaxis by infected macrophages. Notably, most responses impacted infected cells but not non-infected bystander cells, indicating direct effects of parasitization. In DCs, BATF3 is essentially associated with the development of cDC1 (Grajales-Reyes et al., 2015), while IRF4 and NR4A3 are required for mo-DC differentiation and CCR7-mediated migration (Bajaña et al., 2012; Boulet et al., 2019; Briseño et al., 2016). Moreover, ectopic expression of ZBTB46 rescues cDC differentiation from IRF8-deficient bone marrow cells (Satpathy et al., 2012). However, despite the transcription factors induced being strongly associated with DCs, we found no evidence indicating differentiation of macrophages to DCs. Thus, rather than a global transcriptional reprogramming, intracellular *T. gondii* selectively targeted transcription, with alterations in the migratory responses, activation, and cytokine responses of macrophages. Moreover, the phenotypical effects of *T. gondii* infection were not limited to specific types of mouse macrophages, with generally a similar activation in human monocytes and monocyte-derived macrophages. Yet, in diverse cell types, host-cell-type-specific effects are to be expected (Swierzy et al., 2017).

We identify the secreted dense granule protein GRA28 as a mediator of CCR7 upregulation and chemotaxis of *T. gondii*-infected macrophages. GRA28 is exported to the host cell nucleus in a MYR1- and ASP5-dependent manner (Nadipuram et al., 2016; Figure 4B) and was recently linked to the transcriptional regulation of the placenta-associated chemokine CCL22 (Rudzki et al., 2021). GRA28 is a 200-kDa intrinsically disordered protein (IDR) expected to be structurally flexible and able to adopt multiple conformations to interact with SWI/SNF and NuRD, probably via independent short linear motifs (SLiMs), usually 3 to 11 residues, which remain to be defined. We can predict a prion-like structure (Zhang et al., 2015) in a central region of GRA28 that is known to phase-separate to form weaker multivalent interactions. In this regard, GRA28 can function as scaffold proteins to recruit chromatin remodelers and form membraneless condensates capable of dynamically exchanging components with opposing functions, i.e., SWI/SNF and NuRD, thereby selectively accelerating or inhibiting host gene expression.

GRA28 has features in common with the dense granule protein TgIST that it binds to the NuRD repressor complex, but the nucleosome deacetylation and ATP-dependent chromatin-remodeling functions of NuRD can be hijacked by both in different ways. TgIST may co-opt NuRD-associated HDACs that compete with HATs (e.g., p300/CBP) to prevent STAT1 acetylation and DNA dissociation, thereby impairing STAT1 recycling and IFN-γ responsiveness (Gay et al., 2016; Olias and Sibley, 2016). TgIST was also shown to prolong STAT1 occupancy on chromatin and allosterically impairs its ability to recruit the acetyltransferase p300/CBP (Huang et al., 2022). GRA28, which binds to chromatin over long distances, may use the ATP-dependent chromatin-remodeling enzymes CHD3 and CHD4 of NuRD to generate a nonpermissive chromatin state by altering the positioning of nucleosomes, but this remains to be shown. In this

(D) The pie chart shows the distribution of GRA28 peaks in the genome of human fibroblasts relative to gene features.
(E) The average distribution of GRA28 and the control GRAx in gene promoters. Average-signal profiles of each protein were plotted over a region from −5 kb to +5 kb relative to the TSS of each gene. Average tag count of the enrichment is shown on the y axis.
(F) IGB images of the gene *CCR7* and ChIP-seq signal peaks for GRA28 and GRAx.
See also Figure S5.

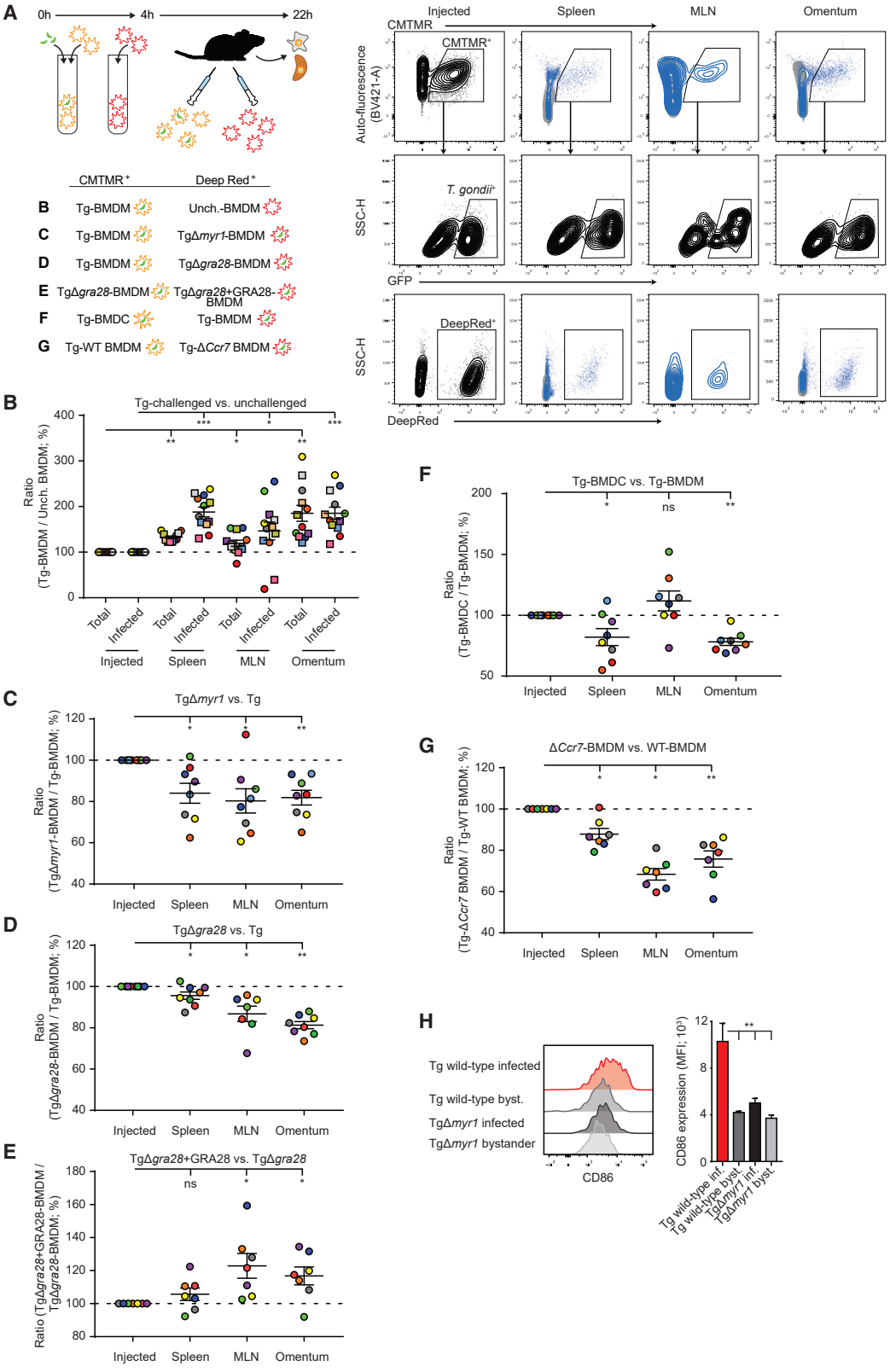

(legend on next page)

regard, the diversification of effectors in *T. gondii*, as exemplified by the interaction of TgIST and GRA28 with the NuRD complex, is likely an evolutionary strategy of the parasite to adapt to multiple hosts and their different cell and organ types. Similarly, TgIST and TgNSM were shown to cooperate and to signal through chromatin by binding to their respective corepressors, NuRD and NCoR/SMRT (Gay et al., 2016; Olias and Sibley, 2016; Rosenberg and Sibley, 2021).

In sharp contrast to the effects of Δ*myr1* and Δ*gra28* mutants, challenge with a Δ*rop16* mutant parasite conversely elevated *Ccr7* expression, with maintained chemotaxis. Because the secreted rhoptry protein ROP16 is a known down-modulator of inflammatory cytokine responses by acting on STAT3/6 (Jensen et al., 2011; Saeij et al., 2007; Yamamoto et al., 2009), our findings phenotypically corroborate the recently described counteracting transcriptional effects of MYR1-dependent and MYR1-independent effectors (Naor et al., 2018; Rastogi et al., 2020). However, the data indicate that *Irf4*/IRF4 and *Batf3* induction are MYR1/GRA28-independent, while MYR1/GRA28-deficient parasites failed to upregulate *Ccr7* expression. This suggests that BATF3 and IRF4 may act in concert to remodel the chromatin in *T. gondii*-infected macrophages, jointly with MYR1-related factors such as GRAs and *Egr1* (Braun et al., 2013; ten Hoeve et al., 2019) that ultimately enable transcription at the *Ccr7* locus. However, the precise contributions of IRF4 and BATF3 to the migratory phenotype remain to be addressed in future studies under IRF4- and BATF3-deficient conditions. Consistent with the above considerations, the IL-12 pro-inflammatory response and the expression of the costimulatory molecule CD86 generally coincided with CCR7 upregulation and downregulation. Jointly, the data demonstrate that *T. gondii* orchestrates the modulation of macrophage migration with both a pro-migratory, pro-inflammatory effector axis (MYR1-dependent GRA secretion) and an alternative activation-mediating effector axis (ROP16) that downmodulates IL-12 responses. This establishes the CCR7-dependent pro-migratory axis as distinct from the M2-like signature driven by ROP16 (Jensen et al., 2011; Patil et al., 2014). Despite CCR7 responses being observed for all strains tested, the existing polymorphisms of effectors between strains are likely of relevance because of their link to virulence in type I/II strains and to dissemination (Barragan and Sibley, 2002; Hitziger et al., 2005; Sibley and Boothroyd, 1992). For example, type I ROP16 activates STAT3 more potently than type II ROP16, which may partly explain these differences (Yamamoto et al., 2009). Consequently, the pro-chemotactic effect of GRA28 is likely partly counteracted by ROP16 in a genotype-related fashion. Also, although GRA28 predominantly mediated CCR7 responses, it is likely that additional GRA proteins contribute to the equilibrium of other responses (Mercer et al., 2020; Mukhopadhyay et al., 2020). For example, the M1-associated effector GRA15 in type II strains (Jensen et al., 2011) modulates leukocyte adhesion in relation to hypermigration (Ross et al., 2021, 2022). Additionally, systemic responses mediated by PAMPs/PRRs are central for immunity in toxoplasmosis (Frickel and Hunter, 2021; Scanga et al., 2002) and MyD88-independent responses in infected cells also mediate protective immunity (Mercer et al., 2020; Mukhopadhyay et al., 2020). Here, GRA24 (type I) suppressed *Il12p40* expression, consistent with a previously reported IL-12-inhibiting role of p38 MAP kinase (Katholnig et al., 2013). This finding is, however, in contrast to previous findings on GRA24 in type II *T. gondii* (Braun et al., 2013; ten Hoeve et al., 2019). Similarly, GRA6-dependent NFAT4 activation impacts immune responses in a strain-dependent manner (Ma et al., 2014). Altogether, this highlights the complex host-pathogen interplay mediated by polymorphic ROPs and GRAs in different parasite strains and host cells, leading to differences in CCR7 and IL-12 regulation.

We report a central role for the MYR1 secretory pathway in the chemotactic and pro-inflammatory responses of macrophages. This was further corroborated with mutants of GRA45 and ROP17, which are constituents of the MYR1 secretory pathway (Cygan et al., 2020). Interestingly, ROP17 has also been

Figure 6. *In vivo* migration of *T. gondii*-challenged adoptively transferred BMDMs

(A) Illustration of experimental setup and conditions for co-adoptive transfers of *T. gondii* (RH)-challenged or unchallenged (unch.) BMDMs or BMDCs pre-labeled with CellTracker Deep Red or CMTMR dyes.

(B–G) Indicate, respectively, conditions and experimental setups for corresponding graphs below. Plots show flow cytometric detection of pre-labeled ($CMTMR^+$/Deep red^+) and parasitized cells (GFP^+) extracted from organs 18 h post-inoculation, as detailed under STAR Methods. Events from organs are displayed in blue or black (inoculated) and in gray (non-inoculated).

(B) Flow cytometric analysis of *T. gondii*-challenged (Tg) and unchallenged (unch.) BMDMs in the spleen, MLNs, and omentum 18 h post-inoculation. Data are presented as the change in ratio between detected challenged $CMTMR^+$ cells and unchallenged Deep red^+ cells (total) or specified by infection (GFP^+/GFP^-) related to the inoculated ratio (normalized to 100%). Mean ratio change ±SE and individual mice (n = 12) are displayed.

(C) Flow cytometric analysis of BMDMs treated as indicated in (A) in the spleen, MLNs, and omentum. The change in ratio between Deep red^+GFP^+ cells (TgΔ*myr1*-infected) and $CMTMR^+GFP^+$ cells (Tg-infected) related to inoculated (=100%) is shown.

(D) Flow cytometric analysis of BMDMs treated as indicated in (A). The change in ratio between Deep red^+CFSE^+ TgΔ*gra28*-infected cells and $CMTMR^+CFSE^+$ Tg-infected cells related to inoculated (=100%) is shown.

(E) Flow cytometric analysis of BMDMs treated as indicated in (A). The change in ratio between Deep red^+CFSE^+ TgΔ*gra28*+GRA28-infected cells and $CMTMR^+CFSE^+$ TgΔ*gra28*-infected cells related to inoculated (=100%) is shown.

(F) Flow cytometric analysis of *T. gondii*-challenged (Tg) BMDM and BMDC in the spleen, MLNs, and omentum 18 h post-inoculation. Data are presented as the change in ratio between infected $CMTMR^+GFP^+$ BMDCs and Deep red^+GFP^+ BMDMs related to inoculated (=100%) is shown.

(G) Flow cytometric analysis of *T. gondii*-challenged (Tg) wild-type (WT) or CCR7-deficient (Δ*Ccr7*) BMDM in the spleen, MLNs, and omentum 18 h post-inoculation. Data are presented as the change in ratio between infected $CMTMR^+GFP^+$ BMDCs and Deep red^+GFP^+ BMDMs related to inoculated (=100%) is shown.

(H) Flow cytometric analysis of anti-CD86 staining in BMDMs challenged as in (D) recovered from the spleen. Bar graph depicts MFI (mean + SE) from 3 mice. Scatter plots display individual mice with symbols (n = 7–12) and mean ± SE (B–G). $^*p \leq 0.05$, $^{**}p \leq 0.01$, $^{***}p \leq 0.001$, ns $p > 0.05$ (one-sample permutation [B–G] or ANOVA and Dunnett's [H] post-hoc tests [H]).

See also Figure S6.

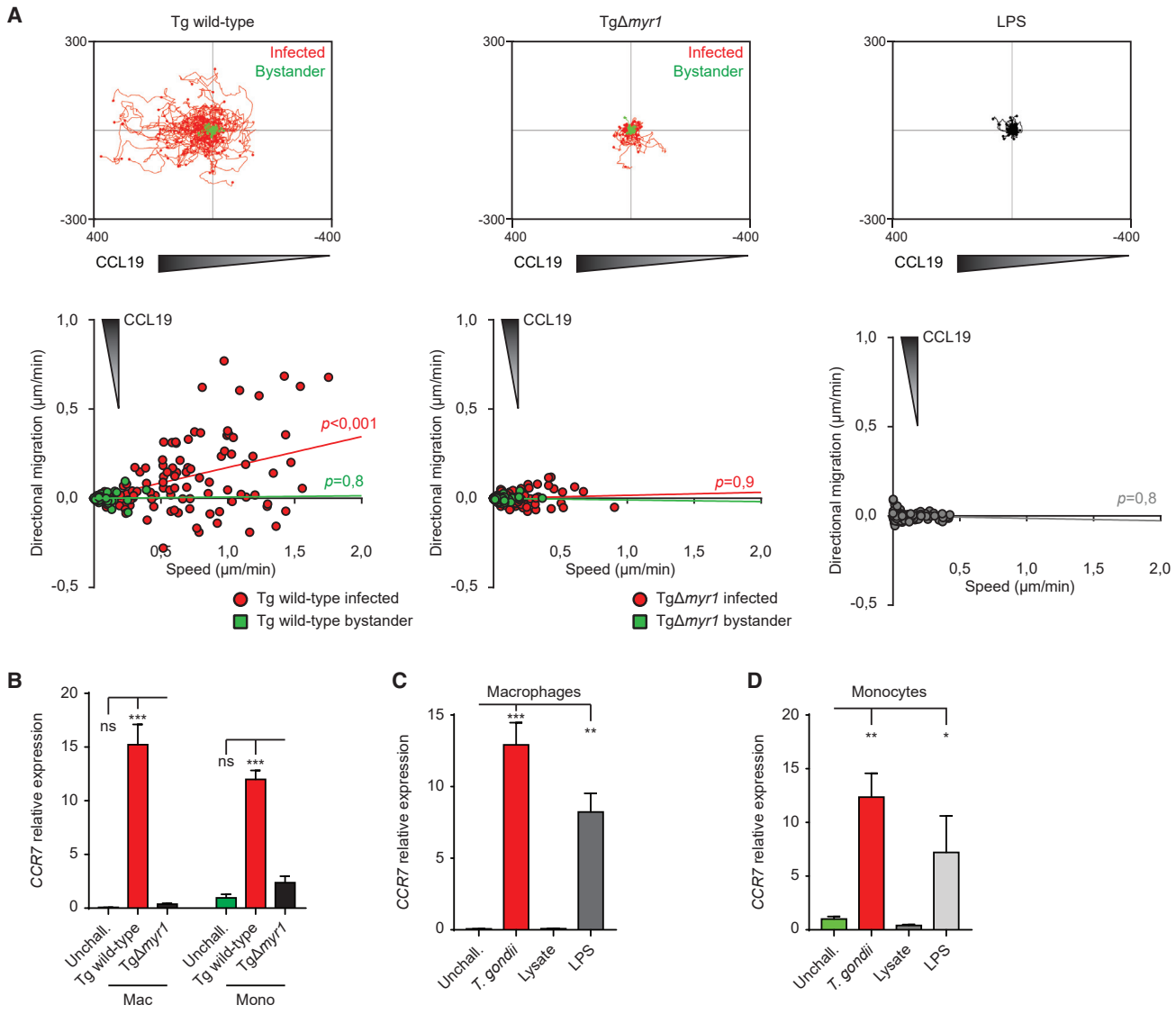

Figure 7. Expression of DC-associated transcription factors and chemotaxis in *T. gondii*-challenged human monocytic cells

(A) Motility plots and analyses (n = 3) of human monocyte-derived macrophages challenged with *T. gondii* type I (RH, Tg) wild type, TgΔ*myr1* or LPS for 12 h in a CCL19 gradient as indicated under methods details.

(B) qPCR analysis of *CCR7* cDNA from human macrophages and monocytes challenged for 18 h as in (A). Relative expression ($2^{-\Delta Cq}$) is shown (mean + SE, n = 4).

(C and D) qPCR analysis of *CCR7* cDNA from human macrophages (C) and human monocytes (D) challenged for 18 h with *T. gondii* type I tachyzoites (Tg), tachyzoite lysate, LPS. For reference cells were or left unchallenged (unchall.). Relative expression ($2^{-\Delta Cq}$) is shown (mean + SE, n = 4–5).

*p ≤ 0.05, **p ≤ 0.01, ***p ≤ 0.001, ns p > 0.05 (B–D; ANOVA, Dunnett's post-hoc test).

See also Figure S7.

implicated in hypermigration of monocytic cells (Drewry et al., 2019), indicating dual or alternative modes of action by ROP17 on hypermigration. In contrast, chemotaxis and the IL-12 response were not abrogated upon deletion of the rhoptry protein TgWIP, implicated in the migratory activation of DCs (Sangaré et al., 2019). However, the velocity of chemotaxing cells was diminished, indicating overlapping effects on cell locomotion. Indeed, hypermigration and chemotaxis jointly promote the migration of infected phagocytes *in vitro* (Fuks et al., 2012; Weidner et al., 2013) and, while the two migratory phenotypes are activated by separate signaling pathways, they commonly share a dependence on calcium signaling and MAP kinase signaling (Bhandage et al., 2020; Ólafsson et al., 2020). Thus, based on the data at hand, rather than being antithetical, we postulate that both signaling cues cooperatively potentiate the migration of infected phagocytes and parasite dissemination. It is also noteworthy that, under the conditions applied, LPS treatment did not induce chemotaxis in human or mouse macrophages. This is in contrast to LPS responses by DCs (Fuks et al., 2012; Weidner et al., 2013) and indicative of the strong activation and rapid onset of chemotaxis upon *T. gondii* infection of macrophages.

Hypermigratory responses by myeloid mononuclear phagocytes (DCs, monocytes, macrophages, microglia) upon challenge with *T. gondii* appear to be a conserved feature across host species (human, mouse, bovine) and are also induced by the related coccidian *Neospora caninum* (Bhandage et al., 2020; Collantes-Fernandez et al., 2012; García-Sánchez et al., 2019; Lambert et al., 2009). Yet, measurable differences exist between parasite strains/lineages in the magnitude of induction of the hypermigratory phenotype *in vitro* (Weidner and Barragan, 2014) and *in vivo* in mice (Lambert et al., 2009). Here, using an *in vivo* adoptive transfer setup (Fuks et al., 2012; Kanatani et al., 2017), we report that parasitized macrophages can potentiate the dissemination of *T. gondii* in a MYR1- and GRA28-dependent fashion. Consistent with these data, we previously showed that MYR1-deficient parasites had no defect in peritoneal survival but a defect in organ colonization (Sangaré et al., 2019). Interestingly, adoptive transfer of CCR7-deficient infected macrophages significantly reduced, but did not abolish, migration to omentum, MLNs, and spleen, indicating a partial dependency on CCR7-mediated chemotaxis for systemic migration. Consistent with this, *in vitro*, CCR7-deficiency abolished chemotaxis of infected macrophages toward CCL19 while hypermotility was maintained. Thus, synergistically with the onset of GABA-mediated hypermigration (Bhandage et al., 2020; Lambert et al., 2006, 2011), the acquired sensitivity of parasitized macrophages and other monocytic cells to CCL19/CCL21 gradients could carry replicating tachyzoites to lymph nodes and beyond, thereby potentiating systemic dissemination. Importantly, the MYR1-dependent CCR7 responses were corroborated in human macrophages and monocytes, advocating for conserved signaling across species. Yet, differences in the transcriptional regulation were also noted, indicating that, despite the conserved migratory plasticity of macrophages, regulatory response differences exist between human and murine cells. Altogether, the data highlight the implication of host-cell-related and parasite-genotype-related components in "Trojan horse"-mediated dissemination, which requires further investigation.

It is becoming increasingly clear that bacterial, viral, and fungal microorganisms use elaborate strategies to thrive inside macrophages and other phagocytes (Mercer and Greber, 2013; Sansonetti and Di Santo, 2007; Tan and Russell, 2015). To do this, pathogens need to sense, respond to, and induce alterations in host cells that benefit their survival. Recent findings show that *Mycobacterium tuberculosis* manipulates alveolar macrophage trafficking for rapid localization to the lung interstitium (Lovey et al., 2022). Similarly, *Leishmania* parasites impact transcription and epigenetic regulation in the host macrophage, thereby modulating immune responses (Lecoeur et al., 2022), including the inhibition of macrophage motility (de Menezes et al., 2017). Following oral infection, *T. gondii* encounters sessile macrophages in the intestine and other peripheral tissues. Dissemination of *T. gondii* from the intestine is rapid, asymptomatic, and without generalized inflammation (Gregg et al., 2013). Our study provides a framework for how *T. gondii* manipulates the migration of mononuclear phagocytes to disseminate. The findings reveal a remarkable migratory plasticity (Friedl and Weigelin, 2008) in normally sessile macrophages, which can acquire migratory properties typically attributed to the more migratory DCs upon infectious challenge with *T. gondii*. The data also highlight a transcriptional plasticity linked to the migratory responses of differentiated monocytic cells, which obligate intracellular parasites may utilize to their advantage. Because macrophages and monocytes outnumber DCs in tissues, a migratory activation of these cells may favor the dissemination of *T. gondii*. The findings unveil putative alternative pathways by which mononuclear phagocytes can be made migratory or activated, which could—by extension—be exploited, for example, in cell therapies.

STAR★METHODS

Detailed methods are provided in the online version of this paper and include the following:

- KEY RESOURCES TABLE
- RESOURCE AVAILABILITY
  - Lead contact
  - Materials availability
  - Data and code availability
- EXPERIMENTAL MODEL AND SUBJECT DETAILS
  - Mice
  - Primary human cells
  - Cell lines
  - T. gondii strains
- METHOD DETAILS
  - Mouse cell culture
  - Human cell culture
  - Infection challenges
  - Plasmid construction
  - *T. gondii* transfection
  - Inhibitors
  - Mixed leukocyte reaction (MLR)
  - Quantitative polymerase chain reaction (qPCR)
  - Flow cytometry
  - Western blot
  - Chemotaxis
  - Immunofluorescence microscopy
  - Adoptive transfers
  - Handling of publicly available datasets
  - RNA-seq
  - ChIP-seq assay
  - Chromatographic purification of GRA28-containing complexes
  - Mass spectrometry-based proteomics
- QUANTIFICATION AND STATISTICAL ANALYSIS
  - Statistical analyses

SUPPLEMENTAL INFORMATION

Supplemental information can be found online at https://doi.org/10.1016/j.chom.2022.10.001.

ACKNOWLEDGMENTS

We are grateful to Dr. Reinhold Förster, Hannover University, Germany, for valuable reagents. This work was funded by the Swedish Research Council (Vetenskapsrådet, 2018-02411 to A. Barragan) and the Olle Engkvist Byggmästare Foundation (193-609 to A. Barragan). The proteomic experiments

were partially supported by Agence Nationale de la Recherche under projects ProFI (Proteomics French Infrastructure, ANR-10-INBS-08) and GRAL, a program from the Chemistry Biology Health (CBH) Graduate School of University Grenoble Alpes (ANR-17-EURE-0003). M.-A.H., A. Bougdour, and L.B. were supported by the Laboratoire d'Excellence (LabEx) ParaFrap (ANR-11-LABX-0024), the Agence Nationale pour la Recherche (Project HostQuest, ANR-18-CE15-0023), and Fondation pour la Recherche Médicale (FRM Equipe # EQU202103012571). J.P.J.S. was funded by NIH R21AI151084.

AUTHOR CONTRIBUTIONS

Experimentation, A.L.t.H., L. Braun, M.E.R., G.C.O., A. Bougdour, and L. Belmudes; methodology, A.L.t.H., L. Braun, M.E.R., G.C.O., Y.C., L. Belmudes, and J.P.J.S.; data analysis and curation, A.L.t.H., A. Barragan, L. Braun, A. Bougdour, Y.C., and M.-A.H.; writing, review, and editing, A.L.t.H., A. Barragan, L. Braun, M.-A.H., and J.P.J.S.; funding acquisition and supervision, A. Barragan and M.-A.H.

DECLARATION OF INTERESTS

The authors declare no competing interests.

Received: March 21, 2022
Revised: August 26, 2022
Accepted: October 3, 2022
Published: October 28, 2022

REFERENCES

Alvarez, D., Vollmann, E.H., and von Andrian, U.H. (2008). Mechanisms and consequences of dendritic cell migration. Immunity *29*, 325–342. https://doi.org/10.1016/j.immuni.2008.08.006.

Amon, L., Lehmann, C.H.K., Baranska, A., Schoen, J., Heger, L., and Dudziak, D. (2019). Transcriptional control of dendritic cell development and functions. Int. Rev. Cell Mol. Biol. *349*, 55–151. https://doi.org/10.1016/bs.ircmb.2019.10.001.

Attanasio, C., Nord, A.S., Zhu, Y., Blow, M.J., Biddie, S.C., Mendenhall, E.M., Dixon, J., Wright, C., Hosseini, R., Akiyama, J.A., et al. (2014). Tissue-specific SMARCA4 binding at active and repressed regulatory elements during embryogenesis. Genome Res. *24*, 920–929. https://doi.org/10.1101/gr.168930.113.

Aziz, A., Soucie, E., Sarrazin, S., and Sieweke, M.H. (2009). MafB/c-Maf deficiency enables self-renewal of differentiated functional macrophages. Science *326*, 867–871. https://doi.org/10.1126/science.1176056.

Bajaña, S., Roach, K., Turner, S., Paul, J., and Kovats, S. (2012). IRF4 promotes cutaneous dendritic cell migration to lymph nodes during homeostasis and inflammation. J. Immunol. *189*, 3368–3377. https://doi.org/10.4049/jimmunol.1102613.

Barragan, A., and Sibley, L.D. (2002). Transepithelial migration of Toxoplasma gondii is linked to parasite motility and virulence. J. Exp. Med. *195*, 1625–1633.

Barragan, A., and Sibley, L.D. (2003). Migration of Toxoplasma gondii across biological barriers. Trends Microbiol. *11*, 426–430.

Bhandage, A.K., Olivera, G.C., Kanatani, S., Thompson, E., Loré, K., Varas-Godoy, M., and Barragan, A. (2020). A motogenic GABAergic system of mononuclear phagocytes facilitates dissemination of coccidian parasites. eLife *9*, e60528. https://doi.org/10.7554/eLife.60528.

Boulet, S., Daudelin, J.F., Odagiu, L., Pelletier, A.N., Yun, T.J., Lesage, S., Cheong, C., and Labrecque, N. (2019). The orphan nuclear receptor NR4A3 controls the differentiation of monocyte-derived dendritic cells following microbial stimulation. Proc. Natl. Acad. Sci. USA *116*, 15150–15159. https://doi.org/10.1073/pnas.1821296116.

Boyle, J.P., Saeij, J.P., and Boothroyd, J.C. (2007). Toxoplasma gondii: inconsistent dissemination patterns following oral infection in mice. Exp. Parasitol. *116*, 302–305. https://doi.org/10.1016/j.exppara.2007.01.010.

Braun, L., Brenier-Pinchart, M.P., Hammoudi, P.M., Cannella, D., Kieffer-Jaquinod, S., Vollaire, J., Josserand, V., Touquet, B., Couté, Y., Tardieux, I., et al. (2019). The Toxoplasma effector TEEGR promotes parasite persistence by modulating NF-κB signalling via EZH2. Nat. Microbiol. *4*, 1208–1220. https://doi.org/10.1038/s41564-019-0431-8.

Braun, L., Brenier-Pinchart, M.P., Yogavel, M., Curt-Varesano, A., Curt-Bertini, R.L., Hussain, T., Kieffer-Jaquinod, S., Coute, Y., Pelloux, H., Tardieux, I., et al. (2013). A Toxoplasma dense granule protein, GRA24, modulates the early immune response to infection by promoting a direct and sustained host p38 MAPK activation. J. Exp. Med. *210*, 2071–2086. https://doi.org/10.1084/jem.20130103.

Briseño, C.G., Haldar, M., Kretzer, N.M., Wu, X., Theisen, D.J., Kc, W., Durai, V., Grajales-Reyes, G.E., Iwata, A., Bagadia, P., et al. (2016). Distinct transcriptional programs control cross-priming in classical and monocyte-derived dendritic cells. Cell Rep. *15*, 2462–2474. https://doi.org/10.1016/j.celrep.2016.05.025.

Butcher, B.A., Fox, B.A., Rommereim, L.M., Kim, S.G., Maurer, K.J., Yarovinsky, F., Herbert, D.R., Bzik, D.J., and Denkers, E.Y. (2011). Toxoplasma gondii rhoptry kinase ROP16 activates STAT3 and STAT6 resulting in cytokine inhibition and arginase-1-dependent growth control. PLoS Pathog. *7*, e1002236. https://doi.org/10.1371/journal.ppat.1002236.

Cairns, B.R., Erdjument-Bromage, H., Tempst, P., Winston, F., and Kornberg, R.D. (1998). Two actin-related proteins are shared functional components of the chromatin-remodeling complexes RSC and SWI/SNF. Mol. Cell *2*, 639–651. https://doi.org/10.1016/s1097-2765(00)80162-8.

Collantes-Fernandez, E., Arrighi, R.B., Alvarez-García, G., Weidner, J.M., Regidor-Cerrillo, J., Boothroyd, J.C., Ortega-Mora, L.M., and Barragan, A. (2012). Infected dendritic cells facilitate systemic dissemination and transplacental passage of the obligate intracellular parasite Neospora caninum in mice. PLoS One *7*, e32123. https://doi.org/10.1371/journal.pone.0032123.

Courret, N., Darche, S., Sonigo, P., Milon, G., Buzoni-Gâtel, D., and Tardieux, I. (2006). CD11c- and CD11b-expressing mouse leukocytes transport single Toxoplasma gondii tachyzoites to the brain. Blood *107*, 309–316.

Curt-Varesano, A., Braun, L., Ranquet, C., Hakimi, M.A., and Bougdour, A. (2016). The aspartyl protease TgASP5 mediates the export of the Toxoplasma GRA16 and GRA24 effectors into host cells. Cell Microbiol *18*, 151–167. https://doi.org/10.1111/cmi.12498.

Cygan, A.M., Theisen, T.C., Mendoza, A.G., Marino, N.D., Panas, M.W., and Boothroyd, J.C. (2020). Coimmunoprecipitation with MYR1 identifies three additional proteins within the Toxoplasma gondii parasitophorous vacuole required for translocation of dense granule effectors into Host Cells. mSphere *5*. e00858–e00819. https://doi.org/10.1128/mSphere.00858-19.

de Menezes, J.P., Koushik, A., Das, S., Guven, C., Siegel, A., Laranjeira-Silva, M.F., Losert, W., and Andrews, N.W. (2017). Leishmania infection inhibits macrophage motility by altering F-actin dynamics and the expression of adhesion complex proteins. Cell. Microbiol. *19*, 3. https://doi.org/10.1111/cmi.12668.

Dobrowolski, J.M., and Sibley, L.D. (1996). Toxoplasma invasion of mammalian cells is powered by the actin cytoskeleton of the parasite. Cell *84*, 933–939.

Drewry, L.L., Jones, N.G., Wang, Q., Onken, M.D., Miller, M.J., and Sibley, L.D. (2019). The secreted kinase ROP17 promotes Toxoplasma gondii dissemination by hijacking monocyte tissue migration. Nat. Microbiol. *4*, 1951–1963. https://doi.org/10.1038/s41564-019-0504-8.

Dubey, J.P. (1997). Bradyzoite-induced murine toxoplasmosis: stage conversion pathogenesis, and tissue cyst formation in mice fed bradyzoites of different strains of *Toxoplasma gondii*. J. Eukaryot. Microbiol. *44*, 592–602.

Farhat, D.C., Swale, C., Dard, C., Cannella, D., Ortet, P., Barakat, M., Sindikubwabo, F., Belmudes, L., De Bock, P.J., Couté, Y., et al. (2020). A MORC-driven transcriptional switch controls Toxoplasma developmental trajectories and sexual commitment. Nat. Microbiol. *5*, 570–583. https://doi.org/10.1038/s41564-020-0674-4.

Förster, R., Schubel, A., Breitfeld, D., Kremmer, E., Renner-Müller, I., Wolf, E., and Lipp, M. (1999). CCR7 coordinates the primary immune response by establishing functional microenvironments in secondary lymphoid organs. Cell *99*, 23–33. https://doi.org/10.1016/s0092-8674(00)80059-8.

Fox, B.A., Ristuccia, J.G., Gigley, J.P., and Bzik, D.J. (2009). Efficient gene replacements in Toxoplasma gondii strains deficient for nonhomologous end joining. Eukaryot. Cell *8*, 520–529. https://doi.org/10.1128/EC.00357-08.

Franco, M., Panas, M.W., Marino, N.D., Lee, M.C., Buchholz, K.R., Kelly, F.D., Bednarski, J.J., Sleckman, B.P., Pourmand, N., and Boothroyd, J.C. (2016). A Novel Secreted Protein, MYR1, Is Central to Toxoplasma's Manipulation of Host Cells. mBio *7*. e02231–e02215. https://doi.org/10.1128/mBio.02231-15.

Frickel, E.M., and Hunter, C.A. (2021). Lessons from Toxoplasma: host responses that mediate parasite control and the microbial effectors that subvert them. J. Exp. Med. *218*, e20201314. https://doi.org/10.1084/jem.20201314.

Friedl, P., and Weigelin, B. (2008). Interstitial leukocyte migration and immune function. Nat. Immunol. *9*, 960–969.

Fuks, J.M., Arrighi, R.B., Weidner, J.M., Kumar Mendu, S., Jin, Z., Wallin, R.P., Rethi, B., Birnir, B., and Barragan, A. (2012). GABAergic signaling is linked to a hypermigratory phenotype in dendritic cells infected by Toxoplasma gondii. PLoS Pathog. *8*, e1003051. https://doi.org/10.1371/journal.ppat.1003051.

García-Sánchez, M., Jiménez-Pelayo, L., Horcajo, P., Regidor-Cerrillo, J., Ólafsson, E.B., Bhandage, A.K., Barragan, A., Werling, D., Ortega-Mora, L.M., and Collantes-Fernández, E. (2019). Differential responses of bovine monocyte-derived macrophages to infection by Neospora caninum isolates of high and low virulence. Front. Immunol. *10*, 915. https://doi.org/10.3389/fimmu.2019.00915.

Gay, G., Braun, L., Brenier-Pinchart, M.P., Vollaire, J., Josserand, V., Bertini, R.L., Varesano, A., Touquet, B., De Bock, P.J., Coute, Y., et al. (2016). Toxoplasma gondii TgIST co-opts host chromatin repressors dampening STAT1-dependent gene regulation and IFN-gamma-mediated host defenses. J. Exp. Med. *213*, 1779–1798. https://doi.org/10.1084/jem.20160340.

Glasmacher, E., Agrawal, S., Chang, A.B., Murphy, T.L., Zeng, W., Vander Lugt, B., Khan, A.A., Ciofani, M., Spooner, C.J., Rutz, S., et al. (2012). A genomic regulatory element that directs assembly and function of immune-specific AP-1-IRF complexes. Science *338*, 975–980. https://doi.org/10.1126/science.1228309.

Goudot, C., Coillard, A., Villani, A.C., Gueguen, P., Cros, A., Sarkizova, S., Tang-Huau, T.L., Bohec, M., Baulande, S., Hacohen, N., et al. (2017). Aryl hydrocarbon receptor Controls Monocyte Differentiation into dendritic Cells versus Macrophages. Immunity *47*, 582–596.e6. https://doi.org/10.1016/j.immuni.2017.08.016.

Grajales-Reyes, G.E., Iwata, A., Albring, J., Wu, X., Tussiwand, R., Kc, W., Kretzer, N.M., Briseño, C.G., Durai, V., Bagadia, P., et al. (2015). Batf3 maintains autoactivation of Irf8 for commitment of a CD8alpha(+) conventional DC clonogenic progenitor. Nat. Immunol. *16*, 708–717. https://doi.org/10.1038/ni.3197.

Gregg, B., Taylor, B.C., John, B., Tait-Wojno, E.D., Girgis, N.M., Miller, N., Wagage, S., Roos, D.S., and Hunter, C.A. (2013). Replication and distribution of Toxoplasma gondii in the small intestine after oral infection with tissue cysts. Infect. Immun. *81*, 1635–1643. https://doi.org/10.1128/IAI.01126-12.

Guilliams, M., Ginhoux, F., Jakubzick, C., Naik, S.H., Onai, N., Schraml, B.U., Segura, E., Tussiwand, R., and Yona, S. (2014). Dendritic cells, monocytes and macrophages: a unified nomenclature based on ontogeny. Nat. Rev. Immunol. *14*, 571–578. https://doi.org/10.1038/nri3712.

Hakimi, M.A., Olias, P., and Sibley, L.D. (2017). Toxoplasma effectors targeting Host Signaling and Transcription. Clin. Microbiol. Rev. *30*, 615–645. https://doi.org/10.1128/CMR.00005-17.

He, H., Brenier-Pinchart, M.P., Braun, L., Kraut, A., Touquet, B., Couté, Y., Tardieux, I., Hakimi, M.A., and Bougdour, A. (2018). Characterization of a Toxoplasma effector uncovers an alternative GSK3/β-catenin-regulatory pathway of inflammation. eLife *7*, e39887. https://doi.org/10.7554/eLife.39887.

Helft, J., Böttcher, J., Chakravarty, P., Zelenay, S., Huotari, J., Schraml, B.U., Goubau, D., and Reis e Sousa, C. (2015). GM-CSF mouse bone marrow cultures comprise a heterogeneous population of CD11c(+)MHCII(+) macrophages and dendritic cells. Immunity *42*, 1197–1211. https://doi.org/10.1016/j.immuni.2015.05.018.

Hitziger, N., Dellacasa, I., Albiger, B., and Barragan, A. (2005). Dissemination of Toxoplasma gondii to immunoprivileged organs and role of Toll/interleukin-1 receptor signalling for host resistance assessed by in vivo bioluminescence imaging. Cell. Microbiol. *7*, 837–848. https://doi.org/10.1111/j.1462-5822.2005.00517.x.

Huang, Z., Liu, H., Nix, J., Xu, R., Knoverek, C.R., Bowman, G.R., Amarasinghe, G.K., and Sibley, L.D. (2022). The intrinsically disordered protein TgIST from Toxoplasma gondii inhibits STAT1 signaling by blocking cofactor recruitment. Nat. Commun. *13*, 4047. https://doi.org/10.1038/s41467-022-31720-7.

Jensen, K.D., Hu, K., Whitmarsh, R.J., Hassan, M.A., Julien, L., Lu, D., Chen, L., Hunter, C.A., and Saeij, J.P. (2013). Toxoplasma gondii rhoptry 16 kinase promotes host resistance to oral infection and intestinal inflammation only in the context of the dense granule protein GRA15. Infect. Immun. *81*, 2156–2167. https://doi.org/10.1128/IAI.01185-12.

Jensen, K.D., Wang, Y., Wojno, E.D., Shastri, A.J., Hu, K., Cornel, L., Boedec, E., Ong, Y.C., Chien, Y.H., Hunter, C.A., et al. (2011). Toxoplasma polymorphic effectors determine macrophage polarization and intestinal inflammation. Cell Host Microbe *9*, 472–483. https://doi.org/10.1016/j.chom.2011.04.015.

Kanatani, S., Fuks, J.M., Olafsson, E.B., Westermark, L., Chambers, B., Varas-Godoy, M., Uhlén, P., and Barragan, A. (2017). Voltage-dependent calcium channel signaling mediates GABAA receptor-induced migratory activation of dendritic cells infected by Toxoplasma gondii. PLoS Pathog. *13*, e1006739. https://doi.org/10.1371/journal.ppat.1006739.

Katholnig, K., Kaltenecker, C.C., Hayakawa, H., Rosner, M., Lassnig, C., Zlabinger, G.J., Gaestel, M., Müller, M., Hengstschläger, M., Hörl, W.H., et al. (2013). p38α senses environmental stress to control innate immune responses via mechanistic target of rapamycin. J. Immunol. *190*, 1519–1527. https://doi.org/10.4049/jimmunol.1202683.

Kim, K., Eaton, M.S., Schubert, W., Wu, S., and Tang, J. (2001). Optimized expression of green fluorescent protein in *Toxoplasma gondii* using thermostable green fluorescent protein mutants. Mol. Biochem. Parasitol. *113*, 309–313.

Kingston, R.E., and Narlikar, G.J. (1999). ATP-dependent remodeling and acetylation as regulators of chromatin fluidity. Genes Dev. *13*, 2339–2352. https://doi.org/10.1101/gad.13.18.2339.

Lambert, H., Dellacasa-Lindberg, I., and Barragan, A. (2011). Migratory responses of leukocytes infected with Toxoplasma gondii. Microbes Infect. *13*, 96–102. https://doi.org/10.1016/j.micinf.2010.10.002.

Lambert, H., Hitziger, N., Dellacasa, I., Svensson, M., and Barragan, A. (2006). Induction of dendritic cell migration upon Toxoplasma gondii infection potentiates parasite dissemination. Cell. Microbiol. *8*, 1611–1623. https://doi.org/10.1111/j.1462-5822.2006.00735.x.

Lambert, H., Vutova, P.P., Adams, W.C., Loré, K., and Barragan, A. (2009). The Toxoplasma gondii-shuttling function of dendritic cells is linked to the parasite genotype. Infect. Immun. *77*, 1679–1688.

Laouar, Y., Welte, T., Fu, X.Y., and Flavell, R.A. (2003). STAT3 is required for Flt3L-dependent dendritic cell differentiation. Immunity *19*, 903–912. https://doi.org/10.1016/s1074-7613(03)00332-7.

Lecoeur, H., Prina, E., Gutiérrez-Sanchez, M., and Späth, G.F. (2022). Going ballistic: Leishmania nuclear subversion of host cell plasticity. Trends Parasitol. *38*, 205–216. https://doi.org/10.1016/j.pt.2021.09.009.

Lin, Q., Chauvistré, H., Costa, I.G., Gusmao, E.G., Mitzka, S., Hänzelmann, S., Baying, B., Klisch, T., Moriggl, R., Hennuy, B., et al. (2015). Epigenetic program and transcription factor circuitry of dendritic cell development. Nucleic Acids Res. *43*, 9680–9693. https://doi.org/10.1093/nar/gkv1056.

Lovey, A., Verma, S., Kaipilyawar, V., Ribeiro-Rodrigues, R., Husain, S., Palaci, M., Dietze, R., Ma, S., Morrison, R.D., Sherman, D.R., et al. (2022). Early alveolar macrophage response and IL-1R-dependent T cell priming determine transmissibility of Mycobacterium tuberculosis strains. Nat. Commun. *13*, 884. https://doi.org/10.1038/s41467-022-28506-2.

Ma, J.S., Sasai, M., Ohshima, J., Lee, Y., Bando, H., Takeda, K., and Yamamoto, M. (2014). Selective and strain-specific NFAT4 activation by the Toxoplasma gondii polymorphic dense granule protein GRA6. J. Exp. Med. *211*, 2013–2032. https://doi.org/10.1084/jem.20131272.

Mercer, H.L., Snyder, L.M., Doherty, C.M., Fox, B.A., Bzik, D.J., and Denkers, E.Y. (2020). Toxoplasma gondii dense granule protein GRA24 drives MyD88-independent p38 MAPK activation, IL-12 production and induction of protective immunity. PLoS Pathog. *16*, e1008572. https://doi.org/10.1371/journal.ppat.1008572.

Mercer, J., and Greber, U.F. (2013). Virus interactions with endocytic pathways in macrophages and dendritic cells. Trends Microbiol. *21*, 380–388. https://doi.org/10.1016/j.tim.2013.06.001.

Miller, J.C., Brown, B.D., Shay, T., Gautier, E.L., Jojic, V., Cohain, A., Pandey, G., Leboeuf, M., Elpek, K.G., Helft, J., et al. (2012). Deciphering the transcriptional network of the dendritic cell lineage. Nat. Immunol. *13*, 888–899. https://doi.org/10.1038/ni.2370.

Montoya, J.G., and Liesenfeld, O. (2004). Toxoplasmosis. Lancet *363*, 1965–1976.

Morgado, P., Ong, Y.C., Boothroyd, J.C., and Lodoen, M.B. (2011). Toxoplasma gondii induces B7-2 expression through activation of JNK signal transduction. Infect. Immun. *79*, 4401–4412. https://doi.org/10.1128/IAI.05562-11.

Mukhopadhyay, D., Arranz-Solís, D., and Saeij, J.P.J. (2020). Toxoplasma GRA15 and GRA24 are important activators of the host innate immune response in the absence of TLR11. PLoS Pathog. *16*, e1008586. https://doi.org/10.1371/journal.ppat.1008586.

Nadipuram, S.M., Kim, E.W., Vashisht, A.A., Lin, A.H., Bell, H.N., Coppens, I., Wohlschlegel, J.A., and Bradley, P.J. (2016). In vivo biotinylation of the toxoplasma parasitophorous vacuole reveals novel dense granule proteins important for parasite growth and pathogenesis. mBio *7*, e00808–e00816. https://doi.org/10.1128/mBio.00808-16.

Naor, A., Panas, M.W., Marino, N., Coffey, M.J., Tonkin, C.J., and Boothroyd, J.C. (2018). MYR1-dependent effectors are the major drivers of a host cell's early response to Toxoplasma, including counteracting MYR1-independent effects. mBio *9*, e02401–e02417. https://doi.org/10.1128/mBio.02401-17.

Nussenzweig, M.C., and Steinman, R.M. (1980). Contribution of dendritic cells to stimulation of the murine syngeneic mixed leukocyte reaction. J. Exp. Med. *151*, 1196–1212. https://doi.org/10.1084/jem.151.5.1196.

Ólafsson, E.B., Ross, E.C., Varas-Godoy, M., and Barragan, A. (2019). TIMP-1 promotes hypermigration of Toxoplasma-infected primary dendritic cells via CD63-ITGB1-FAK signaling. J. Cell Sci. *132*, jcs225193. https://doi.org/10.1242/jcs.225193.

Ólafsson, E.B., Ten Hoeve, A.L., Li-Wang, X., Westermark, L., Varas-Godoy, M., and Barragan, A. (2020). Convergent Met and voltage-gated Ca(2+) channel signaling drives hypermigration of Toxoplasma-infected dendritic cells. J. Cell Sci. *134*, jcs241752. https://doi.org/10.1242/jcs.241752.

Olias, P., and Sibley, L.D. (2016). Functional analysis of the role of Toxoplasma gondii nucleoside triphosphate hydrolases I and II in acute mouse virulence and immune suppression. Infect. Immun. *84*, 1994–2001. https://doi.org/10.1128/IAI.00077-16.

Panas, M.W., Ferrel, A., Naor, A., Tenborg, E., Lorenzi, H.A., and Boothroyd, J.C. (2019). Translocation of dense granule effectors across the parasitophorous vacuole membrane in Toxoplasma-infected cells requires the activity of ROP17, a rhoptry protein kinase. mSphere *4*. e00276–e00219. https://doi.org/10.1128/mSphere.00276-19.

Pappas, G., Roussos, N., and Falagas, M.E. (2009). Toxoplasmosis snapshots: global status of Toxoplasma gondii seroprevalence and implications for pregnancy and congenital toxoplasmosis. Int. J. Parasitol. *39*, 1385–1394. https://doi.org/10.1016/j.ijpara.2009.04.003.

Patil, V., Zhao, Y., Shah, S., Fox, B.A., Rommereim, L.M., Bzik, D.J., and Yap, G.S. (2014). Co-existence of classical and alternative activation programs in macrophages responding to Toxoplasma gondii. Int. J. Parasitol. *44*, 161–164. https://doi.org/10.1016/j.ijpara.2013.08.003.

Rastogi, S., Xue, Y., Quake, S.R., and Boothroyd, J.C. (2020). Differential impacts on Host Transcription by ROP and GRA Effectors from the Intracellular Parasite Toxoplasma gondii. mBio *11*. e00182–e00120. https://doi.org/10.1128/mBio.00182-20.

Rosenberg, A., and Sibley, L.D. (2021). Toxoplasma gondii secreted effectors co-opt host repressor complexes to inhibit necroptosis. Cell Host Microbe *29*, 1186–1198.e8. https://doi.org/10.1016/j.chom.2021.04.016.

Ross, E.C., Hoeve, A.L.T., Saeij, J.P.J., and Barragan, A. (2022). Toxoplasma effector-induced ICAM-1 expression by infected dendritic cells potentiates transmigration across polarised endothelium. Front. Immunol. *13*, 950914. https://doi.org/10.3389/fimmu.2022.950914.

Ross, E.C., Ten Hoeve, A.L., and Barragan, A. (2021). Integrin-dependent migratory switches regulate the translocation of Toxoplasma-infected dendritic cells across brain endothelial monolayers. Cell. Mol. Life Sci. *78*, 5197–5212. https://doi.org/10.1007/s00018-021-03858-y.

Rudzki, E.N., Ander, S.E., Coombs, R.S., Alrubaye, H.S., Cabo, L.F., Blank, M.L., Gutiérrez-Melo, N., Dubey, J.P., Coyne, C.B., and Boyle, J.P. (2021). Toxoplasma gondii GRA28 is required for placenta-specific induction of the regulatory chemokine CCL22 in human and mouse. mBio *12*, e0159121. https://doi.org/10.1128/mBio.01591-21.

Saeij, J.P., Coller, S., Boyle, J.P., Jerome, M.E., White, M.W., and Boothroyd, J.C. (2007). Toxoplasma co-opts host gene expression by injection of a polymorphic kinase homologue. Nature *445*, 324–327. https://doi.org/10.1038/nature05395.

Sangaré, L.O., Ólafsson, E.B., Wang, Y., Yang, N., Julien, L., Camejo, A., Pesavento, P., Sidik, S.M., Lourido, S., Barragan, A., et al. (2019). In vivo CRISPR screen identifies TgWIP as a toxoplasma modulator of dendritic cell migration. Cell Host Microbe *26*, 478–492.e8. https://doi.org/10.1016/j.chom.2019.09.008.

Sansonetti, P.J., and Di Santo, J.P. (2007). Debugging how bacteria manipulate the immune response. Immunity *26*, 149–161. https://doi.org/10.1016/j.immuni.2007.02.004.

Sathe, P., Metcalf, D., Vremec, D., Naik, S.H., Langdon, W.Y., Huntington, N.D., Wu, L., and Shortman, K. (2014). Lymphoid tissue and plasmacytoid dendritic cells and macrophages do not share a common macrophage-dendritic cell-restricted progenitor. Immunity *41*, 104–115. https://doi.org/10.1016/j.immuni.2014.05.020.

Satpathy, A.T., Kc, W., Albring, J.C., Edelson, B.T., Kretzer, N.M., Bhattacharya, D., Murphy, T.L., and Murphy, K.M. (2012). Zbtb46 expression distinguishes classical dendritic cells and their committed progenitors from other immune lineages. J. Exp. Med. *209*, 1135–1152. https://doi.org/10.1084/jem.20120030.

Scanga, C.A., Aliberti, J., Jankovic, D., Tilloy, F., Bennouna, S., Denkers, E.Y., Medzhitov, R., and Sher, A. (2002). Cutting edge: MyD88 is required for resistance to Toxoplasma gondii infection and regulates parasite-induced IL-12 production by dendritic cells. J. Immunol. *168*, 5997–6001.

Schlüter, D., and Barragan, A. (2019). Advances and challenges in understanding cerebral toxoplasmosis. Front. Immunol. *10*, 242. https://doi.org/10.3389/fimmu.2019.00242.

Schneider, C.A., Rasband, W.S., and Eliceiri, K.W. (2012). NIH Image to ImageJ: 25 years of image analysis. Nat. Methods *9*, 671–675.

Schulz, O., Jaensson, E., Persson, E.K., Liu, X., Worbs, T., Agace, W.W., and Pabst, O. (2009). Intestinal CD103+, but not CX3CR1+, antigen sampling cells migrate in lymph and serve classical dendritic cell functions. J. Exp. Med. *206*, 3101–3114. https://doi.org/10.1084/jem.20091925.

Sibley, L.D., and Boothroyd, J.C. (1992). Virulent strains of *Toxoplasma gondii* comprise a single clonal lineage. Nature *359*, 82–85.

Stuart, R.K., and Hamilton, J.A. (1980). Tumor-promoting phorbol esters stimulate hematopoietic colony formation in vitro. Science *208*, 402–404. https://doi.org/10.1126/science.6245446.

Swierzy, I.J., Händel, U., Kaever, A., Jarek, M., Scharfe, M., Schlüter, D., and Lüder, C.G.K. (2017). Divergent co-transcriptomes of different host cells infected with Toxoplasma gondii reveal cell type-specific host-parasite interactions. Sci. Rep. *7*, 7229. https://doi.org/10.1038/s41598-017-07838-w.

Tan, S., and Russell, D.G. (2015). Trans-species communication in the Mycobacterium tuberculosis-infected macrophage. Immunol. Rev. *264*, 233–248. https://doi.org/10.1111/imr.12254.

ten Hoeve, A.L., Hakimi, M.-A., and Barragan, A. (2019). Sustained Egr-1 response via p38 MAP kinase signaling modulates early immune responses of dendritic cells parasitized by Toxoplasma gondii. Front. Cell. Infect. Microbiol. *9*, 349. https://doi.org/10.3389/fcimb.2019.00349.

Wang, Y., Cirelli, K.M., Barros, P.D.C., Sangaré, L.O., Butty, V., Hassan, M.A., Pesavento, P., Mete, A., and Saeij, J.P.J. (2019). Three Toxoplasma gondii Dense granule proteins are required for induction of lewis rat macrophage pyroptosis. mBio *10*. e02388–e02318. https://doi.org/10.1128/mBio.02388-18.

Wang, Y., Sangaré, L.O., Paredes-Santos, T.C., Hassan, M.A., Krishnamurthy, S., Furuta, A.M., Markus, B.M., Lourido, S., and Saeij, J.P.J. (2020). Genome-wide screens identify Toxoplasma gondii determinants of parasite fitness in IFNgamma-activated murine macrophages. Nat. Commun. *11*, 5258. https://doi.org/10.1038/s41467-020-18991-8.

Weidner, J.M., and Barragan, A. (2014). Tightly regulated migratory subversion of immune cells promotes the dissemination of Toxoplasma gondii. Int. J. Parasitol. *44*, 85–90. https://doi.org/10.1016/j.ijpara.2013.09.006.

Weidner, J.M., Kanatani, S., Hernández-Castañeda, M.A., Fuks, J.M., Rethi, B., Wallin, R.P., and Barragan, A. (2013). Rapid cytoskeleton remodelling in dendritic cells following invasion by Toxoplasma gondii coincides with the onset of a hypermigratory phenotype. Cell. Microbiol. *15*, 1735–1752. https://doi.org/10.1111/cmi.12145.

Weidner, J.M., Kanatani, S., Uchtenhagen, H., Varas-Godoy, M., Schulte, T., Engelberg, K., Gubbels, M.J., Sun, H.S., Harrison, R.E., Achour, A., et al. (2016). Migratory activation of parasitized dendritic cells by the protozoan Toxoplasma gondii 14-3-3 protein. Cell. Microbiol. *18*, 1537–1550. https://doi.org/10.1111/cmi.12595.

Xue, Y., Wong, J., Moreno, G.T., Young, M.K., Côté, J., and Wang, W. (1998). NURD, a novel complex with both ATP-dependent chromatin-remodeling and histone deacetylase activities. Mol. Cell *2*, 851–861. https://doi.org/10.1016/s1097-2765(00)80299-3.

Yamamoto, M., Standley, D.M., Takashima, S., Saiga, H., Okuyama, M., Kayama, H., Kubo, E., Ito, H., Takaura, M., Matsuda, T., et al. (2009). A single polymorphic amino acid on Toxoplasma gondii kinase ROP16 determines the direct and strain-specific activation of Stat3. J. Exp. Med. *206*, 2747–2760. https://doi.org/10.1084/jem.20091703.

Zhang, H., Elbaum-Garfinkle, S., Langdon, E.M., Taylor, N., Occhipinti, P., Bridges, A.A., Brangwynne, C.P., and Gladfelter, A.S. (2015). RNA controls PolyQ protein phase transitions. Mol. Cell *60*, 220–230. https://doi.org/10.1016/j.molcel.2015.09.017.

STAR★METHODS

KEY RESOURCES TABLE

REAGENT or RESOURCE	SOURCE	IDENTIFIER
Antibodies		
PE anti-mouse CCR7 (clone 4B12)	eBioscience	Cat# 12-1971-82; RRID:AB_465905
PE-Cyanine7 anti-mouse CD11c (clone N418)	eBioscience	Cat# 25-0114-82; RRID:AB_469590
APC anti-mouse/human CD11b (clone M1/70)	BioLegend	Cat# 101211; RRID:AB_312794
anti-mouse CD16/CD32 (Mouse BD Fc Block™)	BD Biosciences	Cat# 553142; RRID:AB_394657
anti-mouse CD16/CD32 (clone 93)	eBioscience	Cat# 14-0161-82; RRID:AB_467133
Super Bright 780 anti-mouse CD40 (clone 1C10)	eBioscience	Cat# 78-0401-82; RRID:AB_2762674
Super Bright 645 anti-mouse CD80 (clone 16-10A1)	eBioscience	Cat# 64-0801-80; RRID:AB_2663120
Super Bright 600 anti-mouse CD86 (clone GL1)	eBioscience	Cat# 63-0862-80; RRID:AB_2662861
Brilliant Violet 605 anti-mouse CD115 (clone AFS98)	BioLegend	Cat# 135517; RRID:AB_2562760
Super Bright 702 anti-mouse MHCII I-A/I-E (clone M5/114)	eBioscience	Cat# 67-5321-82; RRID:AB_2717173
PE anti-mouse IRF4 (clone Q9-343)	BD Biosciences	Cat# 566649
PerCP-Cyanine5.5 anti-mouse IL-12/23 p40 (clone C17.8)	eBioscience	Cat# 45-7123-80; RRID:AB_1107021
PE anti-mouse Ly6C (clone HK1.4)	BioLegend	Cat# 128007; RRID:AB_1186133
PE anti-mouse ZBTB46 (clone U4-1374)	BD Biosciences	Cat# 565832; RRID:AB_2739372
APC/Fire 750 anti-mouse F4/80 (clone BM8)	BioLegend	Cat# 123151; RRID:AB_2616724
PE mouse IgG1 Kappa Isotype Control (clone MOPC-21)	BD Biosciences	Cat# 551436; RRID:AB_394195
PE rat IgG2a κ Isotype Control (clone R35-95)	BD Biosciences	Cat# 553930; RRID:AB_479719
Anti-TATA binding protein	Abcam	Cat# ab51841; RRID:AB_945758
Goat anti-Mouse IgG (H+L) Secondary Antibody, HRP	Thermo Fisher	Cat# 32430; RRID:AB_1185566
Chemicals, peptides, and recombinant proteins		
Brefeldin A Solution (1000x)	eBioscience	Cat# 00-4506-51
TPCA-1 STAT3 and IKK-2 inhibitor	MedChemExpress	Cat# HY-10074
AS1517499 STAT6 inhibitor	MedChemExpress	Cat# HY-100614
CellTracker Orange CMTMR Dye	Thermo Fisher	Cat# C2927
CellTracker Deep Red Dye	Thermo Fisher	Cat# C34565
CellTrace CFSE Cell Proliferation Kit	Thermo Fisher	Cat# C34554
LIVE/DEAD™ Fixable Far Red Dead Cell Stain Kit	Thermo Fisher	Cat# L34973
Critical commercial assays		
Nile Blue Fluorescent Particles, 2.5-4.5 μm	BD Biosciences	Cat # 556270
CD14 MicroBeads, human, 2 mL	Miltenyi Biotec	Cat # 130-050-201
MiniMACS Separation columns, type MS	Miltenyi Biotec	Cat # 130-042-201
Lymphoprep	Axis Shield Poc As	Cat# 1115754
Direct-zol RNA Miniprep kit	Zymo Research	Cat# R2052
Deposited data		
https://www.ebi.ac.uk/pride/login		N/A
MS proteomics	ProteomeXchange Consortium	PXD032360
Experimental models: Cell lines		
Human foreskin fibroblasts HFF-1	American Type Culture Collection	Cat# SCRC-1041; RRID:CVCL_3285

(*Continued on next page*)

Continued

REAGENT or RESOURCE	SOURCE	IDENTIFIER
RAW 264.7	American Type Culture Collection	Cat# ATCC TIB-71; RRID:CVCL_0493
THP-1	American Type Culture Collection	Cat# ATCC TIB-202; RRID:CVCL_0006
Experimental models: Organisms/strains		
Mouse C57BL/6NCrl (wild-type)	Charles River Laboratories	Strain code 027; RRID:IMSR_CRL:027
Mouse B6.129P2(C)-*Ccr7*^{tm1Rfor}/J (CCR7$^{-/-}$)	Jackson Laboratory	JAX stock #006621; RRID:IMSR_JAX:006621
T. gondii GT1 F3	American Type Culture Collection	Cat# 50838
T. gondii ME49-PTG GFPS65T	Kim et al., 2001	N/A
T. gondii ME49 RFP	Wang et al., 2019	N/A
T. gondii RH-LDM GFPS65T	Kim et al., 2001; Barragan and Sibley, 2002	N/A
T. gondii RH88 (RH-ERP)	American Type Culture Collection	Cat# 50838
T. gondii RH ΔHPT	Jensen et al., 2011	N/A
T. gondii RH ΔHPTΔrop16	Jensen et al., 2011	N/A
T. gondii RH1-1 cLuc GFP	Boyle et al., 2007	N/A
T. gondii RH Δmyr1 cLuc GFP	Wang et al., 2020	N/A
T. gondii RH Δrop17 cLuc GFP	Wang et al., 2019	N/A
T. gondii RH Δgra45 cLuc GFP	Wang et al., 2020	N/A
T. gondii RH ΔTgwip GFP	Sangaré et al., 2019	N/A
T. gondii RHΔku80	Fox et al., 2009	N/A
T. gondii RHΔku80 Δgra24	Braun et al., 2013	N/A
T. gondii RHΔku80 Δgra28	This manuscript	N/A
T. gondii RHΔku80 Δgra28+GRA28	This manuscript	N/A
T. gondii PruΔku80	Braun et al., 2019	N/A
T. gondii PruΔku80 Δgra28	This manuscript	N/A
T. gondii PruΔku80 Δgra28+GRA28	This manuscript	N/A
Oligonucleotides		
See Table S3		N/A
Software and algorithms		
ImageJ	Schneider et al., 2012	https://imagej.nih.gov/ij/
R version 4.0.2	R Foundation for Statistical Computing	https://www.R-project.org/
RStudio version 1.3.1073	RStudio	https://www.rstudio.com
GraphPad Prism 7.0 / 8.0.2	GraphPad Software	http://www.graphpad.com
Chemotaxis and Migration Tool V2.0	Ibidi	http://www.ibidi.com
FlowJo X 10.0.7r2	Flowjo LLC	http://www.flowjo.com

RESOURCE AVAILABILITY

Lead contact

Further information and requests for resources and reagents should be directed to and will be fulfilled by the lead contact, Antonio Barragan (antonio.barragan@su.se).

Materials availability

New plasmids and materials generated in this study are available from the lead contact.

Data and code availability

- The MS proteomics data have been deposited to the ProteomeXchange Consortium through the PRIDE partner repository with the dataset identifier PXD032360. This paper analyzes existing, publicly available data. The NCBI GEO accession numbers for these datasets are GSE40727, GSE66899, GSE64767, GSE99837 and GSE27972. All data reported in this paper will be shared by the lead contact upon request.
- This paper does not report original code.
- Any additional information required to reanalyze the data reported in this paper is available from the lead contact upon request.

EXPERIMENTAL MODEL AND SUBJECT DETAILS

Mice

Wild-type and CCR7-deficient C57BL/6 (6-10 week old, male and female) and wild-type BALB/c (6 week old, female) mice were used for the isolation of bone marrow. Bone marrow-derived macrophages (BMDMs), dendritic cells (BMDCs) and macrophage-like PMA bone marrow cells (PMA-BMC) were cultured from bone marrow with M-CSF-containing conditioned medium, recombinant GM-CSF or PMA as indicated in the method details. Peritoneal cells were harvested from wild-type C57BL/6 mice (6-10 week old, male and female) via peritoneal lavage. C75BL/6 cells were cultured in RPMI 1640 with 10% fetal bovine serum (FBS), gentamicin (20 μg/mL) and glutamine (2 mM) and BALB/c cells in Dulbecco's modified Eagle's medium, high glucose, with 50 μM 2-mercaptoethanol, 1X non-essential amino acids and 2% penicillin/streptomycin-glutamine at 37°C/5% CO_2. C57BL/6 mice (5-18 week old, male and female) were used for adoptive transfer of BMDMs and BMDCs. The Regional Animal Research Ethical Board, Stockholm, Sweden, approved experimental procedures and protocols involving extraction of cells from mice (permit numbers 9707/2018, 14458/2019 and N 78/16), following proceedings described in EU legislation (Council Directive 2010/63/EU).

Primary human cells

Peripheral blood mononuclear cells (PBMC) were isolated from buffy coats obtained from healthy adult donors at the Karolinska University Hospital Blood Center. The sex or age of these donors are unknown to the authors due to privacy law restrictions. $CD14^+$ monocytes were obtained from PBMC via positive selection and used for generating macrophages with M-CSF. Cells were cultured at 37°C/5% CO_2 in RPMI 1640 with 10% fetal bovine serum (FBS), gentamicin (20 μg/mL) and glutamine (2 mM). The Regional Ethics Committee, Stockholm, Sweden, approved protocols involving human cells (application number 2006/116-31). All donors received written and oral information upon donation of blood at the Karolinska University Hospital Blood Center. Written consent was obtained for utilization of white blood cells for research purposes.

Cell lines

Human foreskin fibroblasts HFF-1 were cultured in Dulbecco's modified Eagle's medium, high glucose, (DMEM; Thermo Fisher scientific) with 10% fetal bovine serum (FBS; Sigma), gentamicin (20 μg/ml; Gibco or Sigma) and glutamine (2 mM; Gibco). Human THP-1 (male) and murine RAW 264.7 (male, BALB/c) cells were used for *in vitro* experiments and cultured at 37°C/5% CO_2.

T. gondii strains

T. gondii tachyzoites were maintained by serial 2-day passages in human foreskin fibroblast HFF-1 monolayers. Freshly egressed tachyzoites were used for all infections. The different strains used are listed in the key resources table. All cell cultures used were periodically tested for mycoplasma and found to be negative.

METHOD DETAILS

Mouse cell culture

Cells from bone marrow of 6-10-week-old male or female wild-type or CCR7-deficient C57BL/6 mice (see key resources table) were cultivated in RPMI 1640 with 10% fetal bovine serum (FBS), gentamicin (20 μg/mL) and glutamine (2 mM), referred to as complete medium (all reagents from Life Technologies), and supplemented with 20 ng/mL recombinant mouse GM-CSF. On day 6 of culture loosely adherent cells were removed and loosely adherent cells on day 7 were harvested as bone marrow-derived dendritic cells (BMDCs). Strongly adherent cells were harvested on day 7-8 as bone marrow-derived macrophages (BMDMs). Macrophage-like PMA bone marrow cells (PMA-BMCs) were generated from C57BL/6 bone marrow in complete medium supplemented with 20 ng/mL phorbol 12-myristate 13-acetate (PMA) and adherent cells were harvested after 6 days of differentiation. The predominant appearance of phagocytic monocyte-macrophages after PMA-supplemented bone marrow culture has been described previously (Stuart and Hamilton, 1980). For peritoneal macrophages (PEMs) C57BL/6 mice were euthanized and peritoneal lavage (10 ml PBS) was collected from the peritoneal cavity. After overnight culture in complete medium, loosely and non-adherent cells were removed by repeated washing and the adherent cells were used as PEM in experiments for RNA isolation. For flow cytometric analysis PEMs were identified phenotypically from peritoneal lavage cells that were challenged *in vitro* as indicated. BALB/c BMDMs were generated as described previously (He et al., 2018). Briefly, bone marrow was isolated by flushing femurs and tibias of six-week-old female BALB/c mice (Janvier Labs) and cultured for 1 week in complete macrophage medium (DMEM supplemented with 10% heat-inactivated FBS (Invitrogen), 20% conditioned medium from macrophage-colony stimulating factor-secreting L929 fibroblasts (Aziz et al., 2009), 50 μM 2-mercaptoethanol, 1X non-essential amino acids, and 2% penicillin/streptomycin-glutamine). After 6 days, the cells were washed with PBS to remove non-adherent cells, harvested in ice-cold PBS supplemented with 1 mM EDTA and replated for the assay. RAW264.7 (RRID:CVCL80493, ATCC, cat. No. TIB-71) cell line was cultured in DMEM (Invitrogen), supplemented with 10% heat-inactivated FBS (Invitrogen), 10 mM Hepes buffer, pH 7.2, 2 mM L-glutamine, and 50 μg/ml penicillin and streptomycin (Thermo Fisher Scientific). THP1 (ATCC, cat. No. TIB-202) cell line was cultured in RPMI (Invitrogen), supplemented with 10% heat-inactivated FBS (Invitrogen), 10 mM Hepes buffer, pH 7.2, 2 mM L-glutamine, 50 μM 2-mercaptoethanol and 50 μg/ml penicillin and streptomycin (Thermo Fisher Scientific). Cell purity was confirmed by microscopy and flow cytometry (Figures 1I and S1H; Data S1).

Human cell culture

Human CD14$^+$ monocytes were isolated from peripheral blood mononuclear cells (PBMC) after density gradient centrifugation on Lymphoprep with CD14 MicroBeads from buffy coats obtained from healthy donors at the Karolinska University Hospital Blood Center and cultured in complete medium. Macrophages were generated from CD14$^+$ monocytes through culture for 6-7 days in complete medium supplemented with 50 ng/mL human recombinant M-CSF.

Infection challenges

Carry-over from routine *T. gondii* culture to experiments was minimized by repeated washing of the freshly egressed tachyzoites before preparation of crude tachyzoites lysates (prepared by repeated freeze-thaw) or challenge with live tachyzoites. For all qPCR and western blot experiments, C57BL/6 BMDMs, PEMs, PMA-BMCs and human monocytes and macrophages were challenged with freshly egressed *T. gondii* tachyzoites at MOI 2 for 18h. Tachyzoite lysates were used at amounts derived from equivalent tachyzoite numbers as indicated live parasites. LPS was used at a final concentration of 10 ng/mL. For qPCR experiments, BALB/c BMDMs, RAW and THP-1 cells were challenged with *T. gondii* tachyzoites for 24h as indicated. For flow cytometry assays, C57BL/6 BMDMs were challenged for 6h or 18h, as indicated, with GFP-expressing *T. gondii* tachyzoites (MOI 1) or with non-fluorescent protein-expressing tachyzoites (MOI 2). Peritoneal cells were challenged with GFP-expressing *T. gondii* type I tachyzoites (RH-LDM; MOI 0,5) for 18h for flow cytometry. Infection frequencies for GFP-expressing type I (RH) *T. gondii* tachyzoites (MOI 1 or 2) were determined by flow cytometry (Data S1). For chemotaxis experiments, cells were challenged for 12-14h with GFP-expressing or CMTMR-labeled *T. gondii* tachyzoites at MOI 1 before seeding in the chemotaxis chamber.

Plasmid construction

To construct vector pLIC-GRA28-HF, the coding sequence of GRA28 was amplified using the primers LIC-231960-F and LIC-231960-R and genomic DNA of PruΔ*ku80* strain of *T. gondii* as the DNA template. The resulting PCR product was cloned into the pLIC-HF-*dhfr* vector using the ligation independent cloning (LIC) method.

The plasmid pTOXO_Cas9-CRISPR::sgGRA28 was generated as previously described (Curt-Varesano et al., 2016) to construct the *gra28* deletion in the RHΔ*ku80* and PruΔ*ku80* strains. Briefly, primers GRA28-gRNA-Fwd and GRA28-gRNA-Rev containing the sgRNA targeting *GRA28* genomic sequence were phosphorylated, annealed and ligated into pTOXO_Cas9-CRISPR plasmid linearized with BsaI, leading to pTOXO_Cas9-CRISPR::sgGRA28.

To construct the pP_{GRA28}-GRA28-HA vector, the promotor sequence of GRA28 and the *GRA28* coding sequence were amplified by PCR using the primers LICF-P_{GRA28}_F and LICR-GRA28_R. The resulting PCR P_{GRA28}-GRA28 DNA fragment was cloned into the plasmid pLIC-3HA-DHFR. The chimeric construct P_{GRA28}-GRA28-3HA-3'DHFR was amplified using the primers UPRT-P_{GRA28}_F and UPRT-3'DHFR_R and inserted within the UPRT locus.

T. gondii transfection

Vectors were transfected into *T. gondii* strains by electroporation. Electroporation was conducted in a 2-mm cuvette at 1.100 V, 25 Ω and 25 μF. Stable integrants were selected in media containing 1 μM pyrimethamine or 10 μM 5-fluorodeoxyuracil and single-cloned in 96 wells plates by limiting dilution.

Inhibitors

When indicated, cells were treated with inhibitors TPCA-1 or AS1517499 at 3 μM or vehicle (DMSO) initiated 1h prior to challenge.

Mixed leukocyte reaction (MLR)

Syngeneic MLR was performed as described (Nussenzweig and Steinman, 1980). Briefly, BMDM were challenged for 6h as indicated, washed and co-cultured with syngeneic unfractionated splenocytes for 18h at 1:20 ratio. Splenocytes were freshly isolated from triturated spleens, filtered through a 40 μm cell strainer and subjected to red blood cell lysis (ammonium chloride).

Quantitative polymerase chain reaction (qPCR)

C57BL/6 BMDMs, PMA-BMCs and PEMs were cultured with complete medium or challenged with freshly egressed *T. gondii* tachyzoites of the indicated strains, lysate of egressed *T. gondii* tachyzoites (ME49) at MOI equivalents or LPS as indicated and lysed in TRI Reagent (Sigma-Aldrich). Total RNA was extracted according to the manufacturers' protocol using the Direct-zol RNA Miniprep kit and reverse transcribed with Maxima H Minus Reverse Transcriptase (Thermo Fisher). Real time qPCR was performed SYBR® green PCR master mix (KAPA biosystems), specific forward and reverse primers at target-dependent concentrations (100 or 200 nM) and cDNA (10-30 ng) in a QuantStudio 5 System (Thermo Fisher) with ROX as a passive reference. qPCR results were analyzed using the ΔΔCq method and displayed as fold change relative to unchallenged or as ΔCq and relative to Importin-8 and TATA-binding protein (TBP) as housekeeping genes. BALB/c BMDMs and RAW and THP-1 cells were either uninfected or *T. gondii*-infected (MOI = 6) for 24 h. Total RNA was isolated using TRIzol reagent (Thermo Fisher Scientific). Complementary DNA was synthetized with random hexamers using the High Capacity RNA-to-cDNA kit (Applied Biosystem). Samples were analysed by real-time quantitative PCR for *CCR7*, *CCL22*, *TNFAIP6*, *CCL24*, *CX3CL1*, *CXCL3*, *CXCL5*, *Vcam1* and *IL1a* using the TaqMan gene expression master mix (Applied Biosystem) according to the manufacturer's instructions. The internal control gene *TBP* was used for normalization. Primers are listed in the key resources table.

Flow cytometry

C57BL/6 BMDMs or BMDCs were challenged as indicated and stained with anti-CD11c, CD11b, MHCII I-A/I-E, CD86, CD115, IRF4, Ly6C, IL-12p40 or isotype control antibodies and live/dead far red stain. For intracellular staining cells were fixed (2% PFA) and then permeabilized in either Tween-20 (1%) in FACS buffer (PBS/0,5% FBS/1mM EDTA; IL-12p40) or Triton X-100 (1%) in PBS/5% BSA (IRF4/isotype) supplemented with anti-CD16/CD32 antibody prior to staining. For IL-12p40 staining cells were cultured in the presence of Brefeldin A (eBioscience) for the last 4h of challenge. Extracellular staining was performed on fixed (2% PFA) or live cells, blocked with anti-CD16/CD32 antibody, in FACS buffer. For bead phagocytosis, PMA-BMCs were mixed with Nile Blue Fluorescent Particles (2.5-4.5 μm, 10 particles/cell) and cultured for 1h on ice or at 37° C, washed and fixed (2% PFA). PMA-BMCs kept on ice were <1% bead$^+$. C57BL/6 peritoneal lavage cells were challenged *in vitro* as indicated, stained with LIVE/DEAD Far Red stain, fixed (2% PFA) and then stained with anti-CD11c, CD11b, CD19, MHCII I-A/I-E, CD86, CD115, Ly6C and F4/80 antibodies. PEMs were defined as CD19$^-$CD11b^{hi}CD11c$^-$ (Figures 1I and S1H). Flow cytometry was performed on a BD LSRFortessa flow cytometer (BD Biosciences) and analyzed with FlowJo X (FlowJo LLC).

Western blot

For Western blotting cells were challenged as indicated, harvested, washed with PBS and then lysed directly in Laemmli buffer for whole cell lysates. Proteins were separated using 8% or 10% SDS-PAGE, blotted onto a PVDF membrane and blocked (10% BSA in TBS/0,5% Tween-20) followed by incubation with primary and secondary antibodies: anti-TATA-binding protein, anti-ZBTB46, anti-mouse IgG-HRP or anti-rat IgG-HRP jn 10% BSA/0,5% Tween-20 in TBS. Proteins were revealed by mean of enhanced chemiluminescence (GE Healthcare) in a BioRad ChemiDoc XRS+. Densitometry analysis was performed using ImageJ (NIH, MD, USA).

Chemotaxis

BMDCs, BMDMs or human macrophages were challenged as indicated, washed, resuspended in CM with 1 mg/mL bovine collagen type I (Sigma) and seeded into gelatin (1%)-coated or uncoated ibiTreat μ-slide chemotaxis chambers (Ibidi, Martinsried, Germany). Collagen was allowed to polymerize for 45 minutes and media, inhibitors and 1,25 μg/mL murine (BMDCs, BMDMs) or human recombinant CCL19 (human macrophages) were added as indicated conform the manufacturer's instructions (application note 23). Cells were then imaged every 2,5 (BMDCs) or 5 (BMDMs, human macrophages) min for 4h (BMDCs) or 8h (BMDMs, human macrophages; Zeiss Observer Z.1). Motility tracks for 35-60 cells per condition were analyzed using ImageJ software for each experiment.

Immunofluorescence microscopy

BMDMs were seeded on gelatin (1%)-coated glass coverslips, challenged freshly egressed *T. gondii* tachyzoites (RH1-1; MOI 2) for 18h and fixed with 2% PFA. Cells were then permeabilized with 0,1 or 1,0% Triton X-100 in PBS and stained with phalloidin Alexa Fluor 594 (Thermo Scientific) or anti-IRF4 and DAPI. Images were acquired on a Leica DMi8 with 63x objective.

Adoptive transfers

Adoptive transfers were performed as previously described (Bhandage et al., 2020). Briefly, BMDMs or BMDCs were stained with CellTracker CMTMR (2 μM) or Deep Red (1 μM) dyes (2,5x10^6 cells each), washed and challenged with freshly egressed *T. gondii* GFP-expressing or CFSE-stained RH tachyzoites (MOI 1,5) or left unchallenged in complete medium for 4h. Cells were then washed and injected i.p. into C57BL/6 mice. Mice were sacrificed 18h post-injection to collect spleens, mesenteric lymph nodes and omenta. The organs were triturated, filtered through 40 μm cell strainer and fixed (4% PFA). Cells from the spleen were briefly subjected to red blood cell lysis (ammonium chloride) prior to fixation, blocked with anti-CD16/32 antibody in FACS buffer (PBS/0,5% FBS/1mM EDTA) and stained with CD11c antibody.

Handling of publicly available datasets

ChIP-seq data available from NCBI GEO series GSE40727 (IRF4), GSE66899 (H3K27ac), GSE64767 (H3K4me3), which are described elsewhere, was visualized in the USCS genome browser (Glasmacher et al., 2012; Grajales-Reyes et al., 2015; Lin et al., 2015). Changes in gene expression by 1 or 2 day treatment of sorted monocytes with GM-CSF and IL-4 were determined from RNA-seq read counts in NCBI GEO serie GSE99837 (Boulet et al., 2019). Microarray data from NCBI GEO series GSE27972 was analyzed with R packages oligo and limma to derive differentially expressed genes upon 6h *T. gondii* (RH) challenge of BMDMs (Morgado et al., 2011).

RNA-seq

For each biological assay, 3 x 10^6 BMDMs were seeded per well in six-well tissue culture plates. Cells were left uninfected or infected with the PruΔ*ku80* and PruΔ*ku80* Δ*gra28* strains (MOI = 6) for 24 hr. Total RNAs were extracted and purified as described previously (Farhat et al., 2020). RNA-sequencing was performed by GENEWIZ (South Plainfield, NJ, USA) as described previously (Farhat et al., 2020).

ChIP-seq assay

HFF cells were infected (MOI = 6) for 24 h with RHΔ*ku80* GRA28–HA–FLAG or GRAx–HA–FLAG. Cells were then cross-linked with 1% formaldehyde for 10 min before quenching with 125 mM glycine for 5 min. The ChIP assay was performed by using the Transcription

Factor Chromatin Immunoprecipitation kit (Diagenode) according to the manufacturer's protocol. In brief, fixed cells were sonicated to shear the cross-linked chromatin into an average DNA fragment size of 200–600 bp. We used 40 × 106 sorted nuclei in 300 μl immunoprecipitation buffer supplemented with fresh proteinase inhibitors. By using a Diagenode Bioruptor precooled to 4 °C, shearing was achieved in 1.5-ml- low-binding tubes in the appropriate tube adaptor with 18 high-energy cycles of 30 sec on and 30 s off. The aforementioned antibodies were used for immunoprecipitation. After an overnight incubation, the DNA–protein–antibody complex was eluted. The crosslinks were reversed by heating the samples at 65 °C for 4 h. DNA was purified by using IPure kit (Diagenode) according to the manufacturer's protocol. 10 ng of your DNA samples were prepared for Illumina sequencing as the following steps: 1) DNA samples were blunt-ended; 2) A dA base was added to the 3' end of each strand; 3) Illumina's genomic adapters were ligated to the DNA fragments; 4) PCR amplification was performed to enrich ligated fragments; 5) Size selection of ~200-1500bp enriched product using AMPure XP beads. The completed libraries were quantified by Agilent 2100 Bioanalyzer. The libraries were denatured with 0.1 M NaOH to generate single-stranded DNA molecules, captured on Illumina flow cell, amplified in situ. The libraries were then sequenced on the Illumina NovaSeq 6000 following the NovaSeq 6000 S4 Reagent Kit (300 cycles) protocol. After the sequencing platform generated the sequencing images, the stages of image analysis and base calling were performed using Off-Line Basecaller software (OLB V1.8). Sequence quality was examined using the FastQC software. After passing Solexa CHASTITY quality filter, the clean reads were aligned to human genome (UCSC HG19) using BOWTIE software (V2.2.7). Aligned reads were used for peak calling of the ChIP regions using MACS V1.4.2. Statistically significant ChIP-enriched regions (peaks) were identified by IP, using a p-value threshold of 10-4. The peaks in samples were annotated by the nearest gene using the newest UCSC RefSeq database. The annotation of the peaks which were located within -2Kb to +2Kb around the corresponding gene TSS in samples can be found from the Peaks_ Promoter_Annotation.xls file. The signal profile (at 10 bp resolution) with UCSC WIG file format was generated from ChIP-seq data, which can be visualized on UCSC genome browser or IGB browser (Integrated Genome Browser, Java Runtime Enviroment needed, http://www.bioviz.org/igb/). All wig flies and a brief guide of visualizing the profiles can be found in Data_Visualization folder.

Chromatographic purification of GRA28-containing complexes

Protein extracts from Raw cells infected with RHΔku80 GRA28-HA–FLAG-tachyzoites were incubated with anti-FLAG M2 affinity gel (Sigma-Aldrich) for 1 hour at 4 °C. Beads were washed with ten column volumes of BC500 buffer (20 mM Tris–HCl, pH 8.0, 500 mM KCl, 20% glycerol, 1 mM EDTA, 1 mM dithiothreitol, 0.5% NP-40 and protease inhibitors). The bound polypeptides were eluted stepwise with 250 μg ml−1 FLAG peptide (Sigma-Aldrich) diluted in BC100 buffer. For size-exclusion chromatography, protein eluates were loaded onto a Superose 6 HR 10/30 column equilibrated with BC500. The flow rate was fixed at 0.35 ml min−1 and 0.5-ml fractions were collected.

Mass spectrometry-based proteomics

Proteins contained in fractions from size-exclusion chromatography of GRA28-containing complexes purified by FLAG co-immunoprecipitation were solubilized in Laemmli buffer and stacked in in the top of a 4-12% NuPAGE gel (Invitrogen). After staining with R-250 Coomassie Blue (Biorad), proteins were digested in-gel using trypsin (modified, sequencing purity, Promega), as previously described. The resulting peptides were analyzed by online nanoliquid chromatography coupled to MS/MS (Ultimate 3000 RSLCnano and Q-Exactive Plus, Thermo Fisher Scientific) using a 140 min gradient. For this purpose, the peptides were sampled on a precolumn (300 μm x 5 mm PepMap C18, Thermo Scientific) and separated in a 75 μm x 250 mm C18 column (Reprosil-Pur 120 C18-AQ, 1.9 μm, Dr. Maisch). The MS and MS/MS data were acquired by Xcalibur (Thermo Fisher Scientific). Peptides and proteins were identified by Mascot (version 2.6.0, Matrix Science) through concomitant searches against the *T. gondii* database (ME49 taxonomy, v.30, downloaded from ToxoDB), the Uniprot database (Mus musculus taxonomy, August 2019 version), and a homemade database containing the sequences of classical contaminant proteins found in proteomic analyses (bovine albumin, keratins, trypsin, etc.). Trypsin/P was chosen as the enzyme and two missed cleavages were allowed. Precursor and fragment mass error tolerances were set at respectively at 10 ppm and 25 mmu. Peptide modifications allowed during the search were: Carbamidomethyl (C, fixed), Acetyl (Protein N-term, variable) and Oxidation (M, variable). The Proline software was used for the compilation, grouping, and filtering of the results (conservation of rank 1 peptides, peptide length ≥ 7, PSM score ≥ 25, false discovery rate of peptide-spectrum-match identifications < 1% as calculated on peptide-spectrum-match scores by employing the reverse database strategy, and a minimum of 1 specific peptide per identified protein group). Proline was then used to perform a compilation, grouping and MS1 quantification, based on razor and specific peptides, of the identified protein groups. Proteins from the contaminant database were discarded from the final list of identified proteins. Proteins in each sample were further quantified through calculation of their corresponding intensity-based absolute quantification values (iBAQ). The MS proteomics data have been deposited to the ProteomeXchange Consortium through the PRIDE partner repository with the dataset identifier PXD032360.

QUANTIFICATION AND STATISTICAL ANALYSIS

Western blot analysis was performed by band intensity quantification with ImageJ. qPCR results were analyzed using the ΔCq and ΔΔCq methods from Cq values provided by QuantStudio Design and Analysis Desktop Software. Cell tracks were obtained by manual tracking with ImageJ from image sequence files. Speeds and endpoints from individual cells were calculated and derived from these tracks with the Chemotaxis and Migration Tool and combined with track lengths calculated with R and RStudio. Flow

cytometry data in FCS files was analyzed with FlowJo X. Quantification of RNA-seq and proteomics data was performed as described in the method details. Details on the software used can be found in the key resources table.

Statistical analyses

Volcano plots, scatter plots, and histograms were generated with Prism. Statistical analyses were performed with R, RStudio and packages afex (repeated-measures ANOVA), emmeans (Dunnett's and Holm-Bonferroni post-hoc), DAAG and rcompanion (one sample permutation). Statistical significance is defined as $p < 0,05$. The figure legends detail which hypothesis tests were employed, chosen based on experimental design, the hypothesis to be tested and data distribution, and which statistics are presented. All experiments were performed in biological replicates to allow for statistical analyses and in independent biological replicates as stated for each experiment in the manuscript. The number of *n* denotes the number of biological replicates (adoptive transfer experiments) or independent experiments.

Cell Host & Microbe, Volume *30*

Supplemental information

The *Toxoplasma* effector GRA28 promotes parasite dissemination by inducing dendritic cell-like migratory properties in infected macrophages

Arne L. ten Hoeve, Laurence Braun, Matias E. Rodriguez, Gabriela C. Olivera, Alexandre Bougdour, Lucid Belmudes, Yohann Couté, Jeroen P.J. Saeij, Mohamed-Ali Hakimi, and Antonio Barragan

Fig. S1

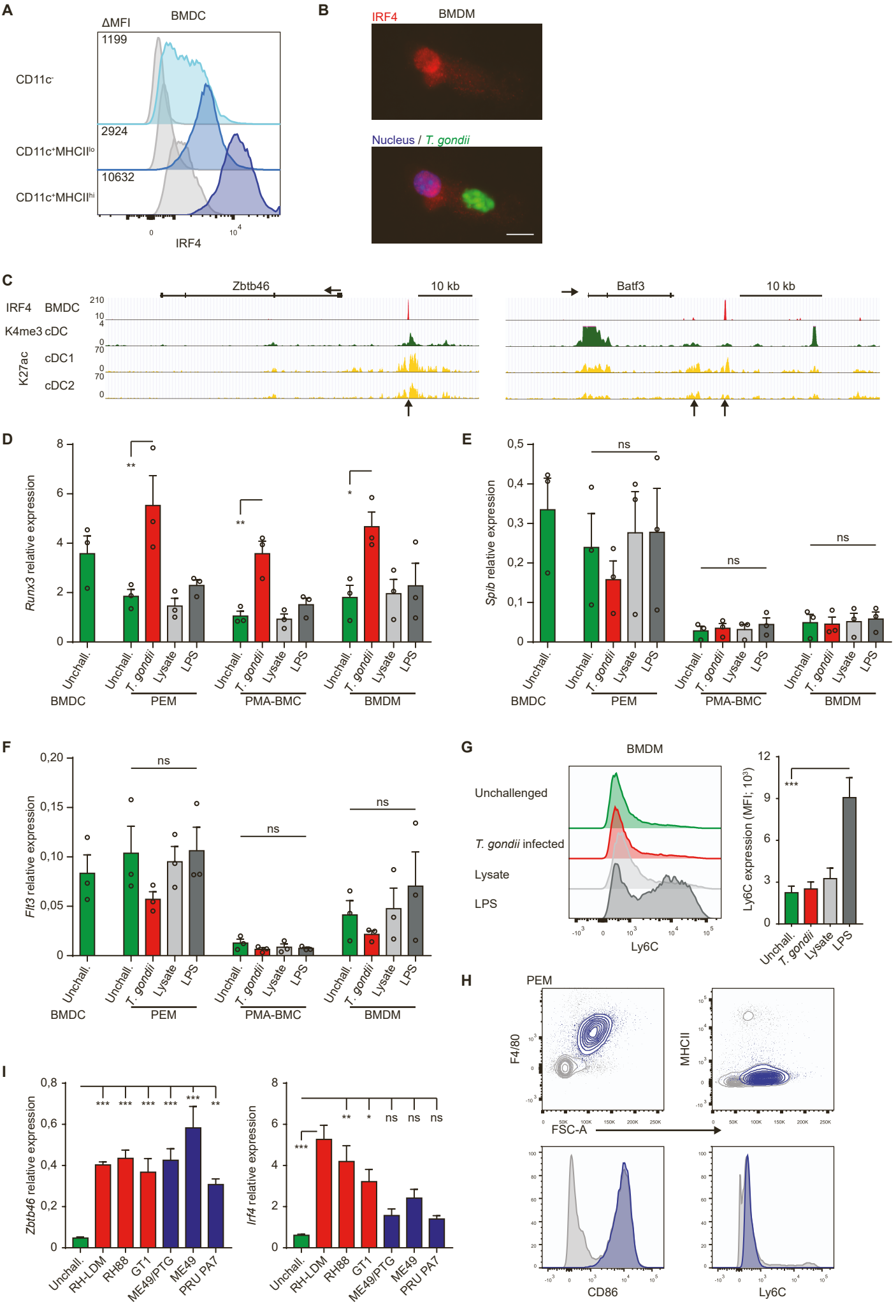
A
ΔMFI
BMDC
1199
2924
10632
CD11c-
CD11c+MHCIIlo
CD11c+MHCIIhi
IRF4
B
IRF4
BMDM
Nucleus / T. gondii
C
Zbtb46
10 kb
Batf3
IRF4 BMDC
K4me3 cDC
K27ac cDC1
cDC2
D
Runx3 relative expression
Unchall.
T. gondii
Lysate
LPS
BMDC
PEM
PMA-BMC
BMDM
E
Spib relative expression
ns
F
Flt3 relative expression
G
BMDM
Unchallenged
T. gondii infected
Lysate
LPS
Ly6C
Ly6C expression (MFI; 10³)
H
PEM
F4/80
FSC-A
MHCII
CD86
Ly6C
I
Zbtb46 relative expression
Irf4 relative expression
Unchall.
RH-LDM
RH88
GT1
ME49/PTG
ME49
PRU PA7

Figure S1. Related to Figure 1.

Expression of DC-associated transcription factors in *T. gondii*-challenged macrophages

(**A**) Flow cytometric analysis of anti-IRF4 and isotype control staining in unchallenged BMDC subsets.

(**B**) Representative micrograph of a BMDMs challenged for 18h and infected with freshly egressed GFP-expressing *T. gondii* type I tachyzoites (MOI 2; green) stained with anti-IRF4 antibody (red) and DAPI (nuclei; blue).

(**C**) ChIP-seq tracks for IRF4, H3K4me3 (K4me3) and H3K27ac (K27ac) at the *Zbtb46* and *Batf3* loci in GM-CSF/IL-4 BMDCs (BMDC), Sirpα^{+} BMDCs (cDC2), CD24^{+} BMDCs (cDC1). Black arrows indicate IRF4 binding associated with H3K4me3 and H3K27ac. Dataset sources can be found in the Method details.

(**D, E, F**) qPCR analysis of *Runx3*, *Spib* and *Flt3* cDNA from BMDCs and macrophages challenged as in (A) with MOI 2 or equivalent. Relative expression ($2^{-\Delta Cq}$) is displayed as mean+SE and individual measurements (n = 3).

(**G**) Flow cytometric analyses of anti-Ly6C staining on BMDMs challenged as in (A). The bar graph depicts the anti-Ly6C MFI (mean+SE) of 3 independent experiments.

(**H**) Representative flow cytometric analysis of anti-F4/80, MHCII, CD86 and Ly6C staining of CD11b^{hi}CD11c^{-}CD19^{-} PEMs as gated in fig. 1I (blue). For reference, all CD19^{-} peritoneal cells are displayed as well (grey).

(**I**) qPCR analysis of *Zbtb46* and *Irf4* cDNA from BMDMs challenged with *T. gondii* type I RH-LDM, RH88 or GT1 or type II ME49/PTG, ME49 or PRU PA7 (MOI 2). Relative expression ($2^{-\Delta Cq}$) is displayed as mean+SE and individual measurements (n = 3).

Statistical comparisons were made with ANOVA and Dunnett's post-hoc tests (D-G, I; * $p \leq 0{,}05$, ** $p \leq 0{,}01$, *** $p \leq 0{,}001$, ns $p > 0{,}05$).

Figure S2

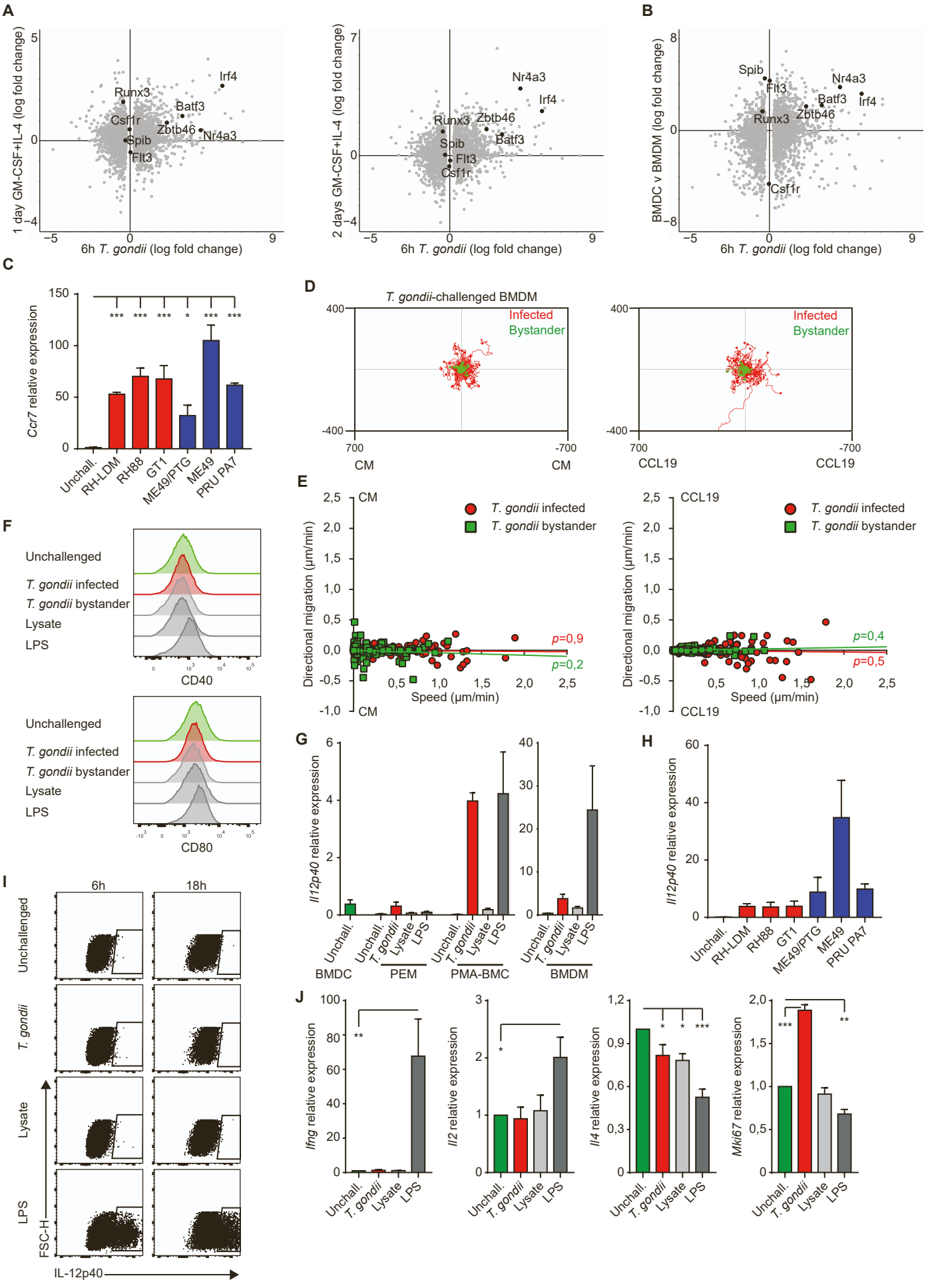
A
1 day GM-CSF+IL-4 (log fold change)
6h T. gondii (log fold change)
Irf4
Runx3
Batf3
Csf1r
Zbtb46
Nr4a3
Spib
Flt3
2 days GM-CSF+IL-4 (log fold change)
B
BMDC v BMDM (log fold change)
C
Ccr7 relative expression
Unchall.
RH-LDM
RH88
GT1
ME49/PTG
ME49
PRU PA7
D
T. gondii-challenged BMDM
Infected
Bystander
CM
CCL19
E
Directional migration (µm/min)
Speed (µm/min)
T. gondii infected
T. gondii bystander
p=0,9
p=0,2
p=0,4
p=0,5
F
Unchallenged
T. gondii infected
T. gondii bystander
Lysate
LPS
CD40
CD80
G
Il12p40 relative expression
BMDC
PEM
PMA-BMC
BMDM
H
I
6h
18h
T. gondii
FSC-H
IL-12p40
J
Ifng relative expression
Il2 relative expression
Il4 relative expression
Mki67 relative expression

Figure S2. Related to Figure 2

Chemotaxis to CCL19 by *T. gondii*-challenged macrophages

(**A**) Dot plot showing the gene expression differences between BMDMs challenged with *T. gondii* type I tachyzoites for 6h and BMDMs left unchallenged and between murine monocytes stimulated with GM-CSF+IL-4 for 1 or 2 days and sorted monocytes. Dataset sources can be found in the Method details.

(**B**) Dot plot showing the gene expression differences between BMDMs challenged with *T. gondii* type I tachyzoites for 6h and BMDMs left unchallenged and between BMDCs and BMDMs.

(**C**) qPCR analysis of *Ccr7* cDNA from BMDMs challenged with *T. gondii* type I RH-LDM, RH88 or GT1 or type II ME49/PTG, ME49 or PRU PA7 (MOI 2). Relative expression ($2^{-\Delta Cq}$) is displayed as mean+SE and individual measurements (n = 3). Statistical comparisons were made with ANOVA and Dunnett's post-hoc tests (* $p \leq 0,05$, *** $p \leq 0,001$).

(**D**) Motility plots depict the displacement of unchallenged BMDMs challenged with freshly egressed *T. gondii* type I over 12 h in a collagen matrix in the absence of CCL19 (CM) or in the presence of CCL19 sources on both sides as detailed in Method details (scale indicates µm).

(**E**) For each condition, directional migration (µm/min) towards the left and speed (µm/min) of individual cells are displayed, with linear regression lines. Infected cells (GFP^+, red) and non-infected bystander cells (GFP^-, green) were analyzed. In the absence of CCL19, infected (0,34 µm/min mean speed) were significantly faster than non-infected bystander cells (0,19 µm/min mean speed, $p < 0,001$). For each condition, p-values indicate the directional migration compared to hypothetical zero directionality (one-sample permutation test). Data from 3 independent experiments.

(**F**) Flow cytometric analyses of anti-CD40 and CD80 staining on BMDMs challenged for 18 h with freshly egressed *T. gondii* type I tachyzoites (MOI 1), tachyzoite lysate (MOI 1 equivalent) or LPS (10 ng/mL). Data is representative of 2 independent experiments.

(**G**) qPCR analysis of *Il12p40* cDNA from macrophages challenged as in (F) with MOI 2 or equivalents. For reference, macrophages and BMDCs were incubated in complete medium, unchallenged (unchall.). Relative expression ($2^{-\Delta Cq}$) is displayed as mean+SE.

(**H**) qPCR analysis of *Il12p40* cDNA from BMDMs challenged as in (C). Relative expression ($2^{-\Delta Cq}$) is displayed as mean+SE.

(**I**) Flow cytometric analyses of anti-IL-12p40 staining in BMDMs challenged for 18 h with *T. gondii* type I tachyzoites (MOI 1), tachyzoite lysate (MOI 1 equivalent) or LPS (10 ng/mL) or left unchallenged (unchall.). Data is representative of 3 independent experiments.

(**J**) qPCR analysis of *Ifng*, *Il2*, *Il4* and *Mki67* in syngeneic mixed leukocytes reactions (MLR) of BMDMs challenged with *T. gondii* tachyzoites, tachyzoite lysate or LPS as in (G) for 4h and mixed with

splenocytes for 18h. Relative expression ($2^{-\Delta\Delta Cq}$) is displayed as mean+SE (normalized to 1; n = 4). Statistical comparisons were made with ANOVA and Dunnett's post-hoc tests on log-transformed (*Ifng*) or non-transformed data (* $p \leq 0{,}05$, ** $p \leq 0{,}01$, *** $p \leq 0{,}001$).

Figure S3

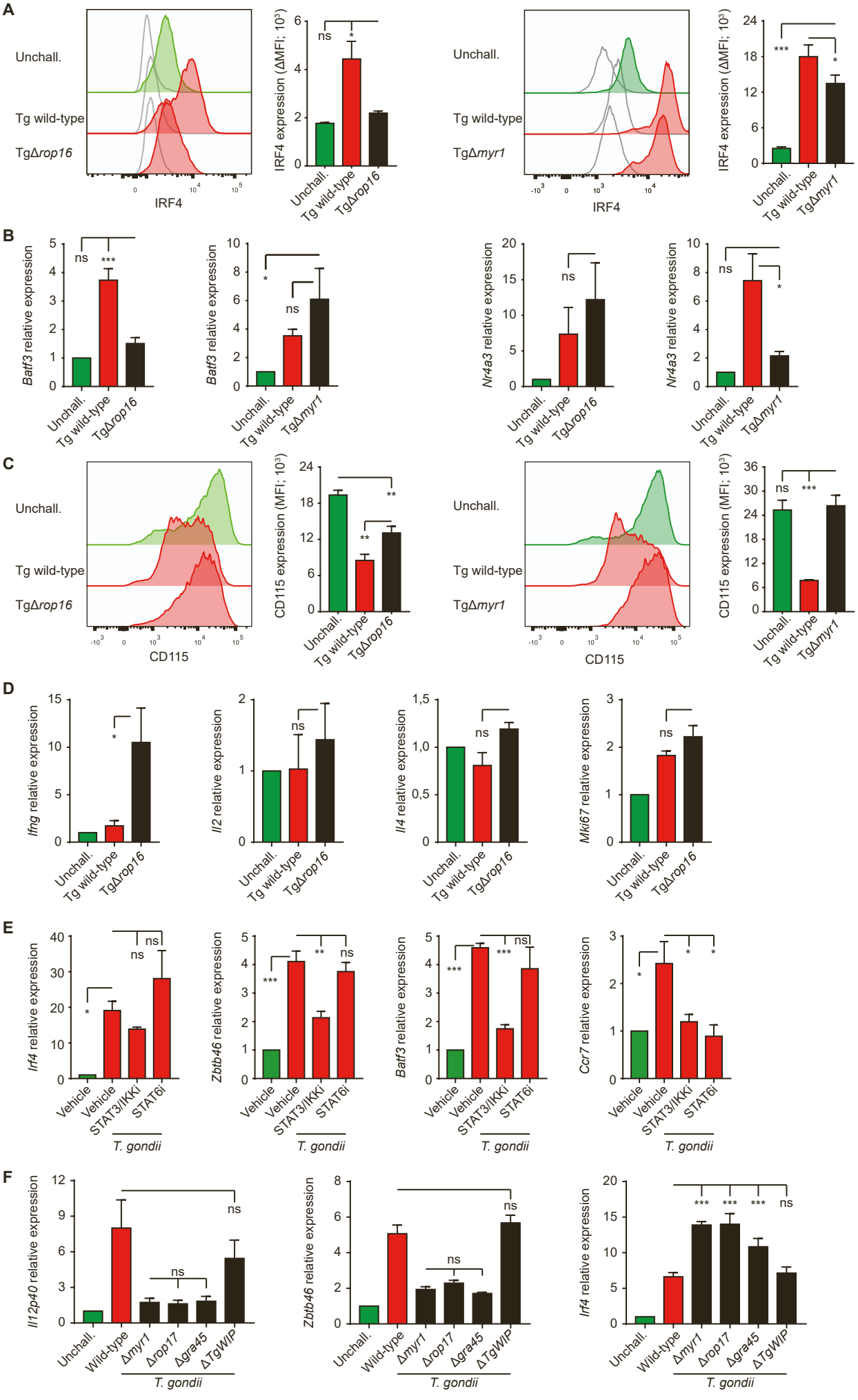
A
Unchall.
Tg wild-type
TgΔrop16
IRF4
IRF4 expression (ΔMFI; 10³)
Unchall.
Tg wild-type
TgΔrop16
Unchall.
Tg wild-type
TgΔmyr1
IRF4
IRF4 expression (ΔMFI; 10³)
Unchall.
Tg wild-type
TgΔmyr1
B
Batf3 relative expression
Unchall.
Tg wild-type
TgΔrop16
Batf3 relative expression
Unchall.
Tg wild-type
TgΔmyr1
Nr4a3 relative expression
Unchall.
Tg wild-type
TgΔrop16
Nr4a3 relative expression
Unchall.
Tg wild-type
TgΔmyr1
C
Unchall.
Tg wild-type
TgΔrop16
CD115
CD115 expression (MFI; 10³)
Unchall.
Tg wild-type
TgΔrop16
Unchall.
Tg wild-type
TgΔmyr1
CD115
CD115 expression (MFI; 10³)
Unchall.
Tg wild-type
TgΔmyr1
D
Ifng relative expression
Unchall.
Tg wild-type
TgΔrop16
Il2 relative expression
Unchall.
Tg wild-type
TgΔrop16
Il4 relative expression
Unchall.
Tg wild-type
TgΔrop16
Mki67 relative expression
Unchall.
Tg wild-type
TgΔrop16
E
Irf4 relative expression
Vehicle
Vehicle
STAT3/IKKi
STAT6i
T. gondii
Zbtb46 relative expression
Vehicle
Vehicle
STAT3/IKKi
STAT6i
T. gondii
Batf3 relative expression
Vehicle
Vehicle
STAT3/IKKi
STAT6i
T. gondii
Ccr7 relative expression
Vehicle
Vehicle
STAT3/IKKi
STAT6i
T. gondii
F
Il12p40 relative expression
Unchall.
Wild-type
Δmyr1
Δrop17
Δgra45
ΔTgWIP
T. gondii
Zbtb46 relative expression
Unchall.
Wild-type
Δmyr1
Δrop17
Δgra45
ΔTgWIP
T. gondii
Irf4 relative expression
Unchall.
Wild-type
Δmyr1
Δrop17
Δgra45
ΔTgWIP
T. gondii

Figure S3. Related to Figure 3.

Impact of parasite-derived secreted effectors on gene expression

(**A**) Flow cytometric analyses of anti-IRF4 and isotype control staining in BMDMs challenged for 18h with freshly egressed *T. gondii* type I (Tg) wild-type (MOI 1 or 2), MYR1-deficient (TgΔ*myr1*; MOI 1) or ROP16 deficient (TgΔ*rop16*; MOI 2) tachyzoites or left unchallenged (unchall.). For Tg wild-type/TgΔ*myr1* experiments cells were gated for GFP^+. The bar graph depicts the difference between anti-IRF4 and isotype MFI (mean+SE).

(**B**) qPCR analysis of *Batf3* and *Nr4a3* in BMDMs challenged as in (A) with MOI 2 or left unchallenged. Relative expression ($2^{-\Delta\Delta Cq}$) is displayed as mean+SE related to unchallenged (normalized to 1).

(**C**) Flow cytometric analyses of anti-CD115 staining in BMDMs challenged and displayed as in (A).

(**D**) qPCR analysis of *Irf4*, *Zbtb46*, *Batf3* and *Ccr7* cDNA of BMDMs treated with TPCA-1 (STAT3/IKKi), AS1517499 (STAT6i) or DMSO (Vehicle) for 1h and then challenged for 6h with freshly egressed *T. gondii* type I wild-type tachyzoites (MOI 3) or left unchallenged, displayed as in (B).

(**E**) qPCR analysis of *Ifng*, *Il2*, *Il4* and *Mki67* in syngeneic mixed leukocytes reactions (MLR) of BMDMs challenged RH or RHΔrop16 tachyzoites (MOI 2) or left unchallenged for 4h and mixed with splenocytes for 18h, displayed as in (B).

(**F**) qPCR analysis of *Il12p40*, *Zbtb46* and *Irf4* in BMDM challenged with type I wild-type (Tg), TgΔ*myr1*, TgΔ*rop17*, TgΔ*gra45* or TgΔ*Tgwip* tachyzoites and displayed as in (B).

All datasets are from 3-4 independent experiments. Statistical comparisons were made with ANOVA and Dunnett's (A-E) or Holm-Bonferroni (F) post-hoc tests (* $p \leq 0{,}05$, * $p \leq 0{,}01$, *** $p \leq 0{,}001$, ns $p > 0{,}05$).

Figure S4

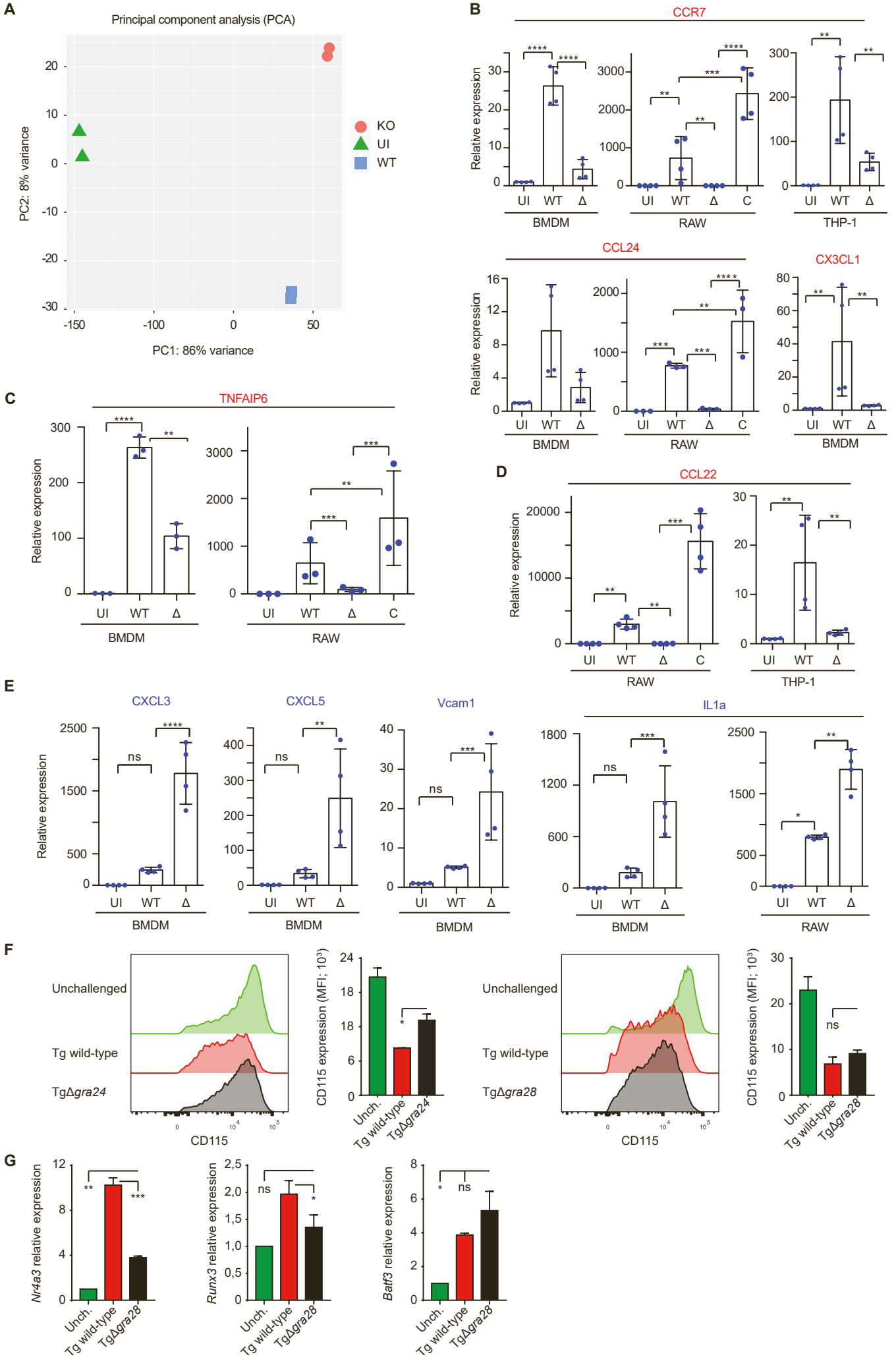
A
Principal component analysis (PCA)
PC2: 8% variance
PC1: 86% variance
KO
UI
WT
B
CCR7
CCL24
CX3CL1
Relative expression
BMDM
RAW
THP-1
C
TNFAIP6
D
CCL22
E
CXCL3
CXCL5
Vcam1
IL1a
ns
F
Unchallenged
Tg wild-type
TgΔgra24
TgΔgra28
CD115
CD115 expression (MFI; 10³)
Unch.
G
Nr4a3 relative expression
Runx3 relative expression
Batf3 relative expression

Figure S4. Related to Figure 4.

GRA28 activates and represses host gene expression.

(**A**) Principal component analysis (PCA) shows the biological and technical variability between samples after Illumina sequencing of mRNA extracted in duplicate from uninfected BMDMs (UI) or infected with WT or Δ*gra28*.

(**B**, **C**, **D** and **E**) BALB/c BMDMs, RAW or THP-1 macrophages were either left uninfected (UI) or infected for 24 h with WT, Δ*gra28* (Δ) or TgΔ*gra28*+GRA28 (C), the complemented line of type II (Pru) tachyzoites. The levels of GOI mRNA were determined by RT–qPCR. The values were normalized to the amount of TBP. Statistical analysis was done by One-way ANOVA followed with Tukey's multiple comparison test (** $p \leq 0,01$, *** $p \leq 0,001$, **** $p \leq 0,0001$, ns $p > 0,05$). Data are the mean ± s.d. of three or more biological replicates.

(**F**) Flow cytometric analysis of anti-CD115 staining on BMDMs challenged with type I (RH) wild-type, GRA24-deficient (Δ*gra24*) or GRA28-deficient (Δ*gra28*) *T. gondii* tachyzoites for 18h (MOI 2) or left unchallenged. The bar graph depicts the staining MFI (mean+SE) of 3 independent experiments. Statistical comparisons were made with ANOVA and Dunnett's post-hoc tests (* $p \leq 0,05$, ns $p > 0,05$).

(**G**) qPCR analysis of *Nr4a3*, *Runx3* and *Batf3* cDNA expression in BMDMs challenged with type I wild-type, Δ*gra24* or Δ*gra28* tachyzoites (Tg) for 18h (MOI 2) or left unchallenged. Relative expression ($2^{-\Delta\Delta Cq}$) is displayed as mean+SE related to unchallenged (normalized to 1; n = 3). Statistical comparisons were made with ANOVA and Dunnett's post-hoc tests (* $p \leq 0,05$, * $p \leq 0,01$, *** $p \leq 0,001$, ns $p > 0,05$).

Fig. S5

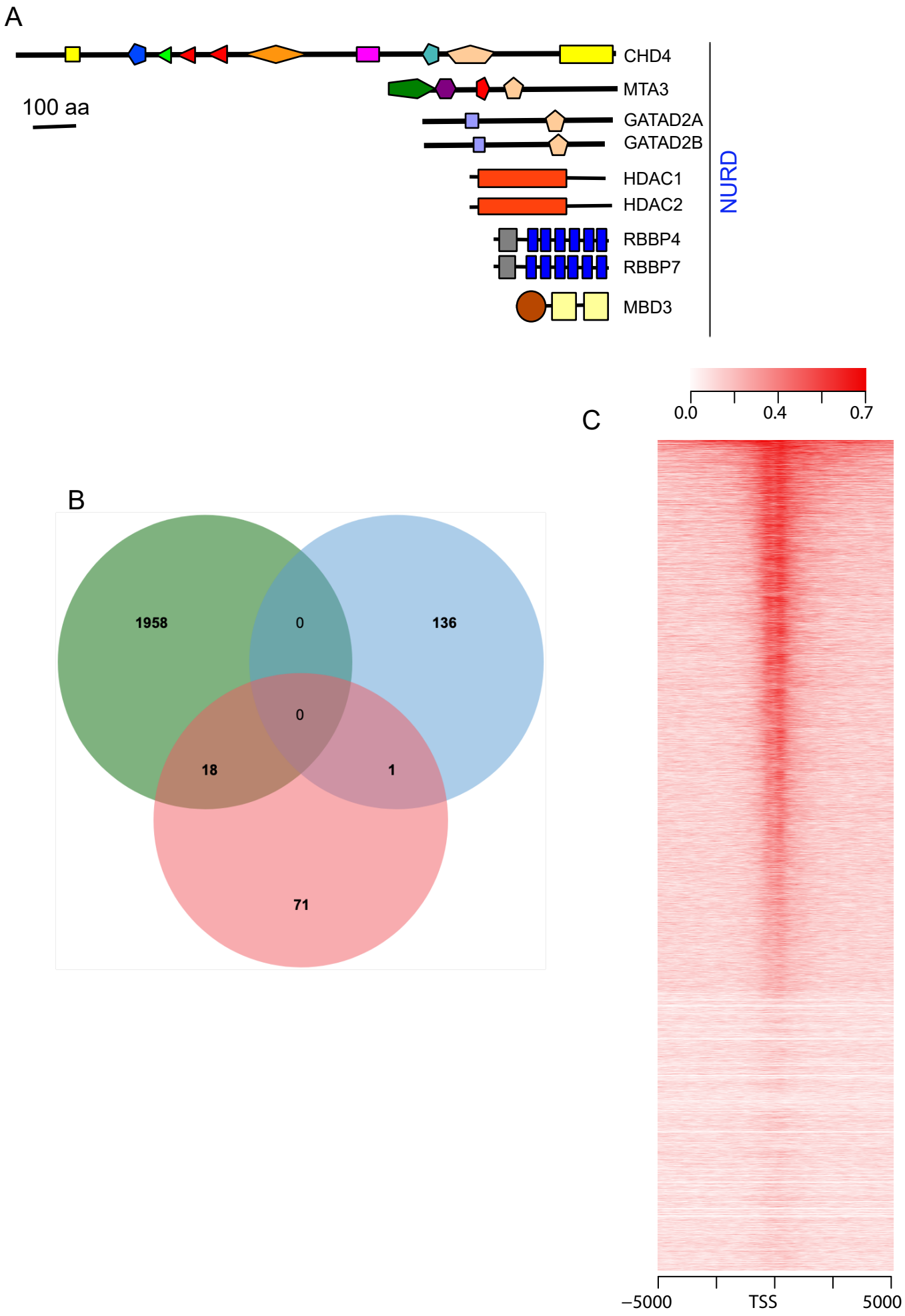
A
100 aa
CHD4
MTA3
GATAD2A
GATAD2B
HDAC1
HDAC2
RBBP4
RBBP7
MBD3
NURD
B
1958
0
136
0
18
1
71
C
0.0
0.4
0.7
−5000
TSS
5000

Figure S5. Related to Figure 5.

GRA28 acts as a chromatin regulator of gene expression.

(**A**) Representative domain architectures of the NuRD subunits associated to GRA28 are shown. Domains were predicted by SMART and PFAM.

(**B**) Venn diagram illustrating the overlap between the number of genes bound by GRA28 (in green), GRAx (in blue) and up-or down-regulated by GRA28 (green).

(**C**) Heatmap of GRA28 ChIP-seq signal genome-wide in HFF cells, ± 5 kb from the center of the binding site.

Figure S6

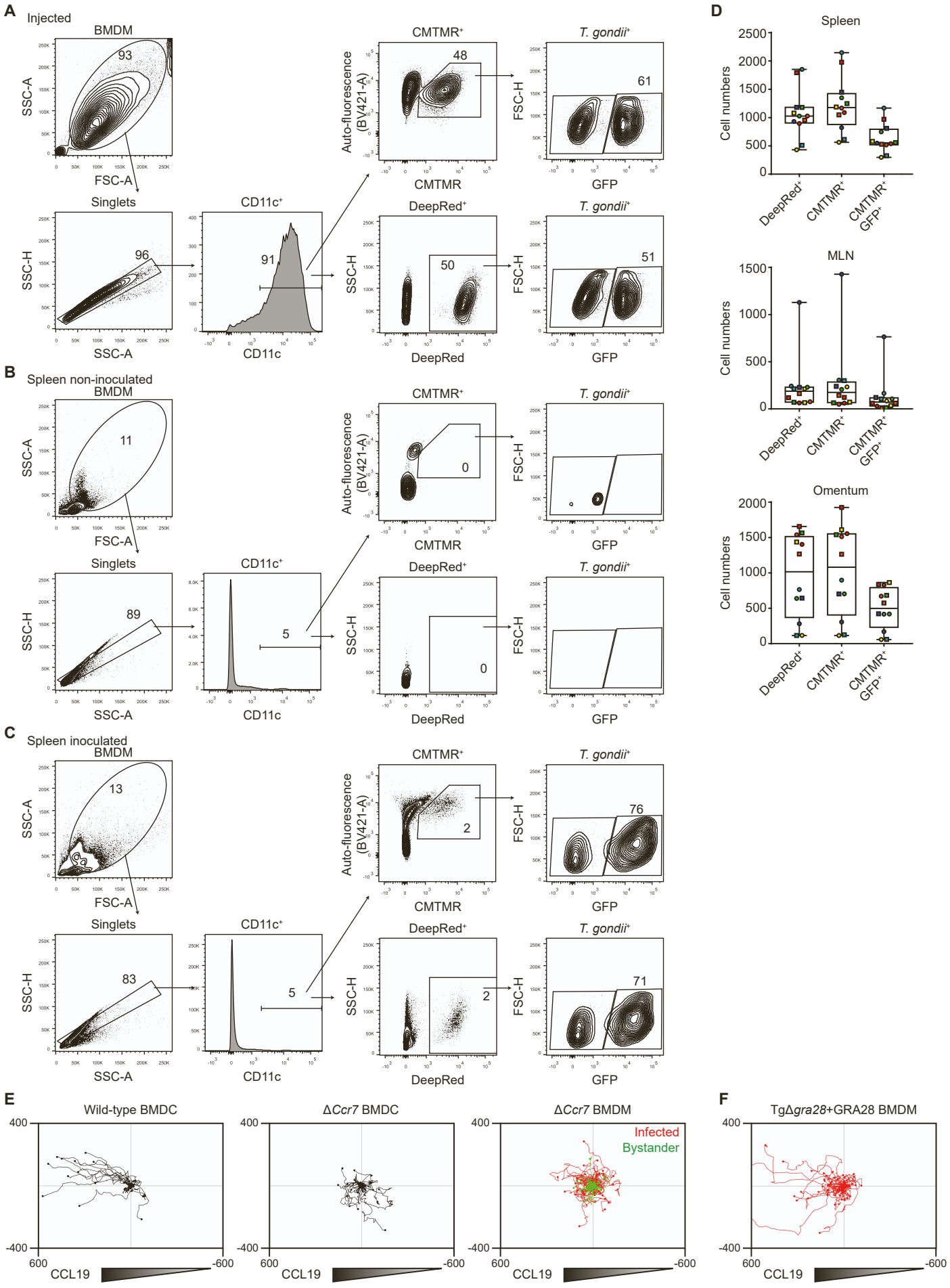
A
Injected
BMDM
93
SSC-A
FSC-A
Singlets
96
SSC-H
SSC-A
CD11c+
91
CD11c
CMTMR+
48
Auto-fluorescence (BV421-A)
CMTMR
T. gondii+
61
FSC-H
GFP
DeepRed+
50
SSC-H
DeepRed
T. gondii+
51
FSC-H
GFP
B
Spleen non-inoculated
BMDM
11
SSC-A
FSC-A
Singlets
89
SSC-H
SSC-A
CD11c+
5
CD11c
CMTMR+
0
Auto-fluorescence (BV421-A)
CMTMR
T. gondii+
FSC-H
GFP
DeepRed+
0
SSC-H
DeepRed
T. gondii+
FSC-H
GFP
C
Spleen inoculated
BMDM
13
SSC-A
FSC-A
Singlets
83
SSC-H
SSC-A
CD11c+
5
CD11c
CMTMR+
2
Auto-fluorescence (BV421-A)
CMTMR
T. gondii+
76
FSC-H
GFP
DeepRed+
2
SSC-H
DeepRed
T. gondii+
71
FSC-H
GFP
D
Spleen
Cell numbers
2500
2000
1500
1000
500
0
DeepRed+
CMTMR+
CMTMR+ GFP+
MLN
Cell numbers
1500
1000
500
0
DeepRed+
CMTMR+
CMTMR+ GFP+
Omentum
Cell numbers
2000
1500
1000
500
0
DeepRed+
CMTMR+
CMTMR+ GFP+
E
Wild-type BMDC
ΔCcr7 BMDC
ΔCcr7 BMDM
Infected
Bystander
400
-400
600
-600
CCL19
F
TgΔgra28+GRA28 BMDM
400
-400
600
-600
CCL19

Figure S6. Related to Figure 6.

Gating strategy of adoptive transfer experiments

(**A**, **B**, **C**) Typical gating for CD11c$^+$ BMDMs stained with CellTracker Deep Red (DeepRed$^+$) or CMTMR and infected with wild-type *T. gondii* tachyzoites (*T. gondii*$^+$) pre-inoculation (A) or in the spleen of non-inoculated (B) or inoculated (C) mice.

(**D**) Numbers of detected cells in spleens, MLNs and omenta of mice inoculated with unchallenged CellTracker Deep Red (DeepRed$^+$) and CMTMR$^+$ *T. gondii* wild-type-challenged BMDMs, 18h post-inoculation, gated as in (C). Graphs depict median (±25/75 percentiles and min/max) and individual mice (n=12).

(**E**) Motility plots of unchallenged wild-type or CCR7-deficient (Δ*Ccr7*) BMDCs and 12h type I (RH) *T. gondii*-challenged CCR7-deficient BMDMs (Δ*Ccr7*) in a CCL19 gradient as detailed in the Method details. Infected cells (GFP$^+$, red, 0,39 µm/min mean speed) were significantly faster than non-infected bystander cells (GFP$^-$, green, 0,27 µm/min mean speed, p = 0,01). Plots are representative of 2 (BMDCs) or display 3 independent experiments (BMDM).

(**F**) Motility plot of wild-type BMDMs challenged with the CFSE-stained RHΔ*gra28*+GRA28 strain for 12-14h in a CCL19 gradient as detailed in the Method details. Infected cells (CFSE$^+$) were analyzed. Cell tracks of 3 independent experiments are displayed.

Related to figure 6.

Figure S7

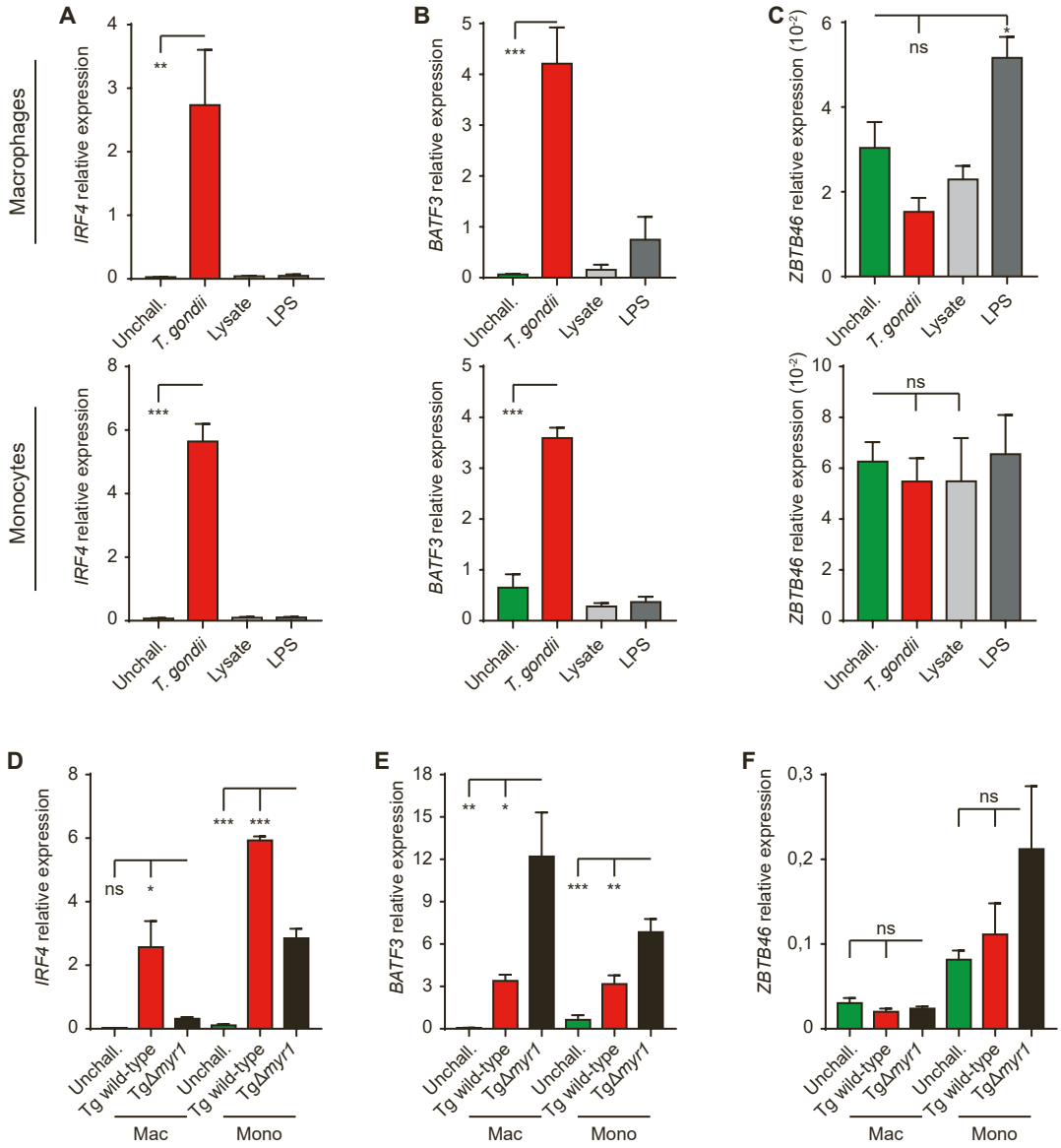
A
B
C
Macrophages
Monocytes
IRF4 relative expression
BATF3 relative expression
ZBTB46 relative expression (10-2)
Unchall.
T. gondii
Lysate
LPS
ns
D
E
F
Tg wild-type
TgΔmyr1
Mac
Mono

Figure S7. Related to Figure 7.

Expression of DC-associated transcription factors in *T. gondii*-challenged human monocytic cells

(**A**, **B**, **C**) qPCR analysis of *IRF4* (A), *BATF3* (B) and *ZBTB46* (C) cDNA from human macrophages and monocytes challenged for 18 h with freshly egressed *T. gondii* type I tachyzoites (MOI 2), tachyzoite lysate (ME49; MOI 2 equivalent) or LPS (10 ng/mL) or left unchallenged (unchall.). Relative expression ($2^{-\Delta Cq}$) is displayed as mean+SE (n = 4-5).

(**D**, **E**, **F**) qPCR analysis of *IRF4* (d), *BATF3* (e) and *ZBTB46* (f) cDNA from human monocytes and macrophages challenged type I (Tg) wild-type or MYR1-deficient (TgΔ*myr1*) tachyzoites as in (A) (n = 4).

Table S3. Primers used in this study, related to STAR Methods

OLIGONUCLEOTIDE	SOURCE	IDENTIFIER
Primer murine Zbtb46 forward: AGAGAGCACATGAAGCGACA	[S1]	N/A
Primer murine Zbtb46 reverse: CTGGCTGCAGACATGAACAC	[S1]	N/A
Primer murine Irf4 forward: CTCATCACAGCTCATGTGG	This manuscript	N/A
Primer murine Irf4 reverse: CCTCAGGAAATGTCCAGTG	This manuscript	N/A
Primer murine Runx3 forward: TGATGAGAACTACTCCGCC	This manuscript	N/A
Primer murine Runx3 reverse: AGCGTGAAACTCTTCCCTC	This manuscript	N/A
Primer murine Spib forward: CCAGAAGGAGTCTTCTACGAC	This manuscript	N/A
Primer murine Spib reverse: CCATGTAGAGTCAAGGCCC	This manuscript	N/A
Primer murine Batf3 forward: AGGTCAAATCTCAGAGCCC	This manuscript	N/A
Primer murine Batf3 reverse: TTCTGGGTCTGCTTCTTCC	This manuscript	N/A
Primer murine Flt3 forward: TACCTACTCCATATTCAGAGCG	This manuscript	N/A
Primer murine Flt3 reverse: CACGTACAGCTGTGTATCTC	This manuscript	N/A
Primer murine Ccr7 forward: CCAGGTGTGCTTCTGCCAAG	This manuscript	N/A
Primer murine Ccr7 reverse: AAAGTTCCGCACATCCTTCT	This manuscript	N/A
Primer murine Nr4a3 forward: ATGGTTAAGGAAGTTGTGCG	This manuscript	N/A
Primer murine Nr4a3 reverse: TTGTAGTGGGCTCTTTGGT	This manuscript	N/A
Primer murine Il4 forward: GATTCATCGATAAGCTGCACC	This manuscript	N/A
Primer murine Il4 reverse: CATGATGCTCTTTAGGCTTTCC	This manuscript	N/A
Primer murine Mki67 forward: AGACAATCATCAAGGAACGG	This manuscript	N/A
Primer murine Mki67 reverse: TTTGATCATTTGTCCTCGGT	This manuscript	N/A
Primer murine Il2 forward: GGATGGAGAATTACAGGAACC	[S2]	N/A
Primer murine Il2 reverse: GAAGATCTTTCAATTCTGTGGC	[S2]	N/A

Primer murine Il12p40 forward: TCCCTCAAGTTCTTTGTTCG	[S2]	N/A
Primer murine Il12p40 reverse: CGCACCTTTCTGGTTACAC	[S2]	N/A
Primer murine Egr1 forward: TTCAATCCTCAAGGGGAGCC	[S2]	N/A
Primer murine Egr1 reverse: AAAGGACTCTGTGGTCAGGTG	[S2]	N/A
Primer murine Tbp forward: GGGGAGCTGTGATGTGAAGT	[S3]	N/A
Primer murine Tbp reverse: CCAGGAAATAATTCTGGCTCA	[S3]	N/A
Primer murine Ipo8 forward: CTATGCTCTCGTTCAGTATGC	[S3]	N/A
Primer murine Ipo8 reverse: GTCCGAAAGATCTCCATCCA	[S3]	N/A
Primer human Zbtb46 forward: CGGGAAGAAGTTCACGCGG	[S4]	N/A
Primer human Zbtb46 reverse: CTGCACACCTTGCACACATAC	[S4]	N/A
Primer human Batf3 forward: TCCATGAGGAATATGAGAGCC	This manuscript	N/A
Primer human Batf3 reverse: CTCCTTCAGTGCCTCTGTC	This manuscript	N/A
Primer human Irf4 forward: CAGGATTGTTCCTGAGGGAG	This manuscript	N/A
Primer human Irf4 reverse: TAGTTGTGAACCTGCTGGG	This manuscript	N/A
Primer human Ccr7 forward: TCAAGACCATGACCGATACC	This manuscript	N/A
Primer human Ccr7 reverse: AGGAGGAAGAGGATGTCTG	This manuscript	N/A
Primer human Ipo8 forward: GCAAAGGAAGGGGAATTGAT	[S2]	N/A
Primer human Ipo8 reverse: CGAAGCTCACTAGTTTTGACCC	[S2]	N/A
Primer human Tbp forward: GAGCTGTGATGTGAAGTTTCC	[S2]	N/A
Primer human Tbp reverse: TCTGGGTTTGATCATTCTGTAG	[S2]	N/A
LIC-231960-F primer: TACTTCCAATCCAATTTAGCaccaaggacacatctgtcctctac	This manuscript	N/A
LIC-231960-R primer: TCCTCCACTTCCAATTTTAGCttcggaataactggagctaccg c	This manuscript	N/A
GRA28-gRNA-Fwd: 5'-AAGTTGCCGCGTCACCTTGAACGCGG-3'	This manuscript	N/A

GRA28-gRNA-Rev: 5'-AAAACCGCGTTCAAGGTGACGCGGCA-3'	This manuscript	N/A
LICF-P_{GRA28}_F primer: 5'-TACTTCCAATCCAATTTAGCGGCCACACAGAGTCCCCTGTGG-3'	This manuscript	N/A
LICR-GRA28_R primer: 5'-TCCTCCACTTCCAATTTTAGCTAAGCATTTTACCAGATGAACGTTGTTGG-3'	This manuscript	N/A
UPRT-P_{GRA28}_F primer: 5'-TTCCAAGATCTGTGGCGTCTCGATTGTGAGAGCTGACGAGTCGATGGAAAGCGGCTTGCGGGCCACACAGAGTCCCCTGTGG-3'	This manuscript	N/A
UPRT-3'DHFR_R primer: 5'-GCCGCGGCAAACTGCCCGCAAGCCGCTTTCCATCGACTCGCTCCACCGCGGTGTCACTGTAGCC-3'	This manuscript	N/A
CCR7 Taqman probe	Applied Biosystem	Assay ID Mm99999130_s1
CCL22 Taqman probe	Applied Biosystem	Assay ID Mm00436439_m1
TNFAIP6 Taqman probe	Applied Biosystem	Assay ID Mm00493736_m1
CCL24 Taqman probe	Applied Biosystem	Assay ID Mm00444701_m1
CX3CL1 Taqman probe	Applied Biosystem	Assay ID Mm00444701_m1
CXCL3 Taqman probe	Applied Biosystem	Assay ID Mm01701838_m1
CXCL5 Taqman probe	Applied Biosystem	Assay ID Mm00436451_g1
Vcam1 Taqman probe	Applied Biosystem	Assay ID Mm01320970_m1
IL1a Taqman probe	Applied Biosystem	Assay ID Mm00439620_m1
TBP Taqman probe	Applied Biosystem	Assay ID Mm01277042_m1

References

S1. Satpathy, A.T., et al., *Zbtb46 expression distinguishes classical dendritic cells and their committed progenitors from other immune lineages.* J Exp Med, 2012. **209**(6): p. 1135-52.

S2. ten Hoeve, A.L., M.-A. Hakimi, and A. Barragan, *Sustained Egr-1 Response via p38 MAP Kinase Signaling Modulates Early Immune Responses of Dendritic Cells Parasitized by Toxoplasma gondii.* Frontiers in Cellular and Infection Microbiology, 2019. **9**(349).

S3. Bhandage, A.K., et al., *A motogenic GABAergic system of mononuclear phagocytes facilitates dissemination of coccidian parasites.* Elife, 2020. **9**.

S4. Wang, Y., et al., *ZBTB46 is a shear-sensitive transcription factor inhibiting endothelial cell proliferation via gene expression regulation of cell cycle proteins.* Lab Invest, 2019. **99**(3): p. 305-318.

Data S1

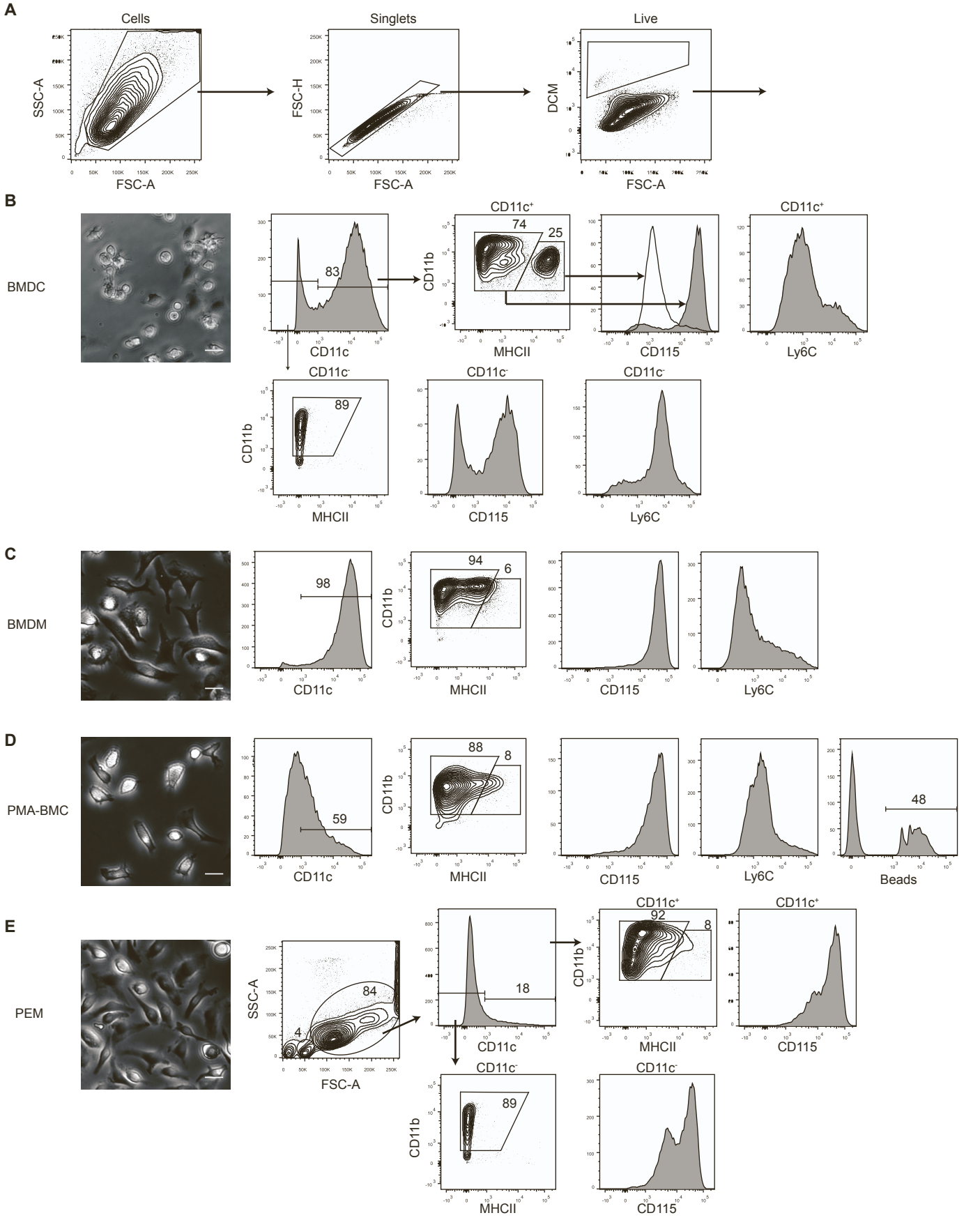
A
Cells
SSC-A
FSC-A
Singlets
FSC-H
FSC-A
Live
DCM
FSC-A
B
BMDC
83
CD11c
CD11c+
74
25
CD11b
MHCII
CD115
CD11c+
Ly6C
CD11c-
89
CD11b
MHCII
CD11c-
CD115
CD11c-
Ly6C
C
BMDM
98
CD11c
94
6
CD11b
MHCII
CD115
Ly6C
D
PMA-BMC
59
CD11c
88
8
CD11b
MHCII
CD115
Ly6C
48
Beads
E
PEM
84
4
SSC-A
FSC-A
18
CD11c
CD11c+
92
8
CD11b
MHCII
CD11c+
CD115
CD11c-
89
CD11b
MHCII
CD11c-
CD115
F
T. gondii
FSC-A
GFP
% infected (GFP+)
100
80
60
40
20
0
MOI 1
MOI 2

Data S1. Related to STAR Methods

Phenotypical analysis of macrophages

(**A**, **B**, **C**, **D**, **E**) Morphological analysis and flow cytometric analysis of anti-CD11c, CD11b, MHCII, CD115, Ly6C staining on uncultured BMDCs (A, B), BMDMs (C), PMA-BMCs (D) and PEMs (E) and of fluorescent particle uptake (beads) by PMA-BMC after 1h incubation at 10 particles/cell (D). Data are representative of ≥2 independent experiments. Scale bars are 20 µm.

(**F**) Representative flow cytometric analysis of infection frequencies of BMDMs challenged with for 18h with GFP-expressing *T. gondii* tachyzoites (RH-LDM; MOI 1 or 2). Bar graph depicts the infection frequency (mean+SE) of the 3 (MOI 2) or 7 (MOI 1) independent experiments.